ABSTRACT

Title of Document: STUDYING mRNA TRANSPORT AND REGULATION OF RETROGRADE INJURY SIGNALING ASSOCIATED AXONAL TRANSCRIPT LEVELS IN THE CONTEXT OF AXONAL REGENERATION

Gunja Keyur Pathak, Doctor of Philosophy, 2014

Directed By: Assistant Professor, Dr. Sameer Shah, Bioengineering

This dissertation focuses on a detailed mechanism of mRNA transport during development of hippocampal neurons, and regulation of retrograde injury signaling (RIS)-associated genes in the context of regeneration. Damaged neurons in the CNS are unable to regenerate leading to neuronal degeneration and cell death. Identifying mechanisms that promote axonal regeneration of the damaged fibers is beneficial. First, I set to explore the detailed quantification of mRNA transport during the development of hippocampal neurons. Rigorous quantitative assessment of mRNA transport concluded that mRNA transport is driven by the functional demands of the cell. I measured the velocity, directionality and the duration of mRNA particles. In the axons, net velocity was highest at day 7 in vitro, which coincides with the initial stage of synapse formation. Within dendrites, it continues to increase through day 12 in vitro coinciding with an increased duration of synaptic contact, suggesting role of protein synthesis in context of sustained synaptic connectivity. Next, I set to explore regulations of genes involved in RIS process, a process stimulated upon injury and required for axonal regeneration. Investigation of regulation of RIS associated axonal transcript levels led to development of a whole hippocampal explant culture system. The hippocampal explant culture system enabled examination of axonal gene and protein expression independent of neuronal cell bodies. The study of RIS process suggests a novel biphasic increase in axonal gene expression (1 & 24 hrs post-injury). These genes are tightly and differentially regulated contributing to early synthesis of corresponding axonal proteins in hippocampal neurons. Additionally, importin β-dependent activity at the nucleus then appears to modulate a second wave (24 hrs) of RIS-associated transcripts, which are likely to further support axonal outgrowth. These studies provide insight into a powerful set of axonal processes that may be exploited to enhance CNS regeneration and repair.

STUDYING mRNA TRANSPORT AND REGULATION OF RETROGRADE INJURY SIGNALING ASSOCIATED AXONAL TRANSCRIPT LEVELS IN THE CONTEXT OF AXONAL REGENERATION

By

Gunja Keyur Pathak

Dissertation submitted to the Faculty of the Graduate School of the
University of Maryland, College Park, in partial fulfillment
of the requirements for the degree of
Doctor of Philosophy
2014

Advisory Committee:
Dr. Sameer Shah, Chair
Dr. Jose Helim Aranda-Espinoza, co-chair
Dr. John P. Fisher
Dr. Amy J. Karlsson
Dr. James N. Culver

Acknowledgements

This work was performed at the Laboratory of Neuromuscular Bioengineering and Cell BioPhysics, University of Maryland under the supervision of Dr. Sameer B. Shah.

I would like to thank:

Dr. Sameer B. Shah for introducing me to the thesis topic and giving me the opportunity to do my PhD thesis in his lab. I have learned a lot in his lab, both about Neuroscience and life in general. I also thank him for his guidance and mentorship throughout my thesis.

Dr. Jose Helim Aranda-Espinoza for welcoming me in his lab, and for being my co-mentor.

Dr. Amy J. Karlsson and Dr. John P. Fisher for helping and supporting this project, and allowing me use their facility.

Dr. James N. Culver for being part of my committee.

All the friends I have in Neuromuscular (at UMD and UCSD) and Cell BioPhysics lab. A special thanks goes to, Matt, Carlos, Heather, Katrina and Susan.

Finally, I would like to thank my parents: Jitendra and Rita Dave; my siblings: Maulik, Chintan and Chakshusha; my in-laws: Mala, Jigar, Purvi; and my husband: Keyur. Their support has been endearing and instrumental.

Table of Contents

List of Tables

List of Figures

List of Illustrations

Chapter 1: Introduction

Section 1: CNS disorder and Causes

Diffuse Axonal Injury (DAI) is a severe type of traumatic brain injury (TBI) resulting in the tearing of axons and eventually, cognitive dysfunction [3,4]. Brain injury occurs when a sudden trauma causes damage to the brain. This type of trauma usually occurs when the head suddenly and violently hits an object. Damage occurs due to moving back and forth in the skull as a result of acceleration or deceleration. Common causes of the injury are automobile accidents, violence, falls, and sports-related accidents [5]. About 1.5 million people in the U.S. suffer from traumatic brain injury each year. About 50,000 people die from TBI each year, and 85,000 people suffer long-term disabilities. In the U.S., more than 5.3 million people live with disabilities caused by TBI [6]. Injury to the central nervous system (CNS, Illustration 1-1) is particularly devastating because of the poor ability for neurons to regenerate their neurites. This injury leads to neuronal degeneration as well as cell death.

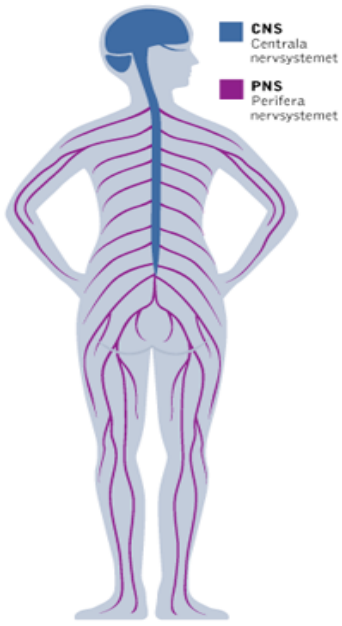

Illustration 1-1: Schematic Showing CNS and PNS [1]

Animal models of injury consist of three main types: compression, crush, and transection injuries. This study proposes to use transection or "cut or repair," type injury. Transection injuries produce a Sunderland type V injury, which result in disruption of all the fibers. Accordingly, recovery is

markedly worse than the lower grade injuries [7]. Hence, it will be beneficial to use transection as a model for a "worst case" regenerative scenario.

Section 2: Post-Injury

After neuronal injury, membranes reseal within 30-60 minutes [8], based on horseradish peroxidase uptake, after which there is a transient period of anatomical remodeling through local sprouting at the lesion site. However, the severed axons ultimately fail to regenerate beyond the lesion site. The distal ends of the severed axons form dystrophic growth cones, which are exposed to the damaged glial environment. At an early phase of the injury, then, myelin-associated inhibitors restrict axon re-growth. Next, inflammatory cells and reactive astrocytes lead to the formation of a glial scar. With the scarring process there is release of chondrotin sulphate proteoglycans that further limit the regenerative process [2]. Illustration1-2 depicts CNS injury site.

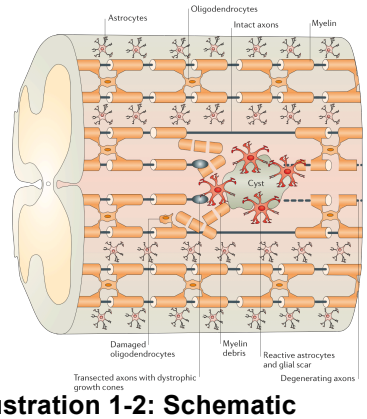

Illustration 1-2: Schematic illustration of CNS injury site [2].

All together, these factors are believed to prevent regeneration of the CNS. As a result, identifying mechanisms that promote axonal regeneration of the damaged fibers is beneficial. I hypothesize that one of the ways that might be able to promote regeneration is through transport of mRNAs to the distal neurites, which would then provide transcripts for protein synthesis, for rebuilding locally within neurites. Some of the current therapies that focus on promoting regeneration are described in Section 3, and evidence in support of a role for local protein synthesis and mRNA transport is provided in Sections 4 and 5, respectively.

Section 3: Current Therapies

Studies to promote CNS regeneration began as early as 1910's. The earlier research illustrated that CNS neurons do have regenerative capabilities when provided with proper environment. More recently, several studies have been looking at different aspects of regeneration process. The regeneration process of CNS requires survival, re-growth and functional synapse formation [9]. There are many studies that focus on promotion of regeneration in the injured CNS.

The many areas of regeneration studies include cellular replacement, neurotrophic factor delivery, axon guidance, removal of growth inhibition, manipulation of intracellular signaling and immune response [10]. The idea of stem cells replacing cells of the CNS morphologically has gained attention. Recent studies have illustrated that stem cells exit in the CNS, and could be used as a source of stem cells for re-implantation. However, the limiting factor is to determine whether the replaced cells are differentiated, and functional [9,10]. Neurotrophins, a family of polypeptides, are believed to be responsible for keeping viability of developing neurons until the axons and dendrites reach appropriate target. These neurotrophins include Nerve growth factor (NGF), Brain-derived neurotrophic factor (BDNF), Neurotrophin-3 (NT3), Neurotrophin-4/5 (NT4/5), and Neurotrophin-6 (NT6). However, an optimal way to utilize these factors in achieving regeneration has not yet been determined. A few axon guidance molecules such as polysialic acid-containing neural adhesion molecules (NCAMs), and proteins such as the SLIT group are known to guide axons during development; however, their role post neuronal damage is not well understood [9]. The two major classes of

CNS regeneration inhibitors are the myelin-associated inhibitors (MAIs) and the chondroitin sulfate proteoglycans. One of the MAI is Nogo-A, genetic deletion of Nogo-A and antibodies targeting Nogo-A promotes functional recovery after spinal cord injury (SCI) [11,12,13,14]. Other therapies such as removal of growth factors, and manipulation of immune response may have potential to manipulate scar tissue that prevents axonal growth, and promote axonal growth by inhibiting microglial and macrophage activation. While these therapies largely address inhibitory factors, the intrinsic growth capacity of neurons is also an imperative determinant of CNS regeneration failure, and has been underappreciated and under-studied. CNS neurons do not up regulate growth-associated genes to the same extent as do PNS neurons. As a result, even in the absence of inhibitors, their ability to regenerate is limited. Increasing the intrinsic growth capacity of neurons will allow modest axon regeneration within the CNS [11,15]. Consequently, the goal of this proposal is to provide a step forward in this direction by understanding intrinsic mechanisms of CNS neurons in the context of development and regeneration. One such intrinsic mechanism is the ability of the cells to synthesize proteins locally.

Section 4: Local Protein Synthesis and Regeneration

Local protein synthesis, or synthesis away from the cell body, in neurites, is important for neuronal survival, development, axon guidance, synapse formation and refinement [16], including plasticity-linked learning and memory, and regeneration [17]. Literature on mechanisms and regulation of local protein synthesis encompasses both the peripheral nervous system (PNS) and central nervous system (CNS), and within the CNS,

dendrites and axons. In the PNS, evidence for local protein synthesis was presented as early as 1970, where ribosome-like particles were visualized by electron microscopy (EM) in axons [18,19]. Since then, studies have confirmed the identity of peripheral ribosomal domains within myelinated mammalian axons [16,20], and gene-profiling studies have revealed many different proteins that can be synthesized locally in axons [21,22]. The examination of local protein synthesis in the central nervous system continues to be a source of some ambiguity. Initial studies concluded that the ribosomes are found in the dendrites of the hippocampal neurons, but not in the axons. Consequently, translational machinery and mRNAs are excluded from the axons of mature neurons [23,24], leading to increased attention on mRNA regulation and local protein synthesis in dendrites. Developmentally, dendritic protein synthesis increases during synaptogenesis and decreases into adulthood [25,26]. Interestingly, the emphasis on dendritic protein synthesis has resulted in an underplaying of evidence supporting protein synthesis within CNS axons. As for the PNS and CNS neurons, axon profiling in the dorsal root ganglion (DRG) and hippocampus suggested that hundreds of different proteins can be locally synthesized [21]. Moreover, multiple components of translational machinery, such as signal recognition particles (SRP), ER proteins, and Golgi components have been observed in the axon [27].

The ability of neurons to re-grow in culture suggests that protein synthesis might be reactivated by injury. The importance of local protein synthesis in regeneration has been elucidated in several studies where it was shown that axonally separated neurons could synthesize proteins for several hours after injury. For instance, the study of Verma et al., demonstrated that axons of injured DRGs formed growth cone within 20 minutes.

And after 4 hours, 80% of neurons successfully regenerated a new growth cone. They also illustrated impaired growth cone regenerative ability after applying protein synthesis inhibitors [28]. It was illustrated that the formation of growth cone requires activity of target of rapamycin (TOR), P38 MAPK, Caspase – 3, where TOR, and P38 MAPK regulate protein synthesis through translation factor activity [28,29,30]. Additionally, in the CNS neurons, particularly in the adult retinal ganglion cells (RGCs), deletion of PTEN (phosphatase and tensin homolog), a negative regulator of the mammalian target of rapamycin (mTOR) pathway promotes axonal regeneration after optic nerve injury. Specifically, PTEN deletion activates the PI3K/mTOR pathway controlling cell growth and size by regulating cap-dependent protein translation initiation [31]. Other observations illustrate protein synthesis inhibitors applied to the proximal nerve after axotomy can attenuate regenerative growth. In addition, immunolocalization studies suggested that the ability of axonal protein synthesis correlates with their regenerative capacity in vivo [29,32,33]. Another piece of evidence that axonally synthesized proteins appear to facilitate injury responses is that injury-conditioned axons show increase in content of protein synthesis compared with axons from naïve neurons [28,29]. Altogether, literature emphasize that axonal protein synthesis is important to initiate and maintain regeneration. However, in order to promote axonal outgrowth and regeneration, it is imperative to elucidate mechanisms that are needed for local protein synthesis (LPS) and that require LPS. This dissertation focuses on two processes underlying protein synthesis: localized mRNA transport during development, and regulation of retrograde injury signaling (RIS) - associated genes in the context of regeneration.

Section 5: mRNA Transport

Local protein synthesis requires transport of mRNA from the cell body to ribosomal sites for synthesis. Regulation of the transport of mRNA transcripts corresponding to proteins is also essential for local synthesis [29,34]. These regulatory pathways have also been studied in models of axonal injury, recovery from which necessitates increased local protein synthesis [35,36]. Of particular interest are the RNA binding proteins ZBP1, Staufen and fragile X Mental Retardation Protein (FMRP).

The RNA binding proteins (RBPs) required to localize mRNAs are known to bind to 3′ untranslated regions (3′UTR) of the mRNAs. As in the PNS, RBP have been implicated in coupling the transport of mRNA into dendrites with local protein synthesis [25]. Among these, FMRP and Cytoplasmic Polyadenylation Element Binding Protein CPEB bind many mRNAs important for development, including, respectively, the α-isoform of calcium–calmodulin-dependent protein kinase II (αCAMKII), involved in long term potentiation, and brain derived neurotrophic factor (BDNF), responsible for initiating a variety of CNS signaling pathways [25,37,38]. Again, FMRP has been found in axons of some CNS neuronal populations [39], and the RBP zipcode binding protein-1 (ZBP1) has been known to associate with β-actin mRNA in the chick forebrain, and influence its axonal transport [40,41]. In fibroblasts, localized translation of β-actin mRNA is needed for polarity of cell migration. It is also evident that the localized β-actin mRNA is translated in the axons [4,27,42,43]. In addition, ZBP1 also act as β-actin mRNA translation repressor since it inhibits translation of β-actin mRNA while bound. The β-actin mRNA translation is de-repressed by phosphorylation of ZBP1 on tyrosine residues by Src-family kinases, allowing dissociation of RNA-protein complex [44].

Another study illustrated the role of ZBP1 in regulating mRNA transport to the activated synapses of hippocampal neurons in response to synaptic activity [45]. Though many mechanisms that regulate mRNA transport have been discovered, further details need to be uncovered.

Defects in several aspects of local mRNA regulation, such as those summarized above, have been linked to neurological disorders [25]. Furthermore, studies in the CNS neurons showed that localized mRNAs play a variety of functions. Most relevant to our work, it was illustrated that the composition of the pool of axonal mRNAs changes after axonal injury and during regeneration [21], and, in support of the intrinsic regenerative capacity of CNS neurons, mRNAs found in injured and naïve CNS axons are similar to those found in the PNS [46]. Detailed quantification of mRNA transport will provide a better understanding of mRNA trafficking in the axons, which will then allow us to understand the mechanisms guiding normal and altered mRNA transport, and its importance in neuronal regeneration. As a result, one of the goals of our project (Chapter 2) was to understand quantitative details of mRNA transport during hippocampal neuron development.

Section 6: Retrograde Injury Signaling (RIS) Mechanisms

Retrograde injury signaling (RIS) may be defined as the transport of injury signals from the site of injury to the nucleus in the cell body. This mechanism appears to play a major role in the regenerative process in the PNS [36,47].

Upon injury, the rapid ion influx at the injury site generates an electrophysiological response that propagates retrogradely to provide the first indication of lesion events [47,48,49]. Slower components of the RIS result in decreased trafficking

of trophic factors to the soma, and increased transport of new-injury induces signals from the site of injury to the nucleus [47,50,51]. RIS complexes require importin α, importin β1 (also known as Karyopherin beta 1), RanBP1, and signaling cargoes in association with dynein motors [47,51,52,53]. The importin β1 mediated RIS mechanism is very important for axonal regeneration, as the axonal knockout of importin β1 attenuates cell body transcriptional responses to nerve injury and delays functional recovery *in vivo* (Illustration 1-3) [54]. In particular, injury induces local translation of importin β1 and Ran-binding protein (RanBP1) in the axons [36], which reverses the prevention of importin-associated cargo complex imposed by RanGTP. Several signaling cargoes and associated signaling molecules have been identified in the RIS complex. Among the cargoes is the type III intermediate filament, vimentin, which links activated Erks to importin-mediated retrograde transport and protects ErK from desphosphorylation [55].

Retrograde signaling has been extensively studied in the PNS, towards new approaches to enhance regeneration. In the CNS, importin β1 is shown to transport the transcriptional regulator STAT after injury, indicating its role in injury-induced axonogenesis of hippocampal neurons [56,57].

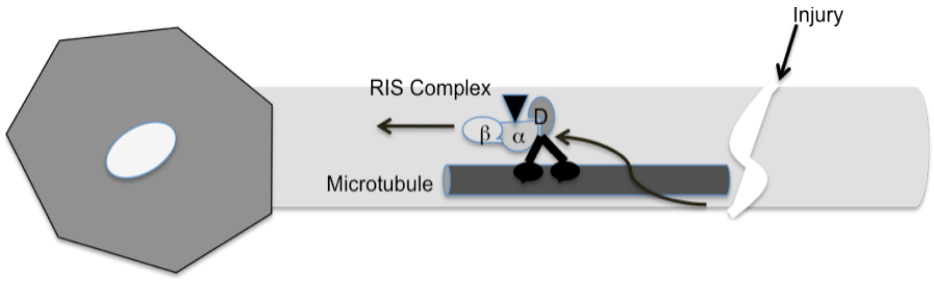

Illustration 1-3: Schematic of Retrograde injury signaling pathway.
Injury triggers translation of several proteins. Upon local synthesis, these proteins form into a complex. The trimeric complex then binds to specific cargo. The cargo is transported back to the nucleus in the cell body causing cell survival and regenerative response.

However, major knowledge gaps exist both in the PNS and CNS, including an unclear understanding of mechanisms underlying the regulation of local transcriptional levels of RIS associated genes, which encode RIS-associated proteins activated in response to injury. Additionally, injury induced local translation of importin β1, and associated proteins RanBP1, and vimentin have not been elucidated in the CNS. In Chapters 3 and 4, I detail the mechanisms underlying the regulation of axonal levels of RIS associated genes in response to injury utilizing whole hippocampal explant culture system.

Section 7: Summary

As described above, CNS neurons' ability to regenerate is less efficient than PNS neurons. In addition, more research has been performed on PNS neurons compared to those in the CNS, due to easily accessible and long peripheral axons, both *in vitro* and *in vivo*. Our goal was to elucidate specific intrinsic mechanisms: mRNA Transport and RIS process in the central nervous system. Unveiling these specific neuronal intrinsic mechanisms will be beneficial in promoting axonal regeneration. First, I have provided the first rigorous quantitative assessment of axonal and dendritic mRNA transport during central neuronal development. Significant differences in the transport parameters for individual and pooled particles at different stages of neuronal maturity emphasize the dynamic nature of transport at multiple levels. As a matter of fact, using our mRNA transport results, average net velocity of .002 μM/sec and maximum velocity of .03 μM/sec suggests that within 1 hour and 24 hours, mRNA can be transported to the distance of 7.2 μM-108 μM within 1 hour, and to the distance of 173μM - 2592 μM within 24 hours. Second, I have unfolded details of the RIS associated mRNAs mechanisms utilizing a novel hippocampal explant culture system. Particularly, our

results suggest a biphasic axonal response, in which levels of several axonal transcripts, including those associated with RIS, increase rapidly in axons after injury, contributing to early synthesis of corresponding proteins. Importin β1-dependent activity at the nucleus then appears to modulate a second wave of RIS-associated transcripts, which are likely to further support axonal outgrowth. These studies provide insight into a powerful set of axonal processes that may be exploited to enhance CNS regeneration and repair.

Chapter 2: A comparative quantitative assessment of axonal and dendritic mRNA transport in maturing hippocampal neurons

Section 1: Abstract

Translation of mRNA in axons and dendrites enables a rapid supply of proteins to specific sites of localization within the neuron. Distinct mRNA-containing cargoes, including granules and mitochondrial mRNA, are transported within neuronal projections. The distributions of these cargoes appear to change during neuronal development, but details on the dynamics of mRNA transport during these transitions remain to be elucidated. For this study, we have developed imaging and image processing methods to quantify several transport parameters that can define the dynamics of RNA transport and localization. Using these methods, we characterized the transport of mitochondrial and non-mitochondrial mRNA in differentiated axons and dendrites of cultured hippocampal neurons varying in developmental maturity. Our results suggest differences in the transport profiles of mitochondrial and non-mitochondrial mRNA, and differences in transport parameters at different time points, and between axons and dendrites. Furthermore, within the non-mitochondrial mRNA pool, we observed two distinct populations that differed in their fluorescence intensity and velocity. The net axonal velocity of the brighter pool was highest at day 7 (0.002 ± 0.001 μm/s, mean ± SEM), raising the possibility of a presynaptic requirement for mRNA during early stages of synapse formation. In contrast, the net dendritic velocity of the brighter pool increased

steadily as neurons matured, with a significant difference between day 12 (0.0013 ± 0.0006 μm/s) and day 4 (-0.003 ± 0.001 μm/s) suggesting a postsynaptic role for mRNAs in more mature neurons. The dim population showed similar trends, though velocities were two orders of magnitude higher than of the bright particles. This study provides a baseline for further studies on mRNA transport, and has important implications for the regulation of neuronal plasticity during neuronal development and in response to neuronal injury.

Section 2: Introduction

The geometry and unusual polarity of neurons imposes a tremendous challenge on biological communication between the cell body and neuronal projections such as axons and dendrites. One such challenge is the appropriate localization of translated proteins, which can vary depending on intracellular and extracellular cues [42]. A large fraction of protein deployment within neuronal projections occurs through the active or passive transport of proteins synthesized in the cell body [58]. Alternately, increasing evidence suggests that proteins may be translated locally, along an axon or dendrite or at their termini [18,19,21,29,59,60]**.** Though synthesis may occur within neurites, mRNA must still be transported, often as part of a granular complex containing additional translational and regulatory machinery, from the cell body to sites of local translation. Local synthesis has been linked to neuronal development, survival, and learning and memory [17]. Specific activities playing a role in these processes include axon guidance, synapse formation and synaptic refinement [16]. Clinically, defects in local mRNA regulation

have been linked to several neurological disorders, including fragile X syndrome and spinal muscular atrophy [25].

Previous work on mechanisms and regulation of local protein synthesis has been performed in both the peripheral nervous system (PNS) and central nervous system (CNS). In the PNS, evidence for local protein synthesis was presented as early as 1970, when ribosome-like particles were visualized in axons by electron microscopy (EM) [18,19,60]. Since then, studies have confirmed the identity of peripheral ribosomal domains within myelinated mammalian axons [16,20], and gene-profiling studies have revealed many different proteins that can be synthesized locally in axons [21,29,59]. Regulation of the transport of mRNA transcripts corresponding to these proteins is also essential for local synthesis. Recent work suggests that mRNA transport is tightly coupled to the activation of local protein synthetic pathways, possibly through signaling pathways initiated by growth factors [34,59]. These regulatory pathways have also been studied in models of axonal injury, recovery from which necessitates increased local protein synthesis [4,36,59]. Of particular interest are RNA binding proteins (RBP) such as Staufen and fragile X mental retardation protein (FMRP), which regulate the distribution of mRNA.

In the CNS, compelling functional roles for local protein synthesis have been identified in development as well as the regulation of synaptic stabilization, long-term potentiation or depression (LTP or LTD), and the consolidation of memory. Translational profiling and localization studies suggest that hundreds of different proteins can be locally synthesized in the axons [21] and dendrites [61]. In addition, multiple components of translational machinery, such as mRNA, signal recognition particles (SRP), ER

proteins, and Golgi components have also been observed in the axons [27] and in dendrites [5, 6]**.** Developmentally, dendritic protein synthesis increases during synaptogenesis and decreases into adulthood [24,25]. As in the PNS, several RBP have been implicated in coupling the transport of mRNA into axons and dendrites with local protein synthesis [25,37].

Collectively, studies in both the PNS and CNS reveal multiple conceptual similarities in hypothesized mechanisms guiding the coupling of mRNA transport and translation. However, a significant gap in our understanding of this coupling persists, in part due to a lack of rigorous criteria by which transport may be assessed and compared. As a first step towards filling this gap, we have developed methods to quantify several parameters that describe the dynamics of mRNA transport and localization. Using these methods, we compared mRNA transport in the axons and dendrites of cultured hippocampal neurons at various stages of neurite outgrowth and developmental maturity. We have validated these methods by comparing mRNA transport to that of mitochondria, a well-characterized transport cargo. Our results provide a baseline for future studies on mRNA transport, and raise interesting hypotheses regarding the plasticity of transport during hippocampal development.

Section 3: Results

Subsection 1: Localization of RNA granules in maturing hippocampal neurites

Immunofluorescence and DIC imaging were performed to examine mRNA localization at different phases of developmental maturity and within hippocampal neurites of different polarity. At days 4, 7, and 12, several criteria were used to determine

the developmental phase of the neurons and to assess polarity. First, we tested whether a neurite contacted another cell. At day 4, the majority of neurites displayed a free growth cone, while at days 7 and 12, the termini of most neurites intersected with other cells. At day 12, there was also significantly more axonal branching per neuron compared to day 7 (9.0 ± 1.3 vs. 2.5 ± 1.08; Mean ± SEM; t-test $p<0.04$), though the total number of projections and dendritic branching per neuron was unchanged. Second, the synaptic vesicle protein synapsin I was labeled to determine synaptic maturity [62,63]. At day 4, as expected based on previous work [23], synapsin localized primarily as small puncta along neurites and as larger densities at terminal growth cones (Fig 1a). By day 7, larger densities of synapsin I were observed, with accumulations of vesicles at sites of neurite contact indicating the presence of stable synapses (Fig 1b).

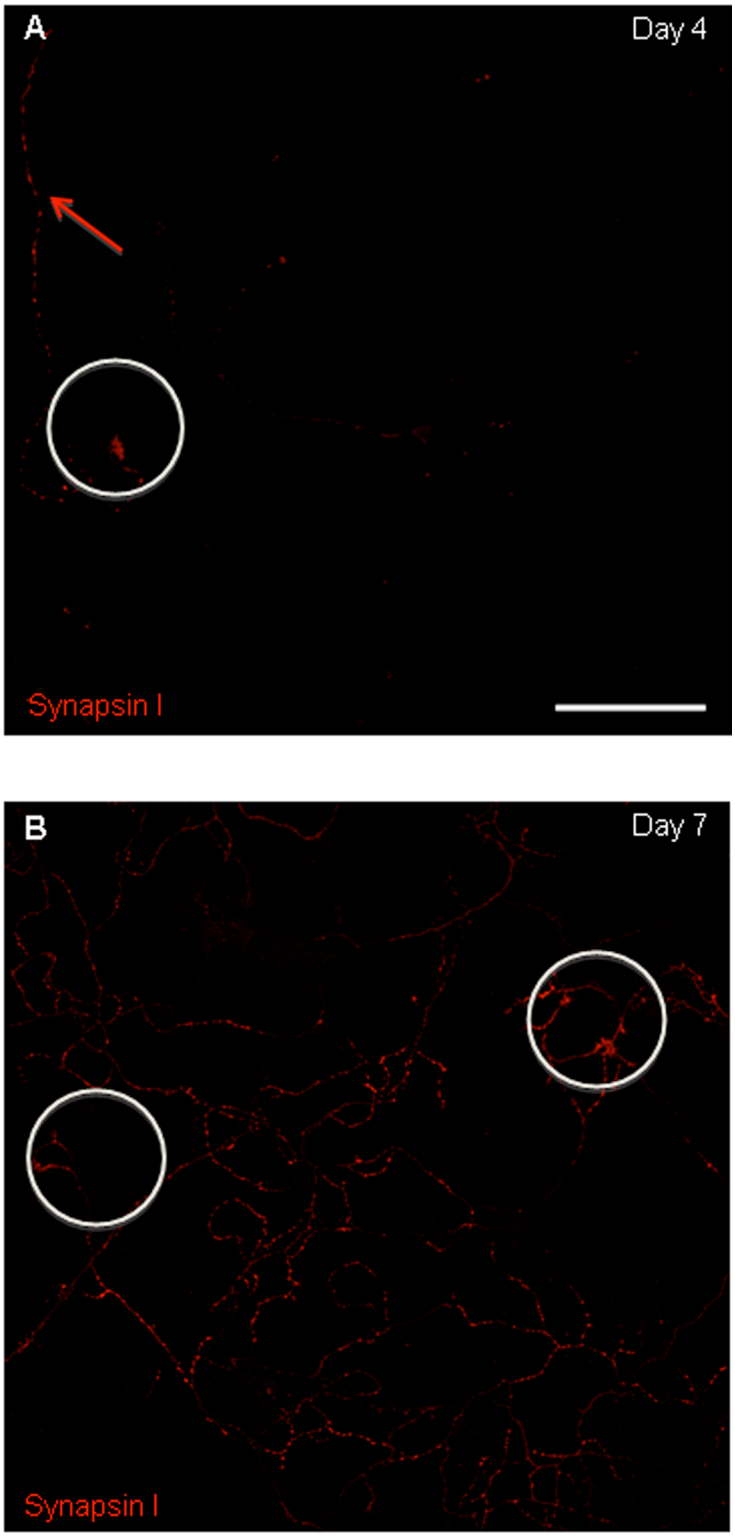

Figure 2-1: Maturity of hippocampal neurons at different days in culture.

The synaptic vesicle protein Synapsin I is a marker for the maturity of the hippocampal neurons [62]. Immunolabeling with Synapsin I at day 4 (A) shows granular proteins concentrated in the distal axon and growth cone, as there is no cell-cell contact (arrow – protein in distal axon, circle- protein in growth cone), while there is a considerable increase in fluorescence intensity at day 7 (B). There is formation of large cluster of vesicles at sites of synaptic contact at day 7 (Circles-shows cell connection). The images illustrated here have been converted to grayscale and contrast enhanced, to emphasize neurites. Bar is 50μm.

To differentiate between dendrites and axons, we examined the geometry of neurites under DIC and fluorescence imaging. As previously described [64,65,66], axons exhibited a long, narrow process that emerged from the cell body with minimal tapering and dendrites displayed a shorter process that tapered more gradually as it emerged from the cell body (Fig 2). We confirmed morphological assessments with immunofluorescence; axons were identified through the labeling of phosphorylated neurofilaments (SMI-31) and dendrites by MAP2 (Fig 2). Spatially distinct SMI-31 and MAP2 labeling was apparent as early as day 3 (data not shown). However, the fluorescence pattern was more continuous within each neurite at days 4, 7, and 12 (Fig 2a-c), confirming that neurons had fully differentiated at our earliest time point. Based on these criteria, then, neurons at day 4 with a free terminal were designated as immature (growing), differentiated neurons. Neurons at days 7 and 12 were both designated as differentiated neurons with stable synapses, with those at day 12 presumably more mature.

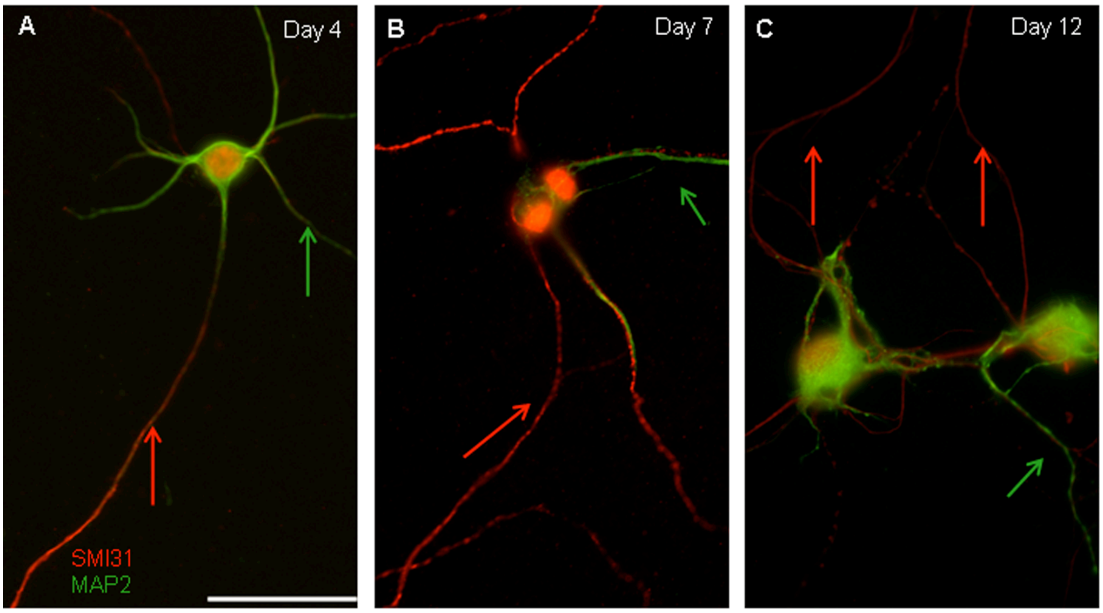

Figure 2-2: Hippocampal neurons are differentiated and present distinct morphology for both the axon and dendrites.

Dendrites have shorter process and taper more gradually (arrows), while axons display a long, narrow process with minimal tapering (arrows in all figures). (A-C) Expression of phosphorylated neurofilaments SMI-31 (red) and microtubule-associated protein MAP2 (green) (A) Double-label immunofluorescence of SMI-31 (red) and MAP2 (green) at 4 DIV (days in vitro). Dendrites (MAP2) are shorter with gradual tapering projections whereas axon (SMI-31) stain display long narrow processes. (B) Double-label immunofluorescence of SMI-31 (red) and MAP2 (green) at 7 DIV. (C) Double-label immunofluorescence of SMI-31 (red) and MAP2 (green) at 12 DIV. Bar is 50μm.

To ascertain the localization of axonal and dendritic mRNA particles at each stage of development, cells were labeled with Syto, a nucleic acid stain that labels RNA in both intra- and extra-nuclear compartments of the cell [67,68]. Syto co-localized with nuclei

labeled with Hoechst dye and also localized to neurites (Fig 3).

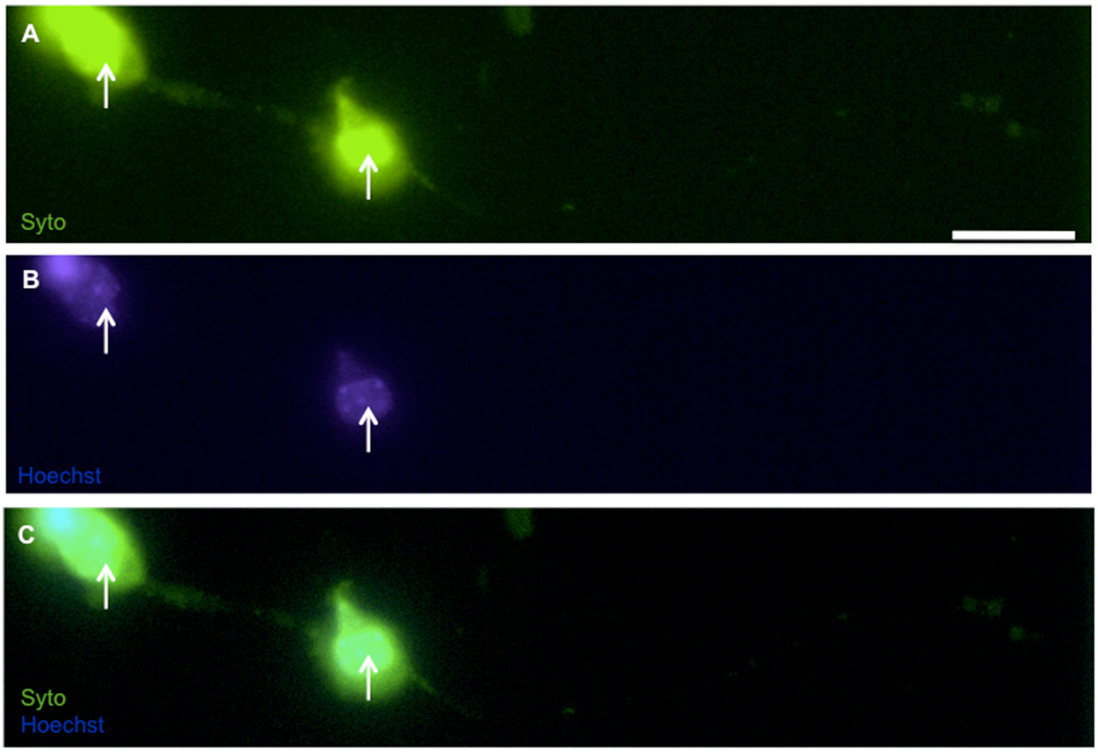

Figure 2-3:Hippocampal neurons were co-labeled with Syto nucleic acid stain and Hoechst nuclear stain.

Syto and Hoechst co-localize within the cell body (arrows), but there is no Hoechst labeling in neurites, which display Syto fluorescence. (A) Neurons stained with Syto nucleic acid stain (green). (B) Neurons stained with Hoechst nuclear stain (blue). (C) Double-label of Syto (green) and Hoechst (blue). Bar is 20µm.

Morphological assessment under DIC imaging conditions and counterstaining with SMI-31 and MAP2 antibodies revealed that RNA localized to both axons and dendrites (Fig 4,5). To differentiate non-mitochondrial RNA from mitochondrial mRNA in these processes, neurons were co-labeled with Syto and MitoTracker. RNA puncta that did not co-localize with MitoTracker within a neurite were designated as non-mitochondrial particles of mRNA (Fig 6b-d). The likelihood of a particle being mistakenly labeled as

non-mitochondrial (i.e., a false positive) was low, given the high affinity and fluorescence intensity of MitoTracker. Subsequent kymograph analysis was performed on labeled non-mitochondrial mRNA (referred to from now as mRNA) and mitochondria to distinguish between the movements of these two spatially and functionally distinct cargoes (Fig 6b-d).

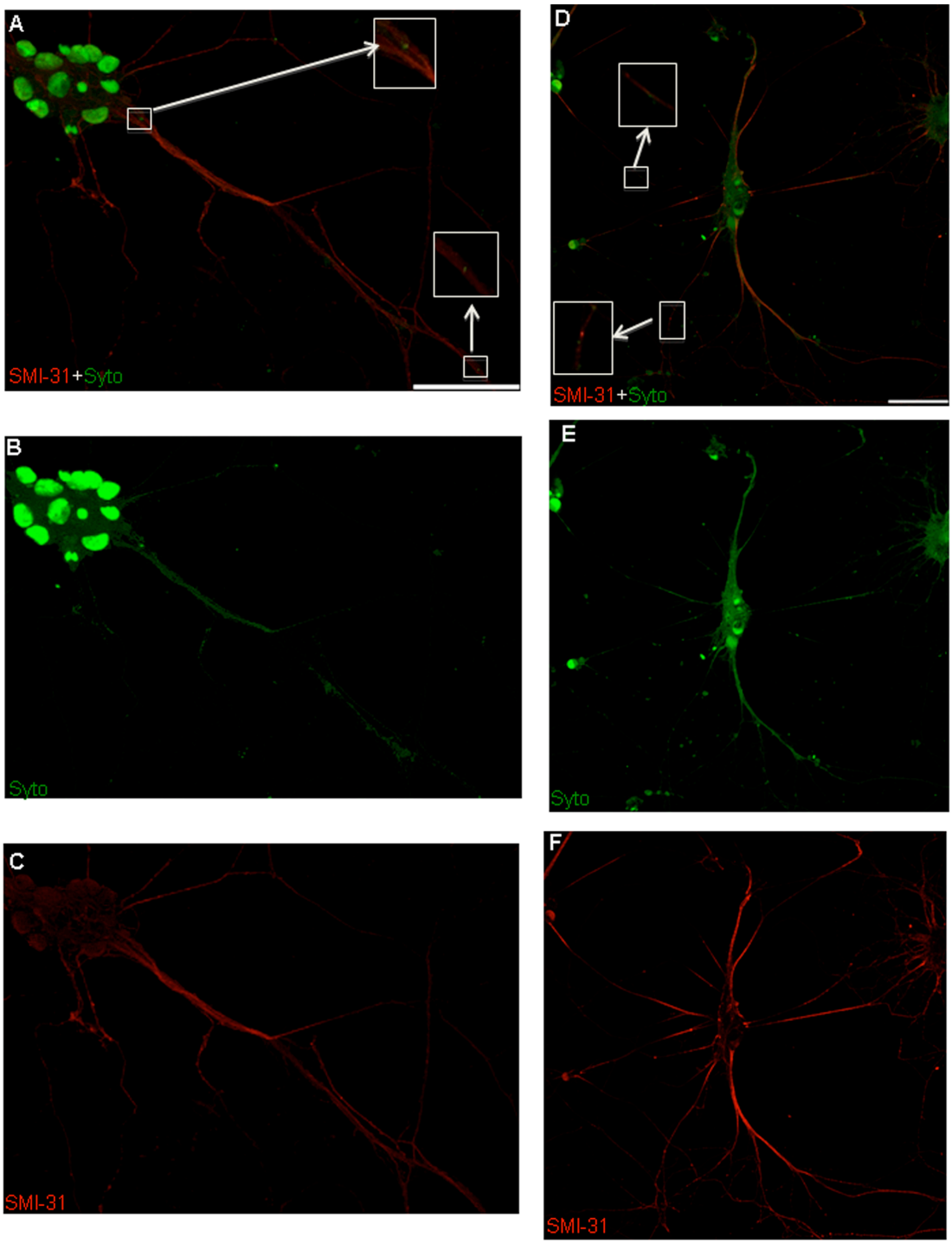

Figure 2-4:Confocal microscopy of mRNA localization in axons.

(A,D) Double-label immunofluorescence shows Syto labeling in cell bodies (nuclear) and co-localization of mRNA (Syto, green) with an axonal marker (SMI-31, red). Green puncta (Syto) that are not co-labeled correspond to localization within dendrites. (Inset – expanded for more clear

visualization). (B, E) Immunofluorescence of mRNA (Syto, green). (C,F) Immunofluorescence of axonal marker only (SMI-31, red). Bar is 50μm.

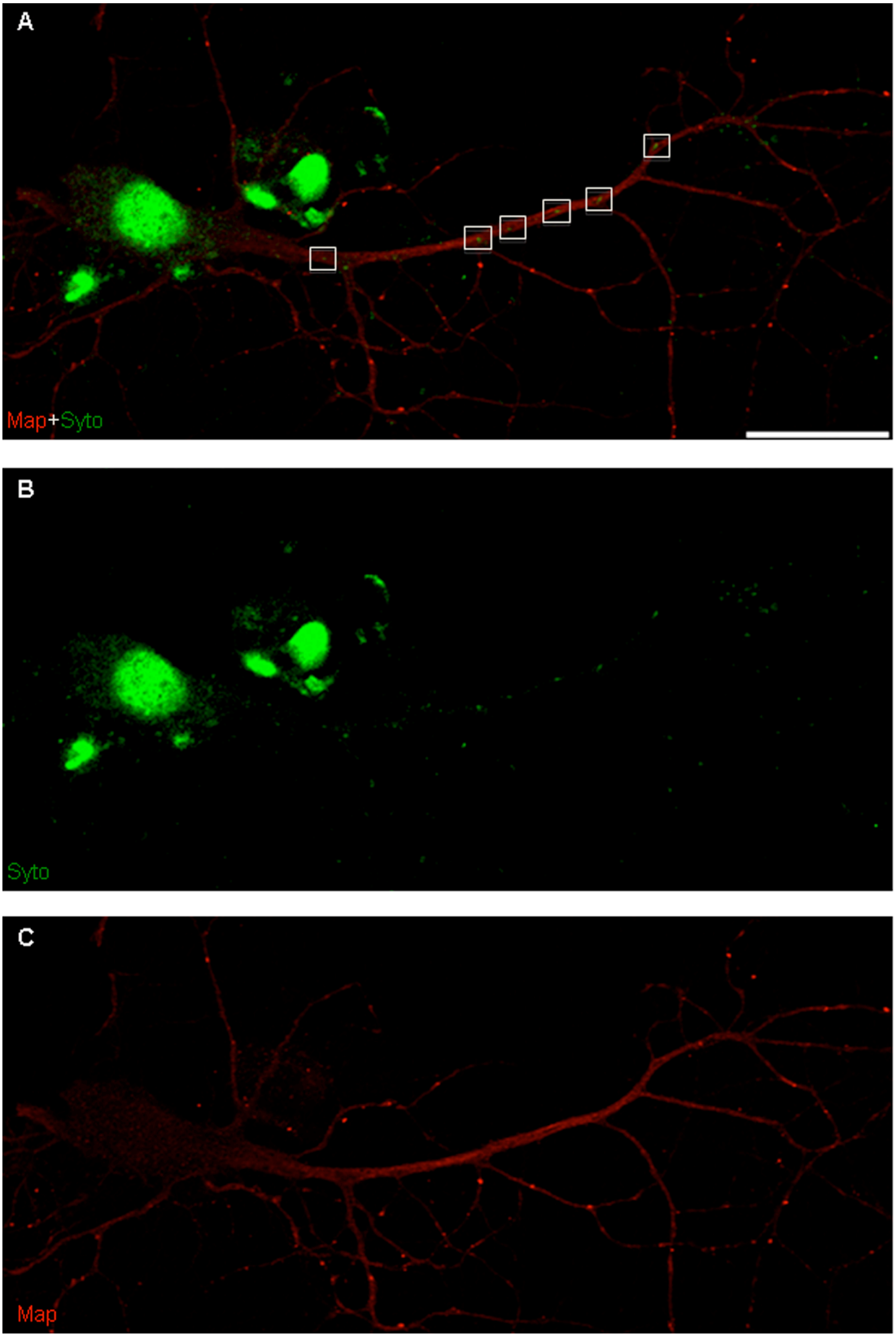

Figure 2-5:Confocal microscopy of mRNA localization in dendrites.

(A) Double-label immunofluorescence shows Syto labeling in cell bodies (nuclear) and co-localization of mRNA (Syto, green) with a dendritic marker (MAP2, red). Green puncta (Syto) that are not co-labeled correspond to localization within axons. (B) Immunofluorescence of mRNA (Syto, green). (C) Immunofluorescence of dendritic marker (MAP2, red). Bar is 50μm. To differentiate non-mitochondrial RNA from mitochondrial mRNA in these processes, neurons were co-labeled with Syto and MitoTracker. RNA puncta that did not co-localize with MitoTracker within a neurite were designated as non-mitochondrial particles of mRNA (Fig 6b-d). The likelihood of a particle being mistakenly labeled as non-mitochondrial (i.e., a false positive) was low, given the high affinity and fluorescence intensity of MitoTracker. Subsequent kymograph analysis was performed on labeled non-mitochondrial mRNA (referred to from now as mRNA) and mitochondria to distinguish between the movements of these two spatially and functionally distinct cargoes (Fig 6b-d).

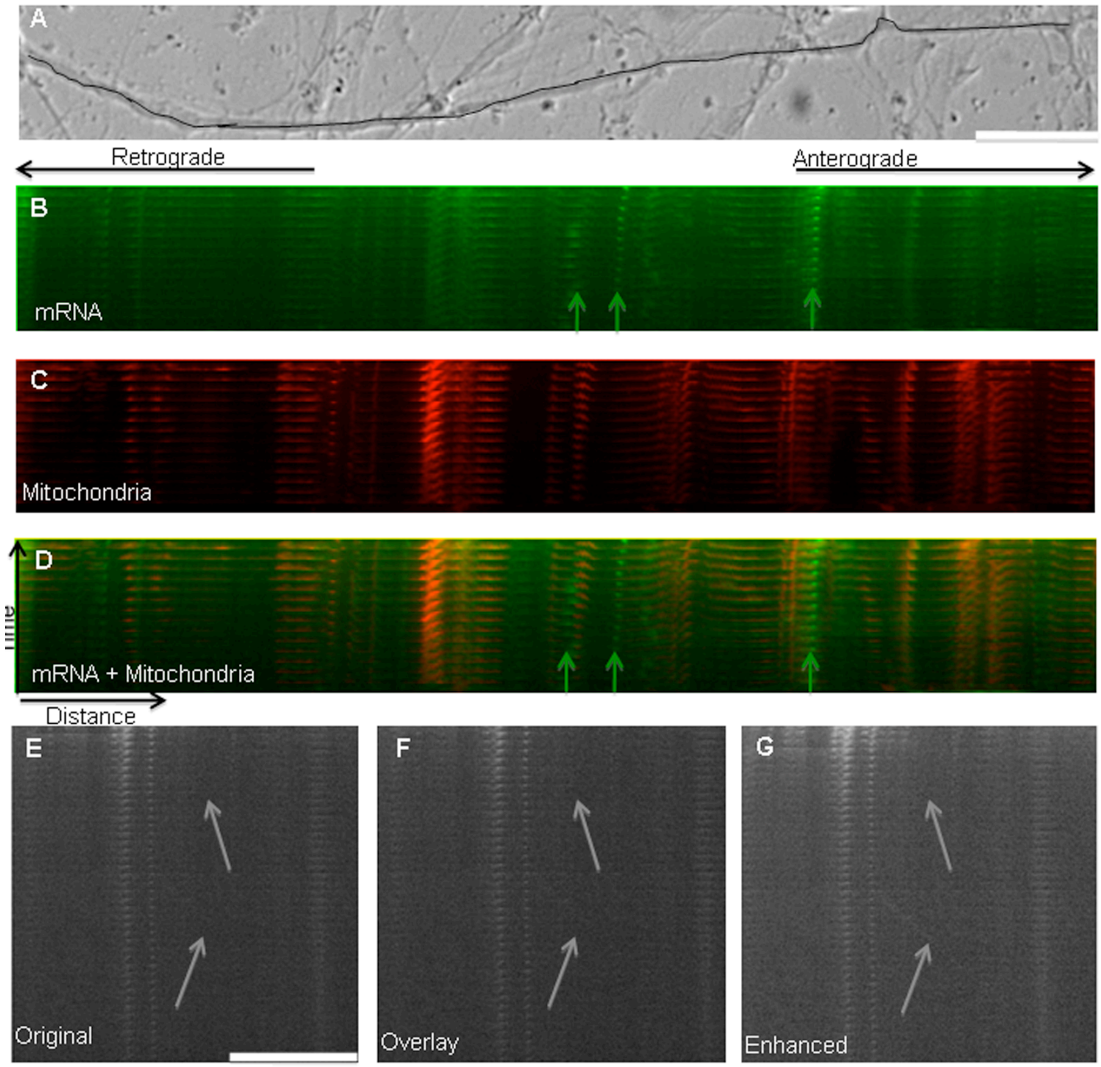

Figure 2-6: Methods of image analysis.

Time-lapse images of neurites were taken under DIC and fluorescence conditions. After classifying the neurite as an axon or dendrite using the DIC image, RNA particles (Syto, green) and mitochondrial particles (Mitotracker, red) were fluorescently labeled. (A) DIC image of a neurite (B) Both mitochondrial (B) and non-mitochondrial RNA and (C) non-mitochondrial kymographs were generated along the length of the neurite visible in the imaging field. Particles that were present in both of the kymographs were concluded to be mitochondrial mRNA whereas particles that were only present in the non-mitochondrial RNA kymograph were considered mRNA particles (arrows). (D) Overlay of mRNA kymograph (green) and mitochondrial kymograph (red). (E) mRNA kymograph without contrast enhancement. (F) Kymograph from (E) following iterative overlay of 50%

transparent image to visualize dim moving particles. (G) Kymograph from (E) following contrast enhancement to visualize dim mRNA moving particles. Additional details on enhancement of dim particles are shown in Figure S1. Bar is 20μm.

RNase treatment was performed to test whether "dim" particles labeled with Syto were mRNAs (Fig 7). Bright and dim mRNA particles were observed in kymographs of Syto, captured for only 5 minutes to minimize bleaching artifacts. Ribonuclease A treatment resulted in complete deletion of Syto signal in the neurites, and a strong suppression of signal in the cell body. Post-RNase, no puncta along the axon were as intense as the dimmest visible particle pre-RNase, suggesting that Syto indeed labeled both bright and dim mRNA particles (Fig 7b-e).

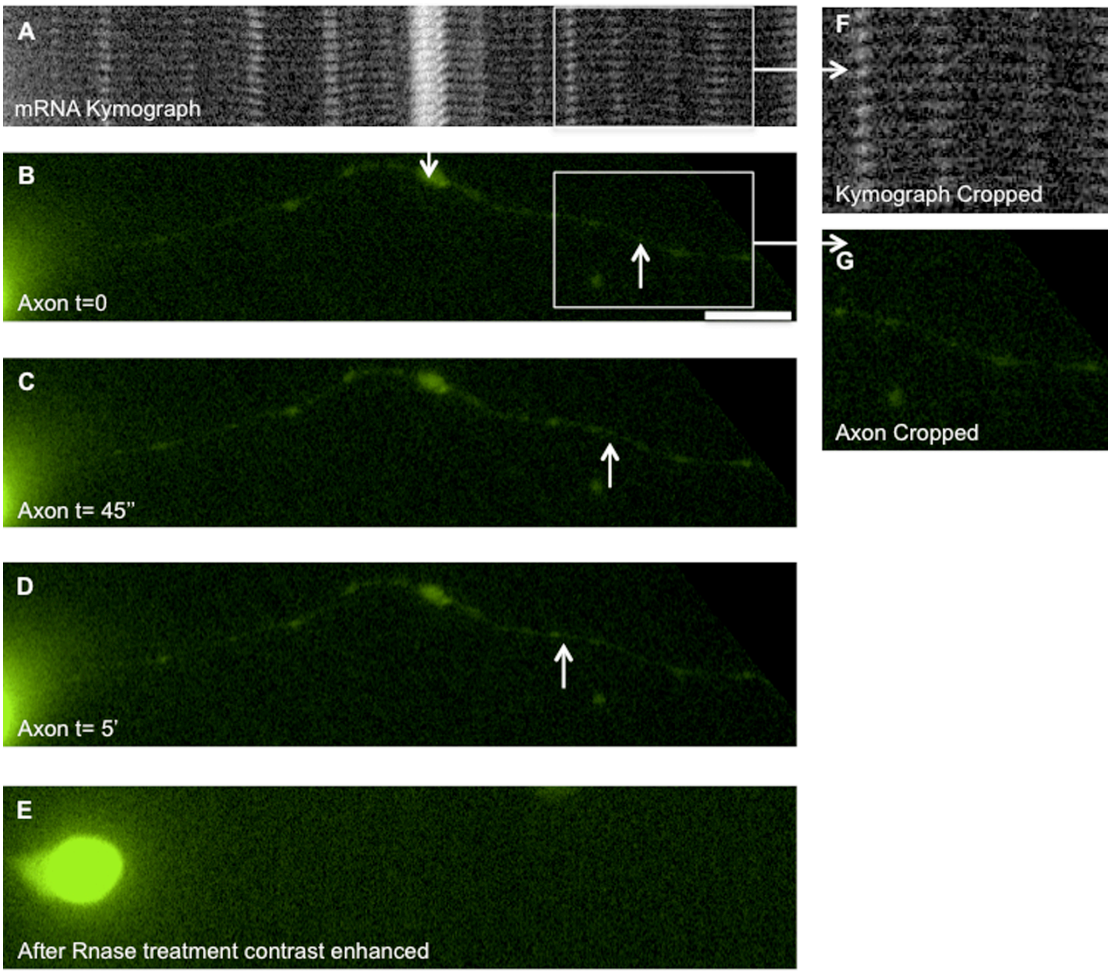

Figure 2-7: RNase A treatment was done to ascertain that dim particles are in fact mRNA particles. (A) Kymographs of mRNA particles pre-RNase treatment. (B) Neurons stained with Syto nucleic acid stain (green). (C) Neurons stained with Syto nucleic acid stain frame #3 (green). (D) Neurons stained with Syto nucleic acid stain frame #11 (green). The arrows indicate corresponding “dim” particle as it moves over five minutes. The bright particle indicated with down arrow had an average intensity of 9.26 arbitrary units, and dim particle indicted with up arrow had an average intensity of 0.98 arbitrary units. Values account for background subtraction. (E) Corresponding neuron after RNase treatment showing no Syto signaling in the neurites. Puncta indicated by arrows pre-RNase had intensities indistinguishable from background levels. All images are shown contrast enhanced, confirming full suppression of neurite fluorescence. (F) Cropped kymograph enlarged, from (A). (G) Corresponding region from (B) enlarged, including dim particle. Bar is 20µm.

Subsection 2: mRNA transport in dendrites and axons

Initial inspection of kymographs indicated 20-30 total fluorescent particles in each axon, with about half associated with mitochondria and half unassociated. Qualitatively, these particles appeared to move bidirectionally over short distances at slow rates. Closer inspection after the contrast enhancement of kymographs revealed another population of particles with very low fluorescence (Fig 6e-g). These particles were difficult to find in individual frames of time-lapse movies as well as non-enhanced kymographs; therefore, we applied a sequence of image processing algorithms to enhance their contrast and confirm their presence (Fig 6e-g, Fig 8 and 9). These particles appeared more mobile than their bright counterparts, and did not co-localize with mitochondria. Given the possibility that these visually distinct pools of mRNA, designated as “bright” and “dim,” could have different functional roles, we analyzed their transport profiles separately rather than pooling their data.

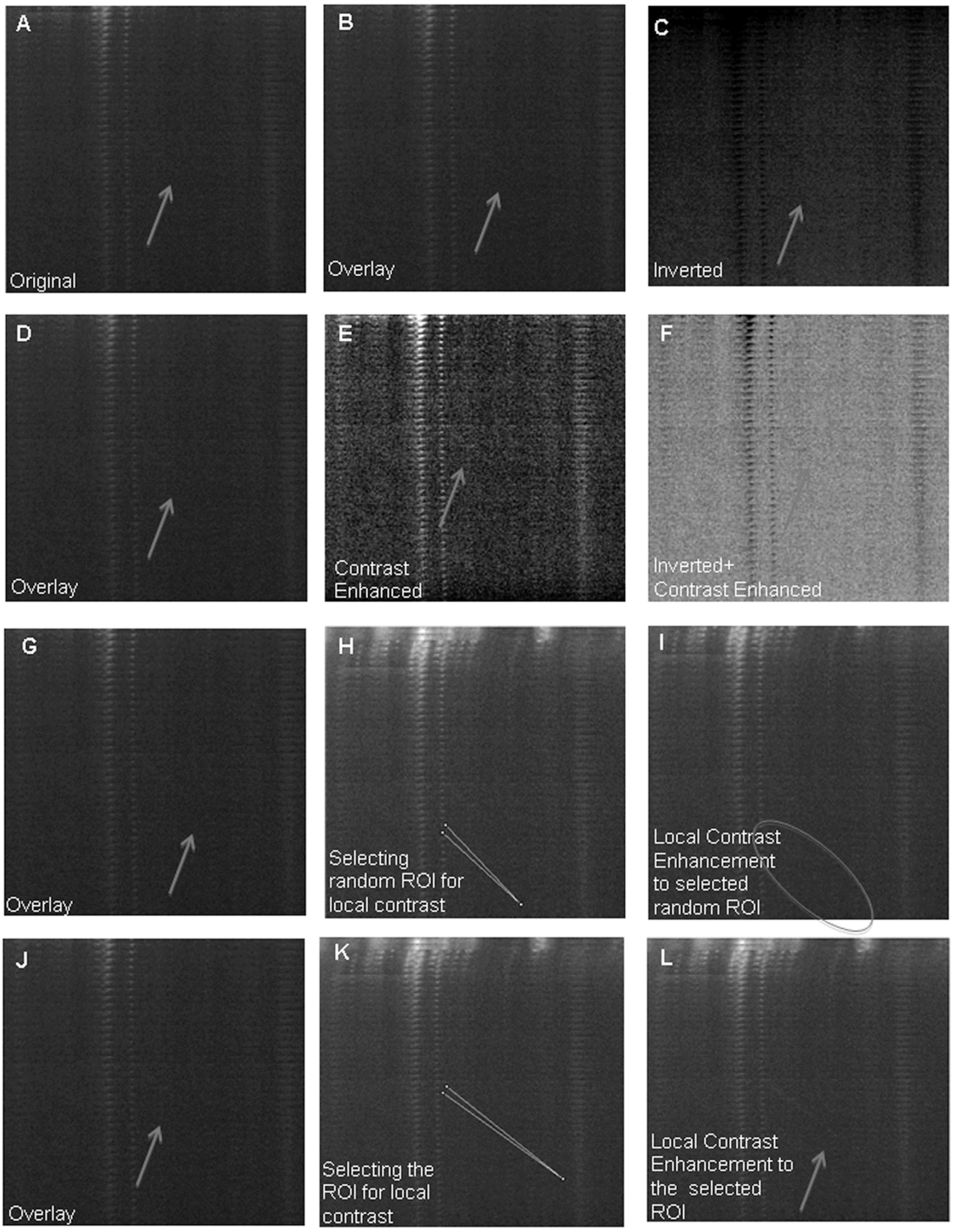

Figure 2-8: Methods of image analysis. Time-lapse images of neurites were taken under DIC and fluorescence conditions.

After classifying the neurite as an axon or dendrite using the DIC image, RNA particles (Syto, green) and mitochondrial particles (Mitotracker, red) were fluorescently labeled to identify respective

particles. Contrast enhancement and several controls were performed to confirm dim particles. (A) Non-mitochondrial mRNA kymograph without contrast enhancement. (B)) Kymograph from (A) following iterative overlay of 50% transparent image to visualize dim moving particles (C) Kymograph from (B) inverted using ImageJ to visualize dim particles (arrow). (D) Kymograph from (B). (E) Kymograph from (D) following contrast enhancement in ImageJ to visualize dim particles (arrow). (F) Kymograph from (D) inverted and contrast enhanced (arrow). (G) Kymograph from (B). Local contrast enhancement improved dim particle visualization. (H) Selection of background region with no apparent particles (yellow lines) for contrast enhancement. (I) Kymograph from (H) following local contrast enhancement does not indicate a particle trajectory in selected region (oval), confirming validity of contrast enhancement. (J) Kymograph from (B). (K) Selection of region of interest (ROI-yellow lines) for local contrast enhancement to visualize dim particles. (L) Kymograph from (K) following local contrast enhancement to visualize dim particles (arrow).

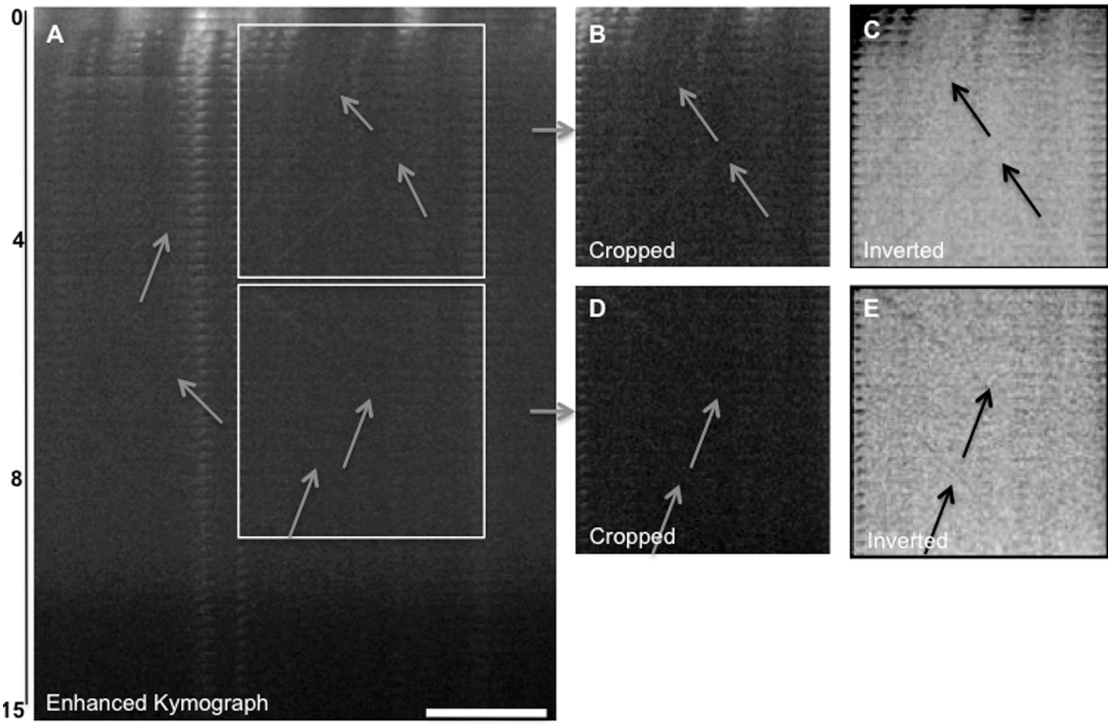

Figure 2-9: Time-lapse images of neurites were taken under DIC and fluorescence conditions.

After classifying the neurite as an axon or dendrite using the DIC image, RNA particles (Syto, green) and mitochondrial particles (Mitotracker, red) were fluorescently labeled to identify respective particles. (A) Whole kymograph following iterative overlay of 50% transparent image to visualize

dim moving particles (arrows). (B) Kymograph from (A) cropped upper region to visualize dim particles (arrows). (C) Kymograph from (B) inverted to visualize dim particles (arrows). (D) Kymograph from (A) after cropping lower region to visualize dim particles (arrows). (E) Kymograph from (C) inverted to visualize dim particles (arrows). Bar is 20µm.

A detailed assessment of transport involved the extraction of several parameters, which are summarized in Table 1. The comparison of pooled particles of a particular identity (directionality and net velocity) is presented in Fig 10 and Fig 11. These parameters are attained from comprehensive raw data that describe the movement of individual particles (particle velocity and duration). For convenience, Tables 2 and 3 summarize results for all parameters and may serve as a useful roadmap through the extensive datasets. Raw data and their statistical comparisons are also presented as figures and supplementary tables (Fig 12-14, Table S1-S4).

Table 2-1: Summary of measured parameters used to describe transport profiles for individual particles or groups of particles. Detailed definitions are found in the Methods section.

Parameter	*Definition*
Maximum Velocity	The maximum velocity achieved during the lifetime of a particle in each direction
Average Velocity	The average velocity during the lifetime of a particle in each direction
Duration	The amount of time spent by a particle moving in each direction during its lifetime
Directionality	The net direction that a given particle moves over its lifetime within a neurite

Net Velocity	The overall directionality and velocity of individual particles

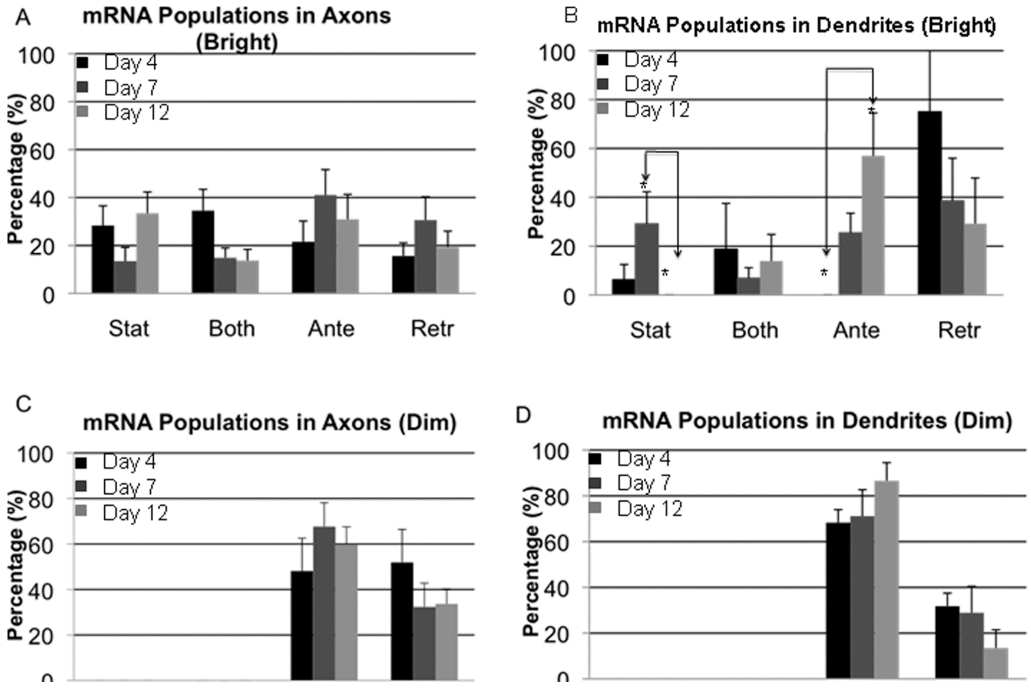

Figure 2-10: Net directionality of particle movement over its lifetime.

mRNA and mitochondrial particles were categorized as either moving or stationary. They were considered moving if their average velocity in either direction was greater than 0.001 μm/sec (0.1mm/day). Particles that did not meet this criterion were designated stationary. (A) percent of bright mRNA particles in axons in each state for days 4, 7, and 12. (B) Percentage of bright mRNA particles in dendrites in each state for days 4, 7, and 12. There are significantly more moving particles in anterograde direction at day 12 compared to day 4 $p < 0.02$ (ANOVA:Tukey). In contrast, there are significantly more stationary particles at Day 7 compared to Day 12 $p<0.05$ (ANOVA:Tukey). (C) Percentage of dim mRNA particles in axons in each state for days 4, 7, and 12. (D) Percentage of dim mRNA particles in dendrites in each state for days 4, 7, and 12.

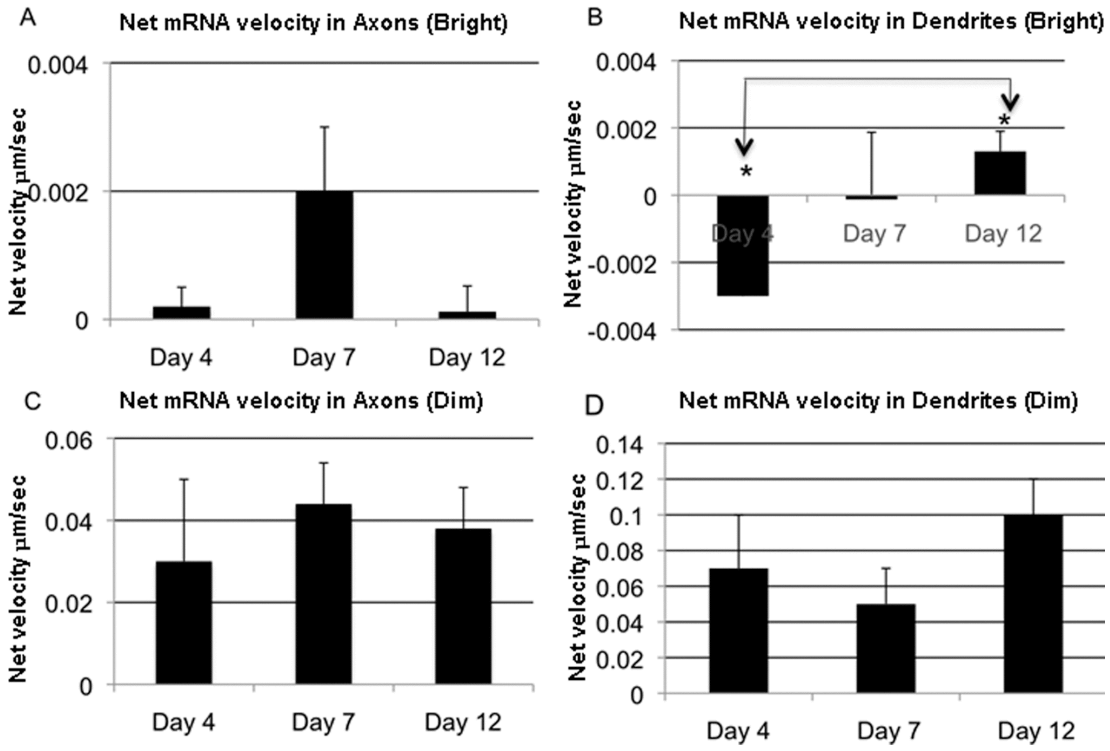

Figure 2-11: Average net velocity of individual dim and bright mRNAs particles in axons and dendrites.

(A*)* Average of net bright mRNA velocity moving through axons. (B) Average of net bright mRNA velocity moving through dendrites. The net velocity is higher at day 12 compared to day 4 $p< 0.05$ (ANOVA:Tukey). (C) Average of net dim mRNA velocity moving through axons. (D) Average of net dim mRNA velocity moving through dendrites. Values represent means ± SEM.

Table 2-2: Summary of statistically significant differences in populations and net velocities for various classes of labeled cargoes. Dash indicates no significant difference for a given parameter. Raw data are provided in supplementary figures and tables.

Cargo	Population Analysis	Net Velocity
mRNA in Dendrites (Dim)	-	day 4 vs. ↑day 12
mRNA in Axons (Bright)	-	-
mRNA in Dendrites (Bright)	↑day 7 vs. day 12 (stat) day 4 vs. ↑day 12 (Ante)	-
Mitochondria in Axons	day 4 vs. ↑day 7 (Ante)	-
Mitochondria in Dendrites	-	day 4 vs. ↑day 7 day 4 vs. ↑day 12

Table 2-3: Summary of statistically significant differences in maximum velocities and track durations for various classes of labeled cargoes. Dash indicates no significant difference for a given parameter. Raw data are provided in supplementary tables.

Cargo	Maximum Track Velocity	Track Duration
mRNA Axon anterograde (Dim)	-	-
mRNA Axon retrograde (Dim)	-	day 4 vs. ↑day 12 ↑day 7 vs. day 12
mRNA Dendrite anterograde (Dim)	day 7 vs. ↑day 12	-
mRNA Dendrite		
Mitochondria Dendrite retrograde (Dim)	-	-
Dendrite retrograde (Bright)	↑day 4 vs. day 12	↑day 4 vs. day 12
mRNA Axon		
Mitochondria Axon anterograde (Bright)	day 4 vs. ↑day 12 ↑day 7 vs. day 12	day 4 vs. ↑day 12 -
anterograde	↑day 7 vs. day 12	day 7 vs. ↑day 12
mRNA Axon		
Mitochondria Axon retrograde (Bright)	↑day 4 vs. day 12 day 4 vs. ↑day 7	↑day 4 vs. day 12 -
retrograde	↑day 7 vs. day 12	↑day 7 vs. day 12
mRNA Dendrite	day 4 vs. ↑day 7	
Mitochondria Axon anterograde (Bright)	day 4 vs. ↑day 12	
anterograde	N/A ↑day 7 vs. day 12	N/A -
Mitochondria	day 4 vs. ↑day 7	
mRNA Dendrite		
Dendrite anterograde	day 4 vs. ↑day 12	
	↑day 7 vs. day 12	-

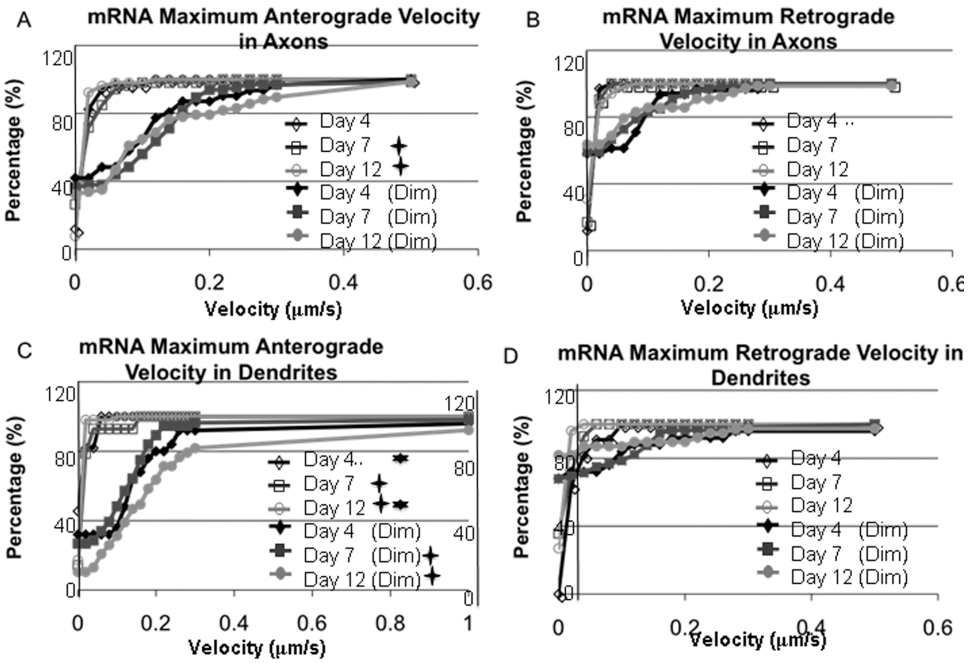

Figure 2-12: Maximum track velocity of mRNA in axons and dendrites. Particles were considered moving if their average velocity in either direction was greater than 0.001 μm/sec (0.1mm/day).

(A) Maximum track velocity of bright and dim mRNAs moving through axons in the anterograde direction. Within the bright mRNA population, particles moved more slowly at day 12 compared with day 7 ($p < 0.002$, K-S test). (B) Maximum track velocity of bright and dim mRNA particles moving through axons in the retrograde direction. Within the bright mRNA population, there is a rightward shift. Overall, more particles moved faster at day 7 compared to day 4 ($p < 0.03$, K-S test). (C) Maximum track velocity of bright and dim mRNA particles moving along dendrites in the anterograde direction. Within the bright mRNA population, there was a leftward shift. Significantly different velocities were observed for all days; however, at day 12 there were more particles that moved slowly ($p < 0.05$, K-S test). Within the dim population, there were significantly more particles that moved faster at day 12 compared to day 7 ($p < 0.01$, K-S test). (D) Maximum track mRNA particles moving through dendrites in the retrograde direction.

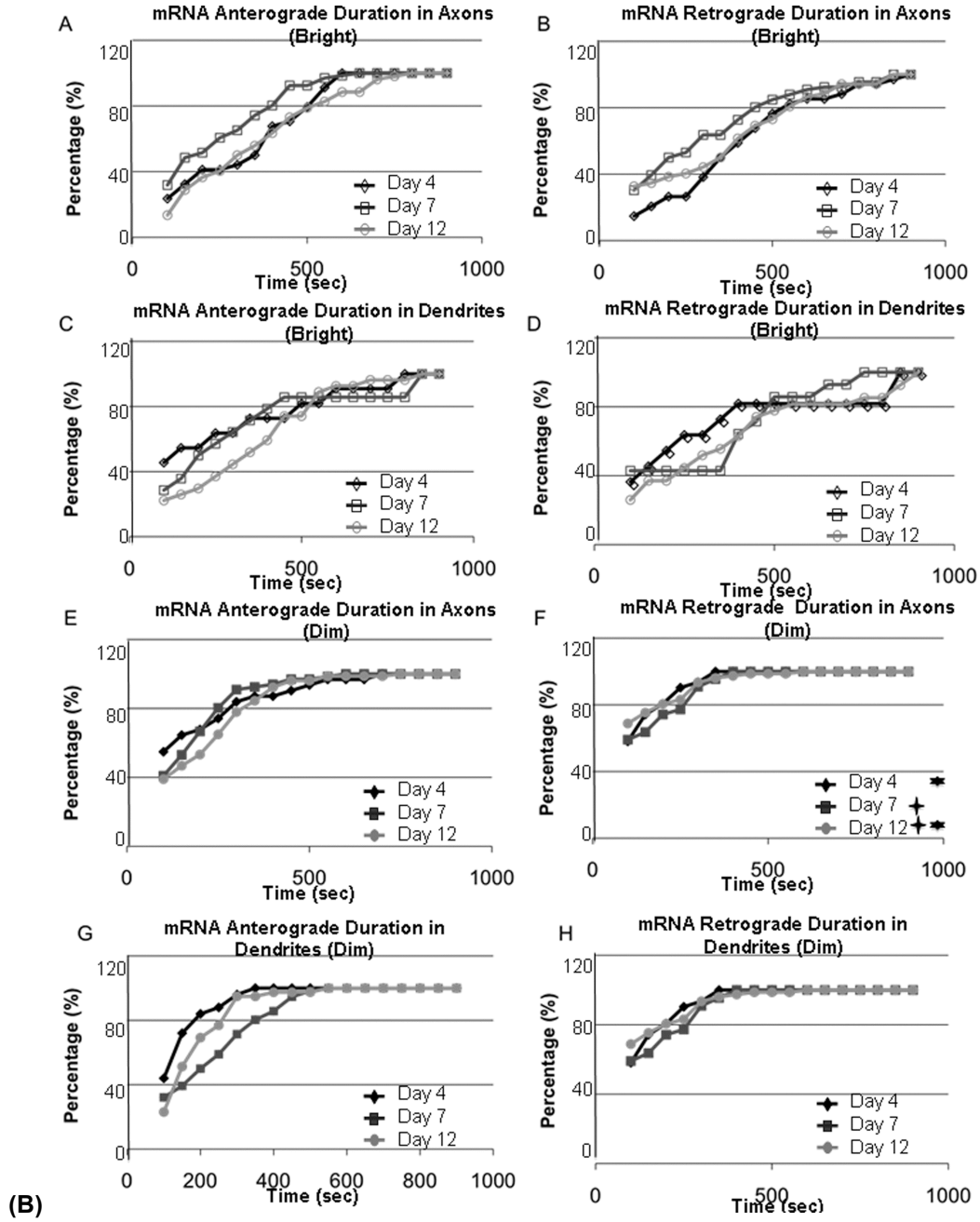

Figure 2-13: Distributions of track movement durations of mRNA in axons and dendrites were calculated from kymographs for days 4, 7, and 12. Only particles classified as moving were analyzed. Individual particle durations are presented as cumulative histograms. (A) Track durations of bright mRNA particles moving through axons in the anterograde direction. (B) Track durations of bright mRNA particles moving through axons in the retrograde direction. (C) Track durations of bright mRNA particles moving through dendrites in the anterograde direction. (D) Track durations of bright mRNA particles moving through dendrites in the retrograde direction. (E) Track durations of

dim mRNA particles moving through axons in the anterograde direction. (F) Track durations of dim mRNA particles moving through axons in the retrograde direction. Distributions were significantly different for days 4 vs. day 12 ($p < 0.03$, K-S test) and at day 7 vs. day 12 ($p < 0.04$, K-S test). (G) Track durations of dim mRNA particles moving along dendrites in the anterograde direction. (H) Track durations of dim mRNAs particles moving through dendrites in the retrograde direction.

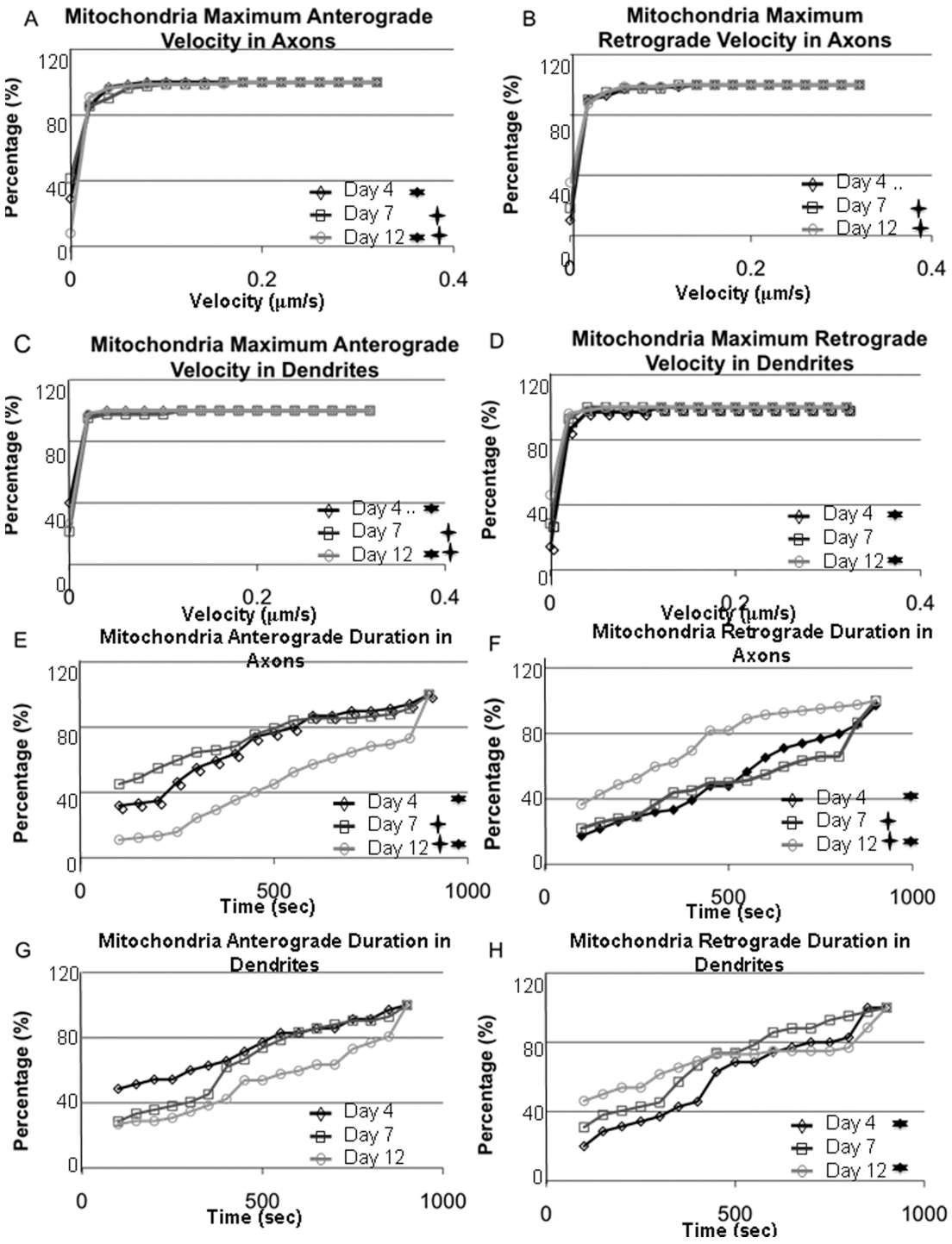

Figure 2-14: Maximum track velocities and movement durations of mitochondria in axons and dendrites were calculated from kymograph for days 4, 7, and 12, and are presented as cumulative histograms.

(A) Maximum track velocity of mitochondria moving through axons in the anterograde direction. Distributions of maximum mitochondrial velocities were significantly different at day 4 compared to day 12 ($p < 0.005$, K-S test), and at day 7 compared to day 12 ($p < 0.001$, K-S test). (B) Maximum track velocities of mitochondria moving through axons in the retrograde direction. Distributions of maximum mitochondrial velocities were significantly different at day 4 compared to day 7 ($p < 0.03$, K-S test), and at day 7 compared to day 12 ($p < 0.03$, K-S test). (C) Maximum track velocities of mitochondria moving through dendrites in the anterograde direction. Distributions of maximum mitochondrial velocities were significantly different at day 4 compared to day7 ($p < 0.02$, K-S test) at day 4 compared to day 12 ($p < 0.001$, K-S test) and at day 7 compared to day 12 ($p < 0.008$, K-S test). (D) Maximum track velocity of mitochondria moving through axons in the retrograde direction. Distributions of maximum mitochondrial velocities were significantly different at day 4 compared day 12 ($p < 0.02$, K-S test). (E) Track durations of mitochondria moving through axons in the anterograde direction. Distributions of durations were significantly different at day 4 compared to day 12 ($p < 0.0007$, K-S test), and at day 7 compared to day 12 ($p < 0.0001$, K-S test). (F) Track durations of mitochondria moving through axons in the retrograde direction. Distributions of durations were significantly different at day 4 compared to day 12 ($p < 0.0001$, K-S test) and at day 7 compared to day 12 ($p < 0.001$, K-S test). (G) Track durations of mitochondria moving through dendrites in the anterograde direction. (H) Track durations of mitochondria moving through dendrites in the retrograde direction. Distributions of durations were significantly different at day 4 compared to day 12 ($p < 0.02$, K-S test).

Maximum and average velocity: Maximum and average directional velocities of mRNA particles in axons and dendrites were measured at different stages of neuronal maturity. For bright mRNA particles, two-way ANOVA indicated no effect of the type of neurite, no effect of stage of maturity and no interaction effect on maximum or average anterograde velocity; however, significant effects of the type of neurite ($p < 0.005$), stage

of maturity ($p < 0.01$), and their interaction ($p < 0.0001$) were observed on maximum and average retrograde velocities (Table S1).

Several interesting features emerged when distributions of velocities were compared. (Similar conclusions were obtained for both maximum and average velocities; for clarity, we have only shown figures for distributions of maximum velocities). In axons, bright mRNA particles showed significant differences in the distribution of maximum velocities in the anterograde direction between days 7 and 12 ($p < 0.002$) and in the retrograde direction between days 4 and 7 ($p < 0.03$; Fig 12a-b). Anterograde particles in dendrites also showed a significant difference in the maximum velocity distributions at day 12 compared to day 4 (Fig 12c-d), associated with a leftward shift of the distribution (decreased velocities). As suggested by the strong rightward shift in their velocity distribution, dim particles were faster than bright particles ($p < 0.0001$, Fig 12a-d). Two-way ANOVA revealed a significant effect of the type of neurite ($p < 0.0013$), and stage of maturity ($p < 0.03$), but no interaction effect on dim anterograde mRNA velocity. There was no significant effect of type of neurite, stage of maturity, or their interaction on dim retrograde mRNA velocity. Comparisons of distributions of velocities also revealed no significant differences.

Directionality analysis: To generate additional perspective on the overall movement patterns of individual mRNA particles, they were classified into anterogradely moving, retrogradely moving, bidirectionally moving, or stationary populations. Within axons, most bright mRNA particles were mobile (at least 75% at all days). Concurrent with a decrease in the proportion of stationary particles, the proportion of directionally moving particles (either anterograde or retrograde) significantly increased between day 4

and day 7 (~35% vs. ~70%) before decreasing again to an intermediate value at day 12 (~50%). Though movement reflected an anterograde bias at all three days (Fig 6a), there were no significant differences in anterograde or retrograde populations across days. This general trend was mirrored in the dim pool of particles as well (Fig 10c). In this case, increases in the anterograde population between days 4 and 7 were balanced by a corresponding decrease in the retrograde pool.

In dendrites, most bright particles were also classified as mobile, with all particles moving by day 12 (Fig 10b). This correlated with significant differences in stationary mRNA particles detected between days 7 and 12. Significant differences in directionality were also observed with increasing dendritic maturity. The proportion of particles moving anterogradely increased steadily with time, with nonsignificant differences being detected between days 4 and 7 (Fig 10b; 0% and 25%, respectively) and significant differences being detected between days 4 day 12 (57%). In contrast, the proportion of particles moving retrogradely decreased steadily over time, though no significant differences were detected between any days. The anterograde bias was more pronounced in the dim pool of mRNA particles (Fig 10d), with ~70% of the particles moving anterogradely at days 4 and 7, and ~85% moving anterogradely at day 12.

Duration of directional movements: We also calculated the percentage of time that mRNA and mitochondria spent moving in each direction within axons and dendrites at each time point. Two-way ANOVA of dim mRNA particles detected effects of the type of neurite ($p < 0.009$), but no effect of maturity or interaction on anterograde and retrograde durations. For bright mRNA particles, analysis of distributions indicated a

trend towards longer durations in both anterograde and retrograde directions at later days in both axons and dendrites, though there were no significant differences in the distributions of the durations in either direction (Fig 12a-d). In contrast, dim particles did not show any trends towards increased duration at later days in axons or dendrites. In fact, anterograde durations in dendrites were actually slower at days 7 and 12 compared to day 4, with significant differences between day 4 and 7 ($p < 0.03$), and day 7 and 12 ($p < 0.04$) in the retrograde direction.

Net velocity: In order to extrapolate transport characteristics of individual mRNA particles to bulk transport at different stages of axonal and dendritic development, we estimated net velocities for specific classes of particles at a given stage of maturity. Net velocity calculations combined the individual characteristics of each particle into an aggregate measure of directional transport. Several interesting trends were observed. The net velocity of bright mRNA within axons was highest at day 7, at early stages of synapse maturity, but decreased sharply at day 12 (Fig 11a). In contrast, net velocity for bright particles moving within dendrites continued to increase through day 12, with significant difference between day 4 and day 12 ($p < 0.05$, Fig 11b). Net velocity attributed to dim mRNA particles revealed similar trends in axons; however, the velocities were two orders of magnitude higher (Fig 11c). In dendrites, net velocity was always positive, and experienced a slight decline at day 7 before rebounding at day 12 (Fig 11d).

To investigate the relative contributions of individual parameters to net velocity, and thus perhaps glean some insight into regulatory mechanisms, we performed multiple

linear regression analysis, with net velocity as the dependent variable and velocity and duration as independent variables. As reflected by their higher beta weights, velocities were for each group predominantly, though not exclusively, the dominant independent variable (Table 4). However, r^2 values were surprisingly low, given that the independent variables reflected parameters used to calculate net velocity (Table 4). This perhaps implies the importance of relative proportions of directionally moving particles, which could not be captured in regression analysis.

Table 2-4:Results comparing beta coefficients. Bold indicates dominant variable

Experiment	**Variable**	**Coefficient**	**R-squared**	**variable**	**coeff**
Mitochondria Axon	**Velocity**	0.18	0.04	duration	-0.047
Mitochondria Dendrites	**Velocity**	0.43	0.15	duration	0.15
mRNA Axon Bright	**Velocity**	0.75	0.58	duration	-0.02
mRNA Axon Dim	**Velocity**	0.52	0.21	duration	0.18
mRNA Dendrites Bright	**Velocity**	-0.34	0.11	duration	-0.001
mRNA Dendrites Dim	**Velocity**	0.54	0.22	duration	0.15

Subsection 3: Mitochondrial transport in dendrites and axons

Maximum and average velocity: For mitochondria, there was an effect of the type of neurite ($p < 0.02$), but no effects of the stage of maturity or interaction effect on maximum anterograde velocities. There were also no effects of the type of neurites, stage of maturity, or their interaction on velocities in the retrograde direction. When distributions were compared, in axons, mitochondria revealed significant differences in

their maximum velocity between days 4 and 12, and days 7 and 12 in both anterograde and retrograde directions (Fig 14a-b). In dendrites, mitochondria also showed significant differences in the maximum anterograde velocity among all three days. However, in the retrograde direction, significant differences were only found between days 4 and 12 (Fig 14c-d). Though significant, differences in the distributions in both axons and dendrites appear subtle visually, and likely reflect differences in the percentage of mitochondria moving at the slowest velocities (left-most bin).

Directionality analysis: Mitochondria displayed a different movement profile than mRNA. In general, mitochondria were less mobile in axons, though there were more moving particles at day 7 (76%) compared to days 4 and 12 (63% and 55%, respectively). Of the unidirectionally moving particles, there were more retrograde particles than anterograde particles at days 4 and 7. Significant differences within a particular population were only found between days 4 and 7; more particles moved anterogradely at day 7 compared to day 4 ($p< 0.05$), concurrent with a reduction in "wiggling" bidirectional particles ($p<0.02$; Fig 15a).

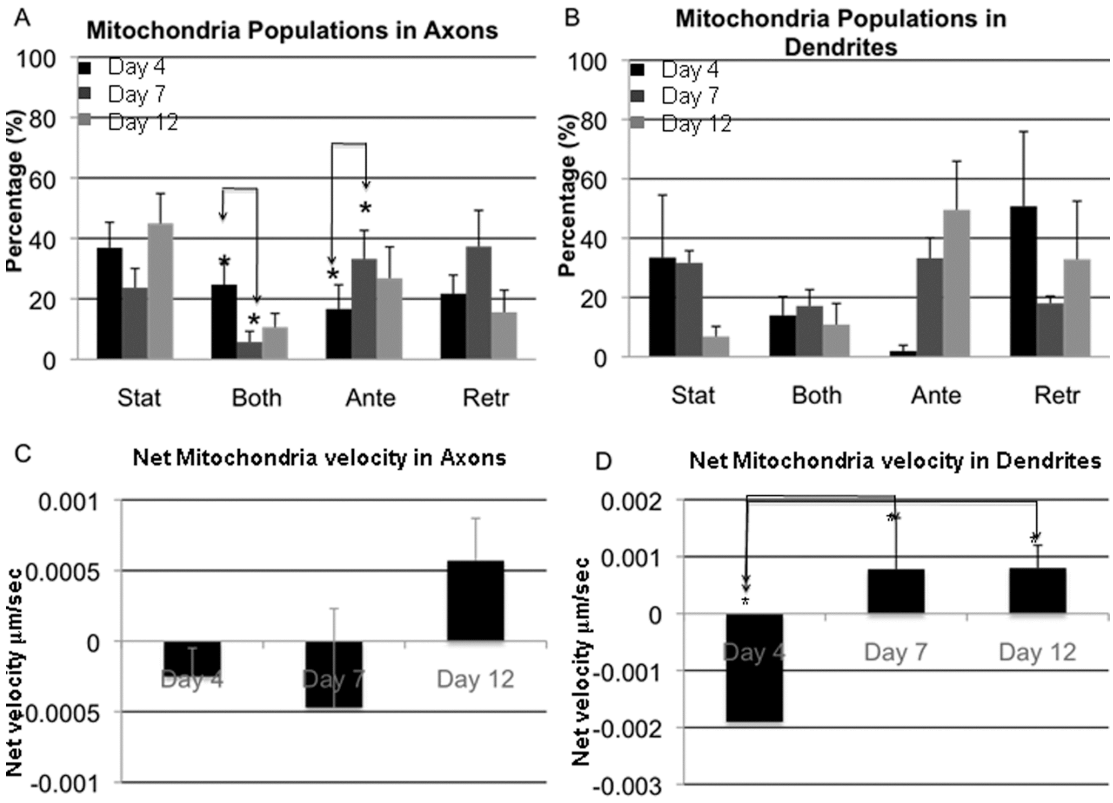

Figure 2-15: Net directionality of mitochondria particle movement over its lifetime.

Particles were considered moving if their average velocity in either direction was greater than 0.001 µm/sec (0.1mm/day). Particles that did not meet this criterion were designated stationary. (A) Percent of mitochondria in axons in each state for days 4, 7, and 12. There are significantly more particles moving in anterograde direction at day 7 compared to day 4 *p<0.05 (ANOVA: Tukey). (B) Percent of mitochondria in dendrites in each state for days 4, 7, and 12. Average net velocity of individual mitochondria particles in axons and dendrites. (C) Average of net mitochondrial velocity moving through axons (D) Average of net mitochondrial velocity moving through dendrites. The net velocity is higher at day 7 compared to day 4 (p< 0.05) and at day 12 vs. day 4 (p<0.05; ANOVA:Tukey). Plotted values indicate mean ± SEM.

In dendrites, there were no significant differences found. However, as was the case for mRNA, there was a strong trend towards increased anterograde mitochondrial transport over time. Between days 4 and 7, this increase occurred concurrently with a

decrease in retrograde particles. Between days 7 and 12, both anterograde and retrograde populations increased as stationary populations decreased.

Duration of directional movements: Mitochondria, like bright mRNA, increased their duration of anterograde movement in both axons and dendrites at later stages of development. Significant differences in the distributions of anterograde durations were found for days 4 vs. 12 ($p < 0.0007$), and between days 7 and 12 ($p < 0.0001$) in axons. No significant differences were found in the dendrites. Unlike mRNA, though, in the retrograde direction, distributions of durations of moving mitochondrial mRNA particles differed in axons, with a leftward shift (shorter) at later time points (4 vs. 12, $p < 0.0001$, and 7 vs. 12 $p < 0.001$), and in dendrites between days 4 and 12 ($p < 0.02$).

Net velocity: The net velocity of mitochondria illustrated a different pattern from mRNA. In axons, net velocity was retrograde at days 4 and 7, before increasing anterogradely at day 12 (Fig 15c). Net velocity also increased over time in dendrites, though in this case a retrograde net velocity was observed at day 4 before changing direction and increasing in magnitude at days 7 and 12, resulting in significant differences among all three days (Fig 15d).

Section 4: Discussion

This work exploited high-resolution imaging, image-processing, and analytical tools to generate a comprehensive quantitative assessment of mRNA transport in axons and dendrites of cultured hippocampal neurons at different stages of maturity. This quantitative approach enabled us to extend previous literature on mRNA transport through the identification and characterization of two distinct classes of non-

mitochondrial mRNA, which appear to differ in mRNA content as well as transport characteristics. Our data also indicated interesting differences between mRNA transport in axons and dendrites, enabling us to propose intriguing hypotheses regarding varying roles for mRNA transport in neurites of different polarity and physiological function. These results provide a baseline for future work to uncover mechanisms involved in the coupling of mRNA transport to local translation.

Though the emphasis of this work was to provide new insights on mRNA transport, our concurrent analysis of mitochondria served multiple purposes. First, co-labeling mitochondria enabled us to distinguish between mitochondrial and non-mitochondrial mRNA, allowing greater clarity in interpreting previous studies that used general mRNA markers. Second, the fact that transport profiles of mRNA were distinct from those of mitochondria provided internal validation for the absence of global effects such as toxicity or changes in cellular geometry that would identically influence all cargoes. Third, we were able to confirm and extend previous quantitative analyses of mitochondrial transport in our cultured rat hippocampal model. Results and discussion pertinent to analysis of mitochondrial transport are presented as supplementary material (Fig 14 and 15).

Subsection 1: Transport profiles differ in bright versus dim populations of mRNA

Several research groups have studied the axonal and dendritic distributions of mRNA and local protein synthetic machinery [69,70,71]. However, details on the role of transport in achieving these distributions are less prevalent. Our quantitative characterization of mRNA transport builds on literature that has examined various aspects of neuronal mRNA transport, both qualitatively and quantitatively.

Brightly fluorescent particles of slowly moving mRNA exist in both axons and dendrites, and appear qualitatively similar to puncta identified as mRNA granules in previous studies on mRNA localization and transport [68,72,73]. Net axonal and dendritic velocities, measured within a 15 minute imaging window and extrapolated to longer time periods, are consistent with slow bulk axonal transport (0.1-1mm/day), and in agreement with previous measurements of 0.5mm/day reported in dendrites in radiolabel pulse-chase experiments [74]. Maximum velocities, both anterogradely and retrogadely, are slightly lower in axons (0.03-0.06μm/sec), but agree exactly in dendrites (~0.09-0.11μm/sec) with the value of 0.1μm/sec provided for motile mRNA granules in cortical neurites of unspecified polarity [68]. Minor differences in these values may result from developmental or physiological differences between our P1 neonatal hippocampal and published E18 cortical neurites. However, the likeliest source of discrepancy is the cutoff used to distinguish between stationary and motile puncta. With respect to the latter, our inclusion of particles with slow, but significant velocities at or above 0.001μm/sec could have lowered the average rate of transport compared to values previously reported [68].

The observation of a weakly fluorescent pool of rapidly moving mRNA was novel and surprising. Net velocities for dim particles were over two orders of magnitude higher than for bright particles. However, the weaker fluorescence implies a smaller quantity of mRNA, offsetting this apparent increase in net transport. Differences in fluorescence intensity and transport parameters suggest different modes of packaging and regulation of transport as well as possible differences in function.

Because of the slow average velocities and our relatively low frame rate, it is not possible to infer the identity of motor proteins responsible for movement in either bright

or dim pools of mRNA. However, cell biological and biochemical studies have identified RNA granule association with KIF5 (kinesin-1) and KIF3 (kinesin-2) in dendrites, KIF3C in axons, and kinesin-1 and dynein in Drosophila S2 cells [75,76,77,78,79]. A role for microtubule-dependent motor proteins in transporting mRNA is also consistent with reductions in mRNA localization within neurites following microtubule destabilization with colchicine [68,80]. mRNA may also piggyback on ribosomes or other cargoes with which it has been reported to co-localize, including cytoskeletal elements such as actin [16,77,81].

Varying functional roles for bright and dim particles can also not be inferred from our analysis. However, based on the increased mobility of this dim pool, one intriguing hypothesis is that dim particles reflect a pool of specific transcripts quickly recruited in response to an unexpected stimulus, such as injury, the termination of axonal outgrowth, or synaptic activity. This hypothesis is consistent with the trafficking of Arc mRNA, which encodes a protein believed to be involved in the maintenance of LTP. Synaptic activity triggers the transport of Arc mRNA to activated synaptic sites [82], and it accumulates near stimulated synapses on a time course that coincides with the duration of protein synthesis during LTP [83]. Such a role would contrast with a more general role for maintenance of cellular infrastructure during growth and homeostasis, which could be reflected in the larger, slower granules. Such posited differences are conceptually similar to differences in mitochondrial populations, which are often stationary along the axon, but are more mobile when recruited to areas of high demand, such as an extending growth cone (Miller and Sheetz, 2006). An alternate hypothesis is that larger, brighter particles represent a multicomponent granular complex, while dim particles represent

particles that are not yet incorporated into a substantial protein synthetic complex or smaller, more specialized translational entities. These hypotheses should be addressed in future studies that elucidate the identity of specific transcripts and components of the translational machinery that are transported in each pool.

Subsection 2: mRNA transport profiles differ in axons and dendrites

We identified several interesting differences in mRNA transport between axons and dendrites at varying stages of neurite maturity, in both bright and dim populations. Net velocities within a given neurite represent the combined influences of run velocities, net directionality, and the duration of movement of individual particles; thus, it was possible to identify the particular parameter or parameters responsible for any differences across experimental groups. For bright particles in axons, net velocities peaked at day 7 before falling again at day 12. This net positive effect stemmed primarily from increased velocity and an increased proportion of anterogradely moving particles on day 7 compared to days 4 and 12 (Fig. 12a and Fig. 13a). The subsequent reduction in net anterograde velocity at day 12 resulted from a slight decrease in anterograde velocity and an increase in stationary particles, at the expense of particles moving both anterogradely and retrogradely. These transport patterns were different from those of bright mRNA particles in dendrites, where net velocities were an order of magnitude smaller than in axons, and were retrograde at day 4 before changing directionality by day 12. This pattern was a result of a sharp transition from a predominantly retrograde pool of moving particles at day 4 to an anterograde pool by day 12 (Fig 10b). In contrast to bright particles, dim particles had comparable net velocities in both axons and dendrites that were up to two orders of magnitude higher than those of bright particles in either type of

neurite. Also in contrast to bright particles, the net velocities of dim particles increased dramatically between day 4 and 7 (Fig 11c), coinciding with the timeline for synapse formation and stabilization (Fig 1).

In comparing transport timelines in axons versus dendrites, the relative increase in net axonal mRNA velocity at an earlier time point compared to dendrites supports a model where local translation initially contributes to synapse stabilization *pre-synaptically*. Indeed, the observed increase in the net axonal velocity of bright and dim mRNA particles at day 7 coincides with the end stages of neurite outgrowth and the initial stages of synapse formation and stabilization (Fig 1, [64,65]). Such a timeline is also consistent with reported relationships between local translation and the effectiveness of neurotrophic signaling both during axonal outgrowth and pre-synaptic signaling [84,85]. Most notably, protein synthesis in both the axon and dendrites is required for effective axonal guidance by brain-derived neurotrophic factor (BDNF) and neurotrophin-3 (NT-3) [4,86]. Neurotrophins may also initiate early stages of synaptic strengthening, as axonally synthesized BDNF has been implicated in potentiating transmitter secretion from nearby synapses [4].

In contrast, net dendritic velocities of bright, slow mRNA particles illustrated a linear relationship between net velocities and the maturity of neurons, with the highest reported net velocities at day 12 coinciding with an increased duration of synaptic contact (Fig 11). Increased and sustained dendritic mRNA transport at later time points is consistent with a role for local protein synthesis in the context of sustained synaptic connectivity for LTP, consolidation of long-term memory, and immunity versus long-term depression [4,17,41,61,83,87,88,89,90]. Several locally synthesized proteins

relevant for such synaptic plasticity are candidates to be found in observed dendritic mRNA pools, including αCAMKII [91] and cytoplasmic polyadenylation element binding protein (CPEB), which upon increased translation, through its long-lasting transmissible conformation, serves to provide a "memory" of the synaptic stimulation [92].

Subsection 3: Mitochondrial transport profiles in axons and dendrites

Mitochondrial transport has been characterized extensively in neurons of both the PNS and CNS. The bulk of this work has been performed in chick sympathetic neurons (e.g., [93,94]), though at least two papers [66,95] have quantified mitochondrial transport in rat hippocampal neurons, and further, axons and dendrites. Consistent with these studies [66,95,96], we observed that individual mitochondria moved with both anterograde and retrograde net directionality in axons and dendrites. The total percentage of directionally moving mitochondria (Fig 14 a-d) was not significantly different in axons and dendrites, and slightly higher than the 20-40% previously observed [66,95,96], though this difference may be a result of our slightly lower cutoff for stationary particles (0.001μm/sec vs. 0.01 μm/sec). In axons, we observed that mitochondria initially demonstrated a slight retrograde net velocity at early stages of growth and synapse formation (days 4 and 7), and an increase in anterograde net velocity as neurons further matured (day 12). These changes were primarily a result of changes in the duration spent moving in a particular direction, rather than differences in the velocity or directionality of individual particles (Fig 14 e,f). In dendrites, mitochondria also displayed a slight retrograde net velocity at day 4 before reversing to a net anterograde velocity at days 7

and 12. In this case, however, differences were a consequence of differing directionalities of individual particles across days (Fig 15d).

The observed differences in mitochondrial transport at varying stages of axonal and dendritic maturity are consistent with previous suggestions that mitochondrial movement is dependent on both the stage of growth and position within a neurite [66,94,95,96]. The specific pattern, though, appears to be heavily dependent on energetic requirements within a particular experimental model. For example, our observed increase in anterograde transport with developmental maturity is opposite to that observed in sympathetic neurons [93,94], which showed net anterograde mitochondrial transport in growing axons, but net retrograde transport in halted axons. This could reflect mitochondrial recruitment for synaptic activity and cytoskeletal stabilization in stationary CNS neurites (Fig 1; [97,98]) but the lack of such recruitment in axons whose growth is truncated by a non-physiological barrier [94]. Mitochondrial transport is also likely to depend heavily on the localization of existing pools of mitochondria. For example, in PNS axons, the highest levels of directional movement occur in regions away from the growth cone [93,94], while a large pool of mitochondria already localizes to the distal axon and growth cone [94]. This is in contrast to our observations of mitochondria more or less evenly distributed along the axon.

Section 5: Conclusions

This work provides the first rigorous quantitative assessment of axonal and dendritic mRNA transport during central neuronal development. Significant differences

in transport parameters for individual and pooled particles at different stages of neuronal maturity emphasize the dynamic nature of transport at multiple levels. As suggested for other cargoes, including mitochondria [24,26,45,55,94,99], the dynamics of mRNA transport are likely to be driven by the functional demands of the cell. Future studies will uncover mechanisms initiating and regulating changes in mRNA transport as well as the identity of specific classes of transcripts that are subject to such regulation. Additionally, datasets of multiple mRNA and mitochondria transport parameters that we generated in this study will be essential for validating theoretical models of neuronal mRNA or mitochondrial transport. It is our belief that multi-disciplinary approaches spanning the computational and biological realms will yield tremendous progress in understanding pathways of local translation and its regulation in neuronal development, disease, and injury.

Section 6: Methods

Ethics statement: All animal protocols were approved by University of Maryland Institutional Animal Care and Use Committee (IACUC).

Primary cell culture

Hippocampi were dissected from one-day-old Sprague-Dawley rats and maintained in ice-cold HBSS (2) media (HBSS 500 mL, D glucose .4g, HEPES .834g, Penicillin 15 mL). They were then incubated with 0.05% DNase (1.4 M $MgSO_4$, HBSS 100 %) and Mixture A (PBS 100%, DL-Cysteine HCL 1.6mM, BSA 3.7μM, D-glucose 34.6 mM,

Papin 21μM) for 30 minutes at 37°C under agitation at 100 rpm. Following trituration, cells were pelleted at 234 × g for 3 minutes before resuspension in growth media (Neurobasal media supplemented with 2% B-27). Finally, cells were plated on coverslips coated with 1mg/ml polylysine at a density of 20,000 cells in 500 μL. All cells were maintained and imaged at 37°C and 5% Co2.

Immunofluorescence

Hippocampal cells were fixed with 4% paraformaldehyde in PBS for 10 minutes and rinsed with PBS three times. Following permeabilization with 0.2% Triton X-100 in PBS, the cells were blocked with 10% Fetal goat serum and 3 % BSA for 30 minutes. A 1:1000 dilution of SMI-31 (Abcam Inc., Cambridge, MA), 1:500 dilution of MAP2 (Abcam Inc., Cambridge, MA), or 1:200 dilution of Synapsin I (Sigma-Aldrich Corp., St. Louis, MO) in BSA was applied for an hour at room temperature, followed by three washes in PBS. Fluorescently labeled secondary antibody was applied subsequently for 1 hr at 37°C, followed again by three washes in PBS. Finally, coverslips were mounted on a slide in the presence of Vectashield (Vector Laboratories, Inc., Burlingame, CA). For co-labeling with RNA, cells were incubated with 500nM of Syto after application of the secondary antibody.

mRNA and mitochondrial labeling

For mRNA labeling, 500 nM solution of RNASelect green fluorescent cell stain (Syto, Excitation 490 nm, Emission 530 nm) in cell media was prepared. This solution was pre-warmed at 37°C prior to application and used immediately. The cells were incubated with

500μL of the 500 nM labeling solution for 20 minutes at 37°C. After this, cells were rinsed once with cell-culture medium. Mitochondria (Excitation 579nm, Emission 599 nm) were labeled by incubating dissociated neurons in a 1:10,000 dilution of mitochondrial dye, MitoTracker Red for 10 minutes at 37°C, followed by rinsing with the cell-culture media. The neurons were labeled on days 4,7, and 12. The imaging was performed immediately after application of the probes.

Fluorescence Microscopy

Imaging was performed on an inverted TE-2000E microscope (Nikon, Melville, NY) outfitted with a Lumen-PRO2000 (Prior Scientific, Rockland, MA) illumination system and Chroma filters (Bellows Falls, VT. EPI: 488 nm, Emission 530 nm). Additionally, a custom built chamber (Precision Plastics, Beltsville, MD) maintained temperature, humidity, and CO2 levels during imaging. DIC and Fluorescence images were captured for 15 minutes every 15 seconds using a 40x objective with 200ms exposure time. DIC, Syto RNA (490nm excitation), and Mitotracker (570nm excitation) channels were captured at the same time point, sequentially within 1-2 seconds, accounting for filter changes.

RNase Treatment

After incubation with Syto, imaging and live imaging was performed as mentioned. Then, cells were fixed with 4% paraformaldehyde for 10 min. After fixation, cells were permeabilized with 0.5% Triton X-100 for 5 min and incubated with RNase A 10 μg/ml

in Tris-buffered solution and for 1 hr at 37°C. A second image was taken of the labeled cell, and the intensities of the two signals were compared.

Image Analysis:

Image analysis was performed either on MATLAB (MathWorks, Natick, MA) or ImageJ (NIH). To analyze the movement of mitochondria and mRNA particles in the axon over time, a custom program was used to create kymographs from time lapse movies as previous described [100]. Trajectories of mRNA particles that did not overlap with those of MitoTracker were concluded to be mRNA particles. The likelihood of a false positive (i.e., a mitochondrial particle that was mistakenly identified as a non-mitochondrial particle) was very low, owing to the considerably brighter fluorescence intensity of MitoTracker compared to Syto. mRNA particles from non-mitochondrial mRNA particles were analyzed separately. A series of image processing steps was performed to confirm and better visualize dim mRNA particles (Fig S3). First, the kymograph of interest was processed by iteratively overlaying 300 images of the same kymograph, which were made 50% transparent (Gnu Image Manipulation Program, http://www.gimp.org). Each overlay resulted in a slight increase in signal to noise ratio, allowing enhancement of dim signals. The resulting kymograph was then contrast enhanced or inverted to visualize the dim mRNA moving particle (ImageJ). Finally, local contrast enhancement was performed on each particle. Contrast enhancement with a similar mask was performed on both regions of interest (ROI) and non-ROI regions, to ascertain that local contrast enhancement did not result in a false positive particle.

Data Analysis:

For directionality analyses, the following sample sizes (numbers of neurons) for each category were used; bright mRNA particles in axons: day 4: N= 11, day 7: N = 10, day 12: N = 11; bright mRNA particles in dendrites: day 4: N = 4, day 7: N = 5, day 12: N = 6; dim mRNA particles in axons: day 4: N = 5, day 7: N = 8, day 12: N = 11; dim mRNA particles in dendrites: day 4: N = 3, day 7: N = 5, day 12: N = 6; mitochondria in axons: day 4: N = 11, day 7: N = 10, day 12: N= 11; and mitochondria in dendrites: day 4: N = 4, day 7 N = 4, day 12: N = 6.

In addition, for net velocity, velocity, and distribution analyses, following sample sizes (number of particles) for each category were used: bright mRNA particles in axons: day 4: N = 34, day 7: N = 53, day 12: N = 52; bright mRNA particles in dendrites: day 4: N =11, day 7: N = 14, day 7: N = 27; dim mRNA particles in axons: day 4: N = 31, day 7: N = 66, day 12: N = 77; dim mRNA particles in dendrites: day 4: N = 25, day 7: N = 56, day 12: N = 39; mitochondria in axons: day 4: N = 69, day 7: N= 82, day 12: N = 88; mitochondria in dendrites: day 4: N = 35, day 7: N = 42, day 12: N = 52.

Maximum and average velocity:

Particles with an average velocity of greater than 0.001μm/sec in either direction (0.1mm/day) were classified as moving, based on minimum velocities measured in a previous study [74]. Moving particles were segregated and further analyzed. The maximum velocity in each direction for each particle was calculated. In addition, the average instantaneous velocity in each direction for particles was calculated.

Directionality Analysis:

Particles not scored as moving, as defined above, were considered stationary. Most moving particles spent the majority of their time (>80%) moving unidirectionally; however, a small fraction of particles changed directions multiple times during a trajectory. These wiggling particles were classified as moving bidirectionally if their net displacement was less than 0.001 μm.

Duration of directional movement:

Only particles considered moving, as defined above, were analyzed for this parameter. The cumulative duration that each particle moved during its entire trajectory was calculated for both the anterograde and retrograde direction.

Net Velocity:

The net velocity for each particle was calculated using the equation below.

$$\text{Net Velocity} = \left\langle \frac{\left[\left(v_a \times T_a\right) + \left(v_r \times T_r\right)\right]}{TotalTime} \right\rangle$$

where v_a = average anterograde velocity, v_r = average retrograde velocity, T_a = Time spent in the anterograde direction, T_r = Time spent in the retrograde direction. Graphs of the net velocities were obtained by averaging all particles from all neurites.

Statistics:

Means were compared using ANOVA followed by Tukey's post hoc analysis. Distributions were compared using Kolmogrov-Smirnov Test. We have also performed multiple regressions, with net velocity as the dependent variable and velocity and duration as independent variables. All statistical analysis was performed using SAS software (Cary, NC).

Chapter 3: Mouse whole hippocampal explant culture system to study isolated axons

Section 1: Abstract

We have developed a novel mouse neonate whole-hippocampus explant culture system to study central neuronal survival and axonal gene and protein expression in the context of regeneration. The explant culture system enables axon-specific measurements without the need of additional equipment. In this report, we detail our validation of this model, and implement it to characterize axonal outgrowth following initial explant harvest and a secondary axonal injury. We also compare the advantages and limitations of this model with existing models.

Section 2: Introduction

Damaged axons of the central nervous system (CNS) regenerate poorly, for reasons that are still being understood. Current studies have probed numerous outcomes in the context of regeneration, including neuronal survival, gene expression, alterations in the mechanical and chemical environments, and axonal outgrowth [101,102,103]. Despite this progress, though, due to their unique size and polarity, it is often necessary to examine the response of axons independently of their cell bodies.

Several experimental systems have been developed to spatially separate cell bodies and axons, to measure of a variety of axon-specific outcomes. A number of studies detail devices that physical separate axons and somata of cultured cells, allowing

incubation of each region in distinct cellular media [104,105,106]. These include larger Campenot chambers as well as micropatterned and microfluidic compartmental culture systems [21,105,106,107]. Microfluidic methods range from producing a PDMS stamp to pattern compartmentalized micro-channels on a glass cover slide [108,109,110,111] to fluid compartmentalization by hydrostatic pressure gradients [21]. These methods have been well-validated for examining peripheral neurons. Although some reports have demonstrated successful use with central neurons [21], shorter axonal processes in the CNS make their use more challenging. From a practical standpoint, despite their efficacy, fabrication and troubleshooting of these systems may be complex, fabricated devices may not be reusable, and additional effort may be required to maintain sterility.

Explant cultures in the absence of compartmentalization have also been used when tissue integrity and connectivity, physical and functional, is desired, but fluidic isolation of axons and cell bodies is not necessarily required [112]. Explants allow manipulation of intact tissues in highly controlled settings, and include whole explant tissue, slice, and fragments of tissue [112,113,114]. Whole explant culture systems, extensively deployed for PNS and spinal hemi-cord models [115,116] are convenient and more completely preserve structural and functional connectivity compared to slice and fragmented culture systems. While a novel Drosophila brain culture system was recently introduced to study axonal regeneration of lesioned neurons [117], in general, whole brain explants have been underutilized, likely due to limitations in gas and nutrient exchange. We have developed a mouse neonate whole-hippocampus explant culture system to study central neuronal survival and axonal gene and protein expression in the context of regeneration. In this report, we detail our validation of this model, and its

implementation to characterize axonal outgrowth following initial explant harvest and a secondary axonal injury. We also compare the advantages and limitations of this model with existing models

Section 3: Results

Subsection 1: Whole explant culture system enables pure isolation of axons

We harvested and cultured whole mouse hippocampal explants for seven days on either plastic culture dishes or on glass cover slips, with the lateral explant surface face-up. A ~0.4 mm ring of migrating cells emerged from the explant periphery, beyond which long projections extended over a distance of several millimeters. We confirmed that these projections were axons by co-labeling phosphorylated neurofilaments (SMI-31, axonal marker) and MAP2A (dendritic marker) (Fig 1c). This labeling also confirmed structural integrity within the explant itself as well as appropriate morphology of cells within and beyond the explant (Fig 1c-e).

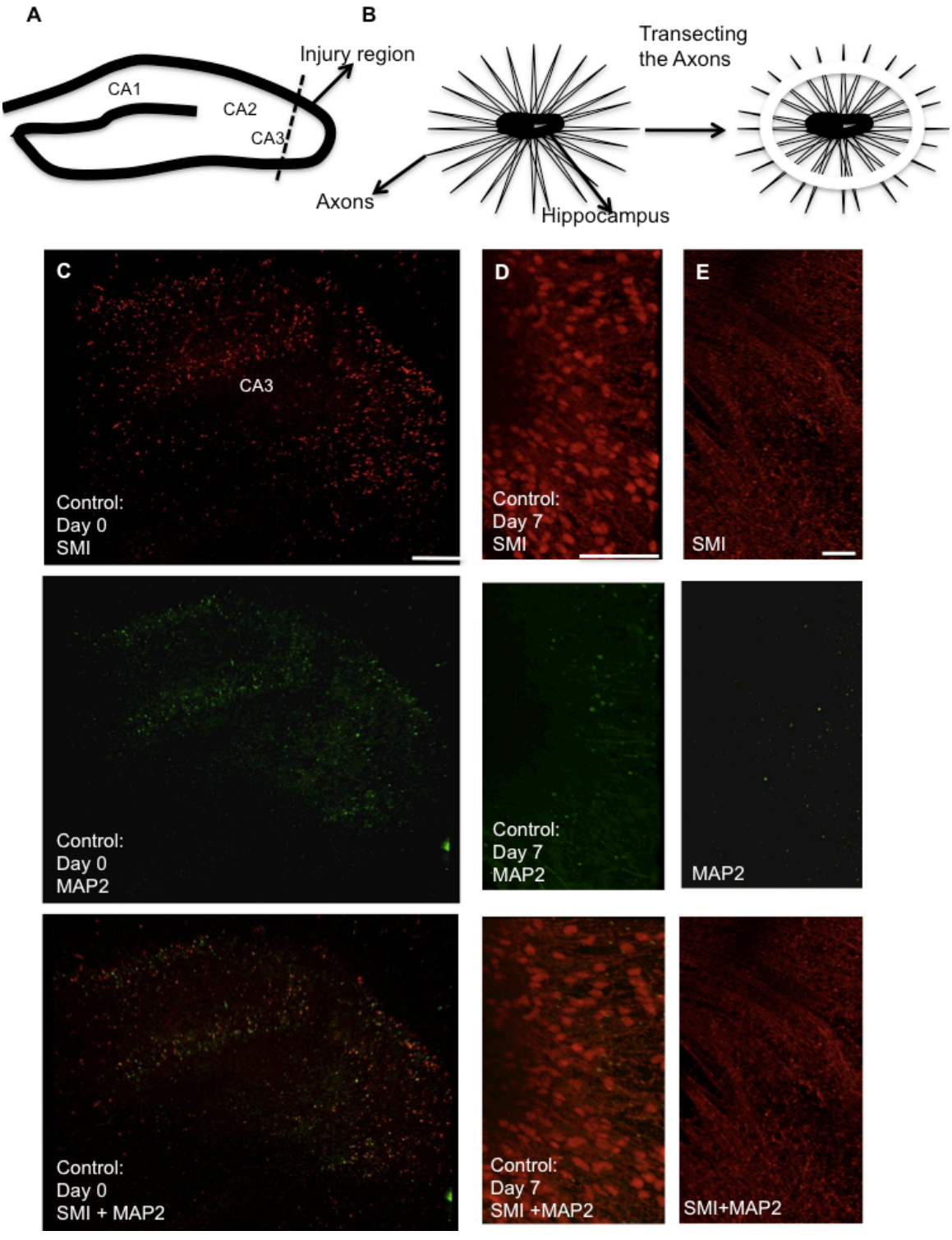
A
B
Injury region
CA1
CA2
CA3
Transecting
the Axons
Axons
Hippocampus
C
CA3
Control:
Day 0
SMI
D
Control:
Day 7
SMI
E
SMI
Control:
Day 0
MAP2
Control:
Day 7
MAP2
MAP2
Control:
Day 0
SMI + MAP2
Control:
Day 7
SMI +MAP2
SMI+MAP2

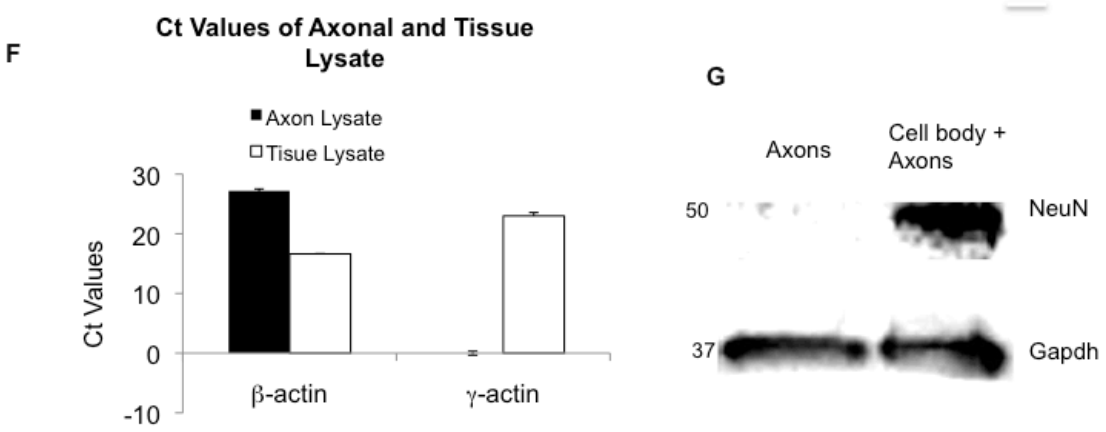

Figure 3-1: Illustration of explant and tissue injury and purity of axons.

(A) Schematic overview of tissue injury to the CA3 region of hippocampus explants. (B) Schematic presentation of axonal injury with a needle, injury was performed 2/3 distance away from the edge of the explant. (C) Panel shows CA3 region of the uninjured explant with axonal marker (SMI), dendritic marker (MAP2), and overlay of both (SMI and MAP2) respectively from top to bottom. (D) Panel shows undamaged CA3 region of hippocampus explant after 7 days in culture with axonal marker (SMI), dendritic marker (MAP2), and overlay of both (SMI and MAP2), showing regions of cell bodies. (E) Panel shows pure axonal region of hippocampus explant after 7 days in culture with axonal marker (SMI), dendritic marker (MAP2), and overlay of both (SMI and MAP2), with no dendritic region (green). RT-PCR and Immunoblots were performed to ascertain exclusive nature of axonal preparation (F) RT-PCR confirms presence of β-actin and absence of γ-acting values (there were some samples with Ct values of >37) in axonal culture and presence of both genes in the tissue lysate. (G) Immunoblots illustrate presence of Neun in positive control (cell body + Axon preparation), and absence of Neun in axonal preparations, whereas GAPDH is present on both the axon and positive control samples. Values represent means ± SEM. Bar is 75μm.

To further assess the exclusive axonal nature of the preparation, as well as test the feasibility and utility of our system to perform gene expression and biochemical assays

on axonal fractions, we performed PCR and Western blot analysis on collected axons and whole explant homogenate. We first compared levels of γ–actin mRNA, which resides only in the cell soma but is restricted from axons [118,119,120], between axon and explant fractions via RT-PCR (Fig 1f). We also compared levels of β-actin mRNA, which is found both in the axon and cell body (Fig 1f). As expected, the results indicate high γ-actin transcript levels in explant fractions, and no γ-actin levels in the axonal population, demonstrating the purity of hippocampal axonal preparation. High β-actin gene levels were found, though at differing levels, in both fractions, confirming our ability to measure and compare gene expression. We then performed Western blot analysis on the isolated axon population, probing for protein levels of a neuronal specific nuclear protein (Neun), which is only found in cell bodies and not in the processes. Consistent with immunolabeling and PCR results, Western-blotting results indicated presence of Neun in the whole lysate, but not in the axonal preparation (Fig 1g). Collectively, these results indicate that isolated axonal processes were not contaminated with protein from neuronal cell bodies.

We then tested the amenability of explant cells to transfection. We lipid-transfected cells with a plasmid encoding soluble GFP tagged with a nuclear localization signal. Numerous fluorescent cells were observed for each label within and beyond the explant (Fig 2a), and a live-dead assay confirmed high cell viability, even following transfection (Fig 2b).

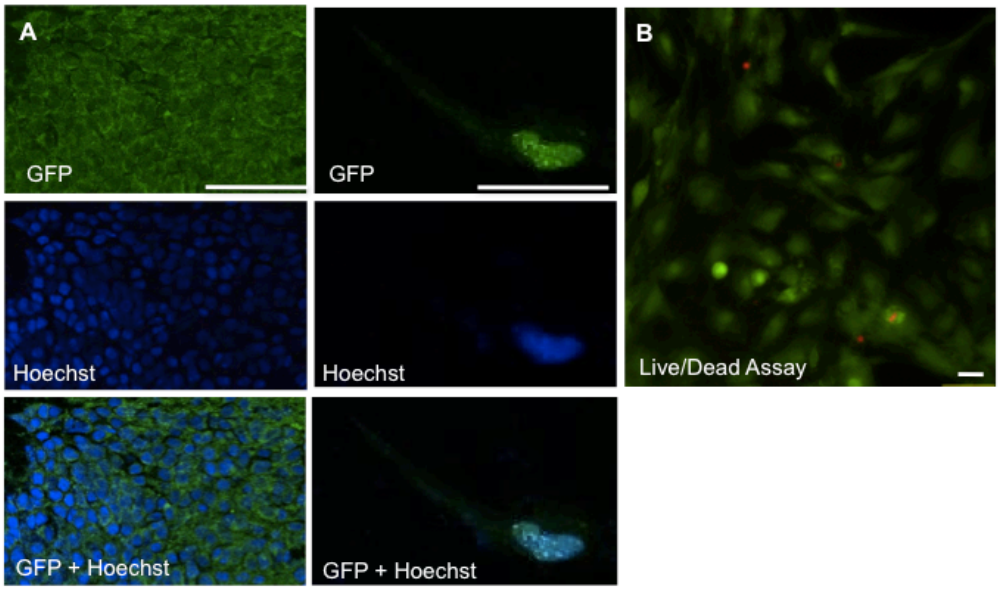

Figure 3-2: Illustrates transfection as well as viability of the cells after 7 days in culture.

(A) Panel shows transfected cells (NFAT-GFP, green) as well as stained nuclear dye(Hoechst, blue), last panel is overlay of both. Two parallel panels showing multiple and single cell transfected. (B) Imaging after live/dead assay show presence of live cells (green). Bar is 75μm.

Subsection 2: Use of hippocampal explant model to examine axonal response to injury

Having validated axonal purity and cell viability, we next used our explant system to probe axonal response to two different types of injury. First, we crushed the presumed CA3 region of the explant at the time of culturing, simulating a traumatic injury to a region particularly affected by traumatic brain injury (Fig 3a). We observed the axon growth of the damaged and undamaged tissue for six days (Fig 3b,d). The axons from damaged tissue lagged in their initial growth rate but extended at a faster rate at later days compared to the control (Fig 3d). Two-way ANOVA (grouping factors: injury, time)

revealed an interaction between injury and time ($p<0.02$) as well as a significant effect of time ($p<0.0001$) on growth rate. We then probed outgrowth of axons after transecting axons projecting from explants that were and were not crushed (Fig 3c,e,f). Two-way ANOVA revealed no effect of crush or axonal transection on instantaneous velocity. However, there was a significant difference between the distributions of the instantaneous velocities of untransected damaged and undamaged tissue (K-S test, $p <0.002$).

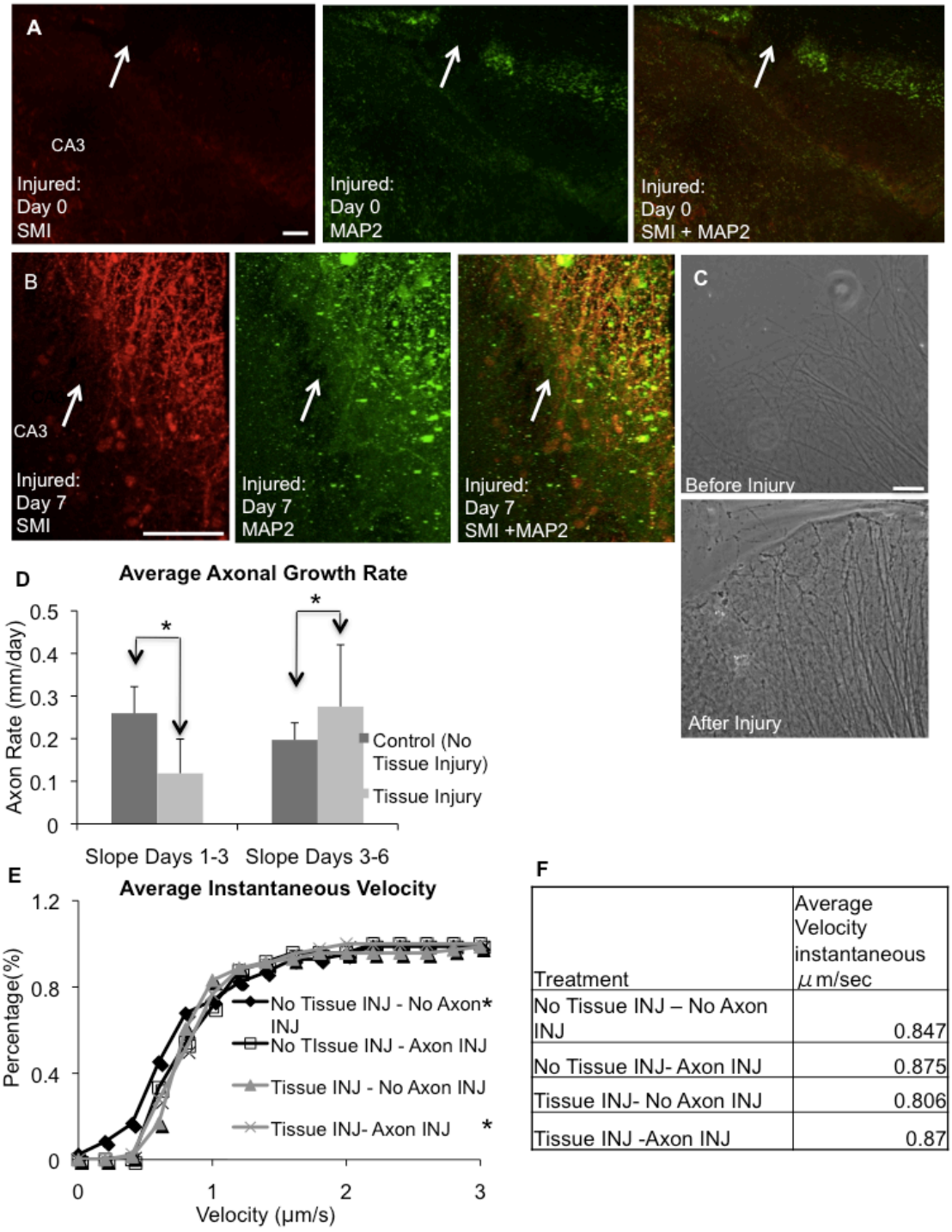

Treatment	Average Velocity instantaneous μm/sec
No Tissue INJ – No Axon INJ	0.847
No Tissue INJ- Axon INJ	0.875
Tissue INJ- No Axon INJ	0.806
Tissue INJ -Axon INJ	0.87

Figure 3-3: Rate of axonal outgrowth of hippocampus axons after tissue and axonal injury.

(A) Injured CA3 region of the explant axonal marker (SMI), dendritic marker (MAP2), and overlay of both (SMI and MAP2) respectively from left to right (arrow = region of injury) at day 0. Fig 1C shows uninjured CA3 region at day 0. (Panel shows damaged CA3 region of hippocampus explant

after 7 days in culture with axonal marker (SMI), dendritic marker (MAP2), and overlay of both (SMI and MAP2), (arrow = region of injury), this illustrates axonal growth over 7 days at the site of injury. Fig 1D shows uninjured CA3 region after 7 days in culture. Figure (C) Bright-field image shows axons before and after injury. (D) Average velocity of axons over 6 days in culture for both the control (no tissue damage) and tissue damage. With tissue injury, there is an initial delay resulting in slower velocity. Two way Anova show interaction between Experimental group and days ($p<0.02$) resulting in significant difference between the days ($p<0.0001$), N (explants) = 2-5 and n (axons) = 20-50 (E) Cumulative histogram showing distribution of instantaneous velocity of axons with and without transection injury as well as with and without tissue damage. Within the no tissue and no axon damage population, there was a leftward shift. The tissue damage with no axonal damage had significantly different distribution compared to the population of no tissue and axonal damage ($p<0.01$, K-S test). N= 3-6 (F) Average of instantaneous velocity shown in figure 3E. Values represent means ± SEM. Bar is 75μm.

Section 4: Discussion

We have characterized and validated in this study a novel whole explant culture system, to further investigate mechanisms associated with neuronal regeneration. Our initial application of this model was to investigate the differential response of axonal outgrowth following tissue or axonal injury. The results of this study highlight the ability to maintain cell viability in explants, perform high-resolution imaging on explants and their axonal projections, and isolate purified axonal populations for biological and biochemical analysis.

Subsection 1: Comparison to other compartmentalization and explant models

A variety of methods have been developed to examine the differential response of axons and neuronal cell bodies. Compartmentalization of dissociated neurons has been performed with a variety of devices, which separate axons and cell bodies and their incubating media with a physical or hydrostatic barrier [121,122]. Such devices are particularly effective for peripheral neurons, which possess the long axons required to pass the barrier in sufficient number. Hydrostatic compartmentalization has also been used to effectively separate central axons from their cell bodies, enabling high-resolution axonal imaging [21]. However, the small numbers of axons that are compartmentalized make such a strategy inefficient for axonal biochemistry or transcriptional analysis. In addition, the variability and ambiguity in axonal orientation of dissociated cells can confound interpretation of polarity-dependent processes (e.g., axonal transport) in dissociated culture systems.

Slice and explant cultures offer the advantage of preserved structural and functional cellular connectivity, and also clear directionality of projections emanating from the tissue mass. Slices maintain neuronal connectivity in the plane of analysis, and also provide cellular accessibility for electrophysiological measurements. However, out-of-plane connectivity is compromised, with particular damage to cells at the edge-planes of slices. In contrast, whole explants provide three-dimensional connectivity of cells within the explant, and a more physiological cellular environment with respect to localization and mechanical environment of supporting cells. DRG explants are an especially popular experimental model for the PNS [123]. Spinal cord explants, including ventral roots as

well as hemi-cord explants have also been used, and straddle the PNS and CNS [113,114,124,125,126,127].

Whole explants for the brain or its sub-domains are used less frequently, though a recent in vitro Drosophila brain explant culturing system demonstrated the value of such a system [117]. We implemented a conceptually similar whole explant culture system, and confirmed explant viability and axonal outgrowth from the explant over at least seven days. In addition, we were able to harvest and analyze purified axon fractions using PCR and Western blotting. Thus, for applications that do not require separation of culture media, we have developed a simple method, which does not require specialized equipment or tools, to analyze the activity of well-aligned, predictably oriented axons decoupled from that of cell-bodies. While culture of hippocampi from mouse genetic models, of which there are many, is in itself of value, the ability to transfect cells further enhances its utility in dissecting mechanistic pathways for injury and repair.

It is important to note that our methodology too has its limitations. Viability is likely restricted in part by the size/thickness of explant, which correlates with the efficiency of nutrient exchange with incubating media; hence, we speculate that our system may be restricted to a scale comparable to that of embryonic or neonatal rodent tissue. Thus, as for other culture models, this may confound the ability to perform experiments requiring an adult model. Finally, in contrast to slice models, though structural integrity is better maintained, targeting of a specific population of neurons for electrophysiological assessment may be more difficult due to overlying tissue

Subsection 2: Influences of primary and secondary injury on axonal outgrowth

In the PNS and spinal cord, previous studies have demonstrated that conditioning lesions (secondary injury) enhance axonal regeneration, either by reducing the initial lag in outgrowth or by increasing the initial rate of axonal outgrowth [128,129]. We therefore tested, using two types of injury, whether a conditioning lesion influenced neuronal outgrowth in neurons from brain. Our results suggest that tissue crush initially delays axonal outgrowth, but there is no change to overall length over six days. It is likely that the damage to the tissue injures resident cells and causes damage causing initial lag in axonal outgrowth [130]. Although no direct comparison can be made given differences in the model system, a comparison with axonal outgrowth rates in slice culture models indicates a similar range of axonal outgrowth rate (0.01 -0.6 mm/day) [131,132].

Axotomy, with or without the initial crush, allowed evaluation of instantaneous velocities at the site of injury. These velocities were unaltered up to 1 hour post-injury, irrespective of experimental group. Future experiments should be performed to measure velocities at later time points or following different lags following crush injury. For example, secondary injury was performed within two days of first injury, whereas it is typical to wait seven days before the second injury. Also, the hippocampal excision itself may have created a primary lesion to some neurons that ultimately extended beyond the explant. Thus, crush injury may in fact be a secondary lesion, and axonal severing either a secondary lesion (no crush) or even a tertiary lesion (with crush).

Section 5: Conclusions

We have characterized and validated a novel hippocampal whole explant model. We have also demonstrated the feasibility of probing axonal biology, biochemistry, and extension

free from confounding effects of neuronal cell bodies. Recent literature in the peripheral nervous system has elucidated many details regarding pathways by which local axonal response influences neuronal regeneration. Our model may be particularly useful in probing similar mechanistic questions in central axons. We anticipate that the simplicity of our experimental system will provide a versatile tool, amenable to genetic and pharmacological manipulation, to probe multiple aspects of neuronal injury and regeneration.

Section 6: Methods

Ethics statement: All animal protocols were approved by the University of Maryland Institutional Animal Care and Use Committee (IACUC).

Dissection and explant culture: C57/Black 6 mouse neonates (P1) were euthanized. Brains were harvested and maintained in cold Hank's Balanced Salt Solution (HBSS) (HBSS 500 mL, D glucose .4g, HEPES .834g, and Penicillin 15 mL). Curved forceps were used to split the left and right hemispheres of the brain, meninges carefully removed, and hippocampus detached from surrounding tissue and maintained in ice cold HBSS (2). For explant culture, the hippocampus was placed on a ~0.2 μL drop of Matrigel on lysine (1mg/ml)-coated glass cover slips. An additional 0.2 μL of matrigel was introduced to the underside of the explant as needed with a micropipette, to further secure the explant to the substrate. After 30 minutes incubation, culture media (Neurobasal media supplemented with 2% B-27) was added. Media was changed

carefully every 3 days, so as not to dislodge the explant. All cells were maintained at 37°C and 5% CO_2. Detached explants or fragmented hippocampi were discarded.

Tissue injury and axonal outgrowth: At the time of plating, explants were either plated immediately or after crushing the presumed CA3 region with forceps (Fig 1a). Axons were allowed to grow out from the explant for six days. Axonal outgrowth was measured every 1, 3, & 6 days after plating using Image J, from images captured using an inverted TE-2000E microscope (Nikon, Melville, NY; described below).

Axonal injury and instantaneous outgrowth: Uncrushed and crushed explants were allowed to grow for two days, after which axons were severed with a 30-gauge needle at a 2/3 distance away from the explant edge (Fig 1b). After transection, time-lapse imaging (every 5 minutes for 1 hour) of axonal outgrowth was captured with an inverted TE-2000E microscope (Nikon, Melville, NY). The instantaneous velocity was measured using Manual Tracking in Image J.

Axon Isolation: Explants were allowed to grow for seven days. Injured (as above) or non-injured axons were collected using appropriate lysis buffer and a micropipette through careful observation under a light microscope. To avoid any cell body and dendritic contamination, we avoided regions at the explant edge. For severed axons, tissue was collected both proximal and distal to the injury site, to enable comparison with corresponding control axons. We performed additional analysis on each sample to assess the exclusive axonal nature of the preparation. For gene expression assays, we probed the

absence of γ–actin mRNA by PCR, which resides only in the soma but is restricted from axons [118,119,120]. For protein assays, we probed the absence of Neun, a neuron-specific nuclear, and thus axon-excluded, protein by immunoblotting [133].

PCR: For detection of axonal transcripts, ~ 100 ng of RNA from axons was used as a template for reverse transcription (RT) with M-MLV Reverse Transcriptase (RT)(Invitrogen, Carlsbad, CA) and an oligo (dT) primer at 90°C for 1 h. The RT reactions were diluted 10-fold and used for transcript-specific PCR. To select primer sequences, we used Primer 3, based on nucleotide sequences found on the NCBI mouse genome browser. Primer sequences used for PCR are provided in Table 1. Negative controls were performed on each sample, and consisted of RNA processed without the addition of RT, or water controls (no DNA). For quantitative RT-PCR, the control and sample RT reactions above were amplified using the Thermocycler detection system (Bio-Rad, Hercules, CA). These reactions were performed using the Soo Fast Green Eva Mix Master Mix (Bio-rad, Hercules, CA) for all transcripts. All control and samples were assayed in triplicate for four independent experiments. Thermal cycling was initiated with an initial denaturation at 50°C for 2 min and 95°C for 10 min followed by 40 cycles at 95°C for 15 s and 60°C for 1 min. Ct values for each transcript were determined using the automatic Ct algorithm of the My IQ software to calculate the optimal baseline range and threshold values. Any samples indicating amplification of the γ-Actin transcript were discarded.

Genes	Primers Forward	Primers Reverse

β-Actin	ccaccatgtacccaggcatt	agggtgtaaaacgcagctca
γ-Actin	cttacactgcgcttcttgcc	aatgcctgggtacatggtgg
CSF1 (reference)	agctggatgatcctgtttgc	tcatggaaagttcggacaca

Transfection: Explants were transfected with Effectene Transfection reagent (Qiagen,Valencia, CA), according to manufacturer's instructions. All transfections took place in Neurobasal supplemented with 2% B-27. Explants were washed 12 hrs after transfection.

Live/dead assay: After transfection, cultures were washed three times. Cell viability was assessed using Live/Dead reagent (Invitrogen, Grand Island, NY). Manufacturer's protocol was followed. Briefly, 10 uL of 2mM Eth-D-1 was added to 5 mL of PBS. Then, 2.5 uL of Calcein AM was added to the solution. Then, about 500 uL of the solution was added to the Explants. Explants were incubated for 22 minutes, washed, and imaged via inverted TE-2000E microscope (Nikon, Melville, NY).

Immunofluorescence: Hippocampal explants were fixed with 4% paraformaldehyde in PBS for 10 minutes and rinsed with PBS three times. Following permeabilization with 0.2% Triton X-100 in PBS, the cells were blocked with 10% Fetal goat serum and 3 % BSA for 30 minutes. A 1:1000 dilution of SMI-31 (Abcam Inc., Cambridge, MA), 1:500 dilution of MAP2 (Abcam Inc., Cambridge, MA) in BSA was applied for an hour at room

temperature, followed by three washes in PBS. Fluorescently labeled secondary antibody was applied subsequently for 1 hr at 37°C, followed again by three washes in PBS. Finally, explants were imaged using a Leica SP5X confocal microscope.

Immunoblotting: Axon samples and positive control (whole explant) samples were lysed using NP40 lysis buffer mixed with protease inhibitor (Fisher-Scientific, Houston, TX) and phosphatase inhibitor (Roche Diagnostics, Indianapolis, IN, USA). The homogenate was further lysed using liquid nitrogen, and supernatant was stored at -80ºC. Protein concentration was measured using a bicinchoninic acid protein assay kit (Pierce; Thermo Fisher Scientific, Rockford, IL, USA). An equal amount of the protein (60 μg) was loaded into each lane, run on 4- 15% Mini-Protean Precast gel (Bio-rad,Hercules, CA), and transferred to PVDF membranes (Millipore, MA). Membranes were blocked overnight using casein-blocking buffer (Vector Lab**,** Burlingame, CA**),** and then incubated for 2 h at RT either with GAPDH (diluted 1:60000, Fitzgerald, Acton, MA) or, Neun (diluted 1:500, Millipore, Billerica, MA). Appropriate secondary antibodies, and DuoLux Chemiluminescent was used for detection following protocol given in Vectastain-AMC Amp kit (Vector Lab, Burlingame, CA). The membranes were detected using ChemiDoc™ XRS+ (Bio-rad, Hercules, CA), and analyzed using Image Lab software (Bio-rad, Hercules, CA). All data is presented normalized to GAPDH. Experiments were repeated at least three times. All samples were imaged for observance of Neun protein in the axonal population, and discarded if contaminated.

Fluorescence Microscopy: Imaging was performed on an inverted TE-2000E microscope (Nikon, Melville, NY) outfitted with a Lumen-PRO2000 (Prior Scientific, Rockland, MA) illumination system and Chroma filters (Bellows Falls, VT. EPI: 488 nm, Emission 530 nm). Additionally, a custom built chamber (Precision Plastics, Beltsville, MD) maintained temperature, humidity, and CO_2 levels during imaging. Live imaging for axonal outgrowth analysis was performed using DIC. Images were captured for 60 minutes every 5 minutes using a 40x objective. Leica SP5X confocal microscope was used for explant imaging; they were either imaged using a 10x or 40x objective with SMI-31 (Excitation 579nm, Emission 599 nm) and Map2 (490 nm, Emission 530 nm) markers.

Statistical Analysis:

Two-way analysis of variance (ANOVA) was performed to measure axonal outgrowth rate over days. Kolmogorov-Smirnov (K-S) test was performed to compare distributions. For all comparisons, we used 3- 6 independent explants and 20-50 axons for analysis. All data are presented as mean ± standard error. Distributions are presented as a cumulative histogram.

Chapter 4: Biphasic increase of retrograde injury signaling complex-related genes in central axons following injury

Section 1: Abstract

Axonal injury activates several programs to promote neuronal survival and axonal regeneration. One such response is retrograde injury signaling (RIS), which promotes local axonal protein synthesis (LPS) and enhances neuronal regeneration in the peripheral nervous system (PNS). RIS is also initiated following injury of neurons in the central nervous system (CNS). However, it remains unknown how the localization of axonal mRNA required for LPS is regulated. We used a novel whole hippocampal explant system to examine mechanisms influencing changes in axonal levels of RIS-associated genes and proteins following axonal injury. Axonal levels of several transcripts, including importin β1 and RanBP1, were elevated biphasically at 1 and 24 hrs post-axotomy. Transcript levels for β-actin, a prototypic locally synthesized protein, were similarly elevated. Our data suggest that axonal transcript levels are regulated differently for different genes. At 1 hr post-injury, experiments performed in the presence of actinomycin indicated that RanBP1, but not importin β1, requires de novo mRNA synthesis. At 24 hrs post-injury, experiments performed following importazole treatment indicated that the second wave of increased axonal mRNA levels required importin β mediated nuclear import. Consistent with studies in the PNS, we observed increased importin β1 (90%) axonal protein levels at 6hrs post-injury. Unlike in the PNS, though, we observed reduced RanBP1 levels (60%) at 3 hrs and vimentin levels (50%) at 3 and 6 hrs post-injury. This study revealed temporally complex regulation of axonal gene

expression, and has significant implications for our understanding of neuronal response to injury in the CNS.

Section 2: Introduction

The poor regenerative capability of the central nervous system (CNS), compared to the peripheral nervous system (PNS), limits recovery from a number of traumatic and degenerative conditions. On the other hand, central neuro-regeneration has been observed in limited contexts (e.g., [9,11]), indicating a need to better understand mechanisms underlying regenerative capacity.

A key advance in understanding mechanisms underlying the robustness of PNS regeneration was the identification and characterization of the retrograde injury signaling (RIS) pathway, which requires transport of injury signals from the injury site to the cell body. Details of this pathway in the PNS have been well summarized in several reviews [36,47,51,54,55]. Briefly, rapid ion influx at the injury site generates a rapid response that propagates retrogradely to provide the first indication of lesion events [47,48,49,134]. A slower component of RIS results in increased dynein-dependent transport of an injury-induced signaling complex from the site of injury to the nucleus [47,50,51]. Importantly, injury also induces local axonal translation of several proteins required for RIS complex transport, including importin β1, RanBP1, and vimentin [36,47,51,52,53,55].

Importin β1, among its diverse roles [135,136,137,138], is a key node in RIS pathways, as its knockout attenuates transcriptional responses to nerve injury and delays functional recovery in vivo [54]. Interestingly, recent evidence suggests that importin β1 may also play a role in central neuronal regeneration. Ohara and colleagues indicated that importin β1-associated STAT3 signaling molecules were transported retrogradely after

injury of hippocampal neurons, but only when importin-STAT association was intact [56,57].

Despite these compelling advances, several key gaps remain in understanding RIS mechanisms. A key unknown in both the PNS and CNS is whether and by what mechanisms transcriptional levels of RIS associated genes are altered locally in the axon in response to injury. Additionally, in the CNS, it has not yet been tested whether importin β1 and other proteins associated with importin in the PNS, including RanBP1 and vimentin, are translated. The goals of this study were to further unveil importin β1-dependent RIS mechanisms in the CNS, through the use of a novel hippocampal explant system, which enabled examination of axonal gene and protein expression independent of neuronal cell bodies. Our results suggest a biphasic axonal response, in which levels of several axonal transcripts, including those associated with RIS, increase rapidly in axons after injury, contributing to early synthesis of corresponding proteins. Importin β1-dependent activity at the nucleus then appears to modulate a second wave of RIS-associated transcripts, which are likely to further support axonal outgrowth.

Section 3: Results

Subsection 1: Whole explant model for examining isolated hippocampal axons

To examine the axonal expression and regulation of genes involved in CNS RIS, we developed a novel hippocampal mouse whole explant system, which enabled injury and analysis of isolated axons. For this study, we cultured P1 explants for seven days, and cut the axons on the seventh day to study axonal response to injury at time points up to 24 hours [Fig 1a,b]. Uninjured axons at the same time point were used as controls. Immunofluorescence evaluation of an axonal marker, phosphorylated neurofilament

[SMI-31], and a dendritic marker, microtubule-associated protein 2 [Map-2A], confirmed the axonal nature of long projections from the explant [Fig 1c; cf. Chapter 3]. In addition, the exclusion of nuclear or cell body markers was assessed in the axonal lysate of each sample, and contaminated samples were excluded from analysis [Fig 1d,e].

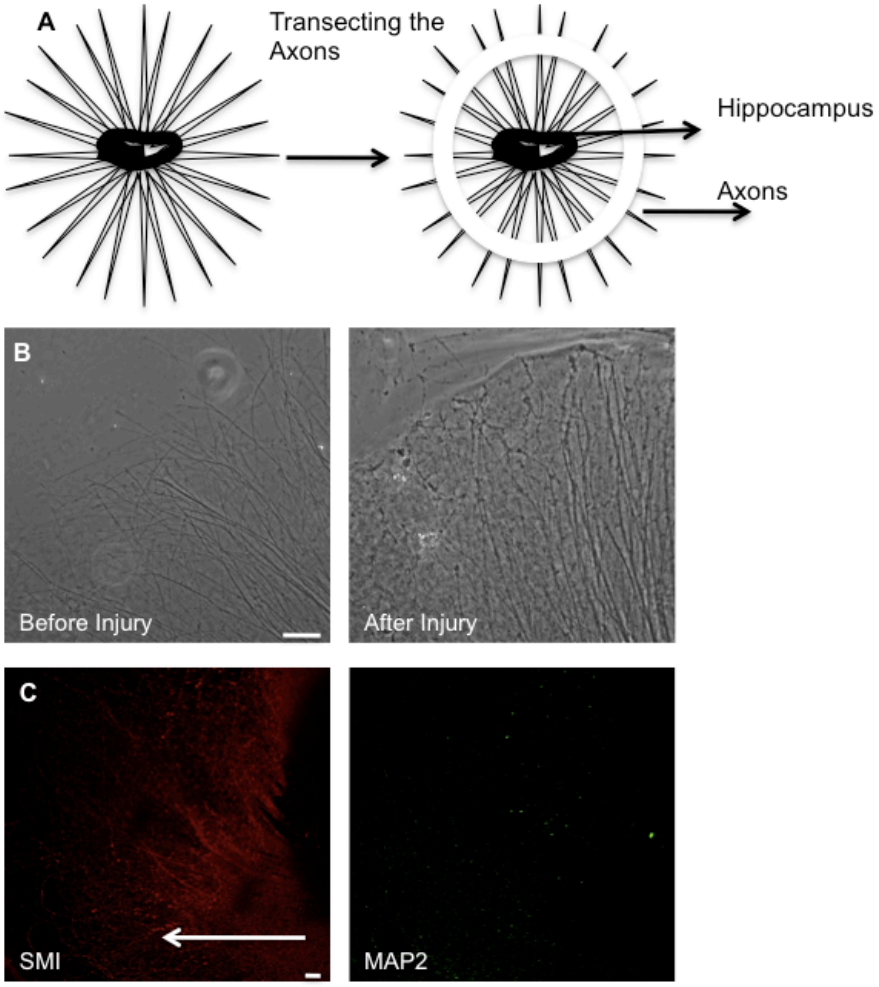

D	CSF1	Importin β1	RanBP1	Vimentin	β-actin	γ-actin
Axon Ct	30+/-3	31+/-3	33+/-3	27+/-2	27+/-3	N/A
Tissue Ct	23+/- .2	27+/-3	31+/-.9	25+/-2	16+/-.05	24+/-.8

Figure 4-1: Illustrating axonal injury and exclusive nature of axonal preparation.

(A) Schematic presentation of axonal injury with a needle, injury was performed 2/3 of distance away from the edge of the explant. (B) Bright-field image illustrating before and after axonal injury. Hippocampal explants are differentiated and present distinct morphology for both the axons and dendrites. Dendrites have shorter process and taper more gradually, while axons display a long,

narrow process with minimal tapering (C) Double-label immunofluorescence of SMI-31 (red) and MAP2 (green), showing presence of axonal outgrowth, and very few or no dendrites proximal to the tissue (green non-specific binding). Arrow indicate direction of growth. RT-PCR and Immunoblots were performed to ascertain exclusive nature of axonal preparation (D) RT-PCR confirms higher levels of genes in the whole tissue compared to only axons validating the presence of for importin β1, RanBP1, Vimentin, β-actin, and γ-actin in whole tissue (positive control).As well as, it confirms presence of β-actin and absence of γ-acting values (there were some samples with Ct values of >37). Bar is 75μm

Subsection 2: Influence of axotomy on axonal mRNA expression

Based on the retrograde transport of RIS signaling complexes observed in both the PNS and CNS [36,47,51,52,56,57], we hypothesized that levels of genes encoding RIS complex components too would be increased in axons. To test this hypothesis, we first performed RT-PCR at 1, 6, 15 and 24 hrs post-injury. Injury caused a significant increase in axonal levels of importin β1 (2.82 ± 1.7, 4.5; $p<0.002$) and RanBP1 (2.70 ± 1.5, 4.9; $p<0.009$), but not vimentin ($p=0.46$), 1 hr after axotomy relative to control (no injury). Transcripts encoding β-actin, which is a well-described locally synthesized protein not believed to play a role in RIS, also significantly increased 1 hour after axotomy compared to controls (4.73 ± 2.1,10.6; $p<0.003$), serving as a "positive control" [Fig 2]. Axonal levels of all four genes were not significantly different between injured and uninjured axons 6 – 15 hours after axotomy ($p>.05$). Interestingly, 24 hrs after axotomy, we observed a second wave of significantly increased levels of importin β1 (2.74 ± 0.7, 10.6; $p<0.06$), and RanBP1 (2.48 ± 0.8, 7.5; $p<0.05$) mRNA compared to controls. β-actin mRNA levels also trended higher at 24 hours ($p=0.45$), but differences

with controls did not reach statistical significance [Fig 2]. These results thus suggest a biphasic elevation in key RIS-associated genes associated with nuclear import.

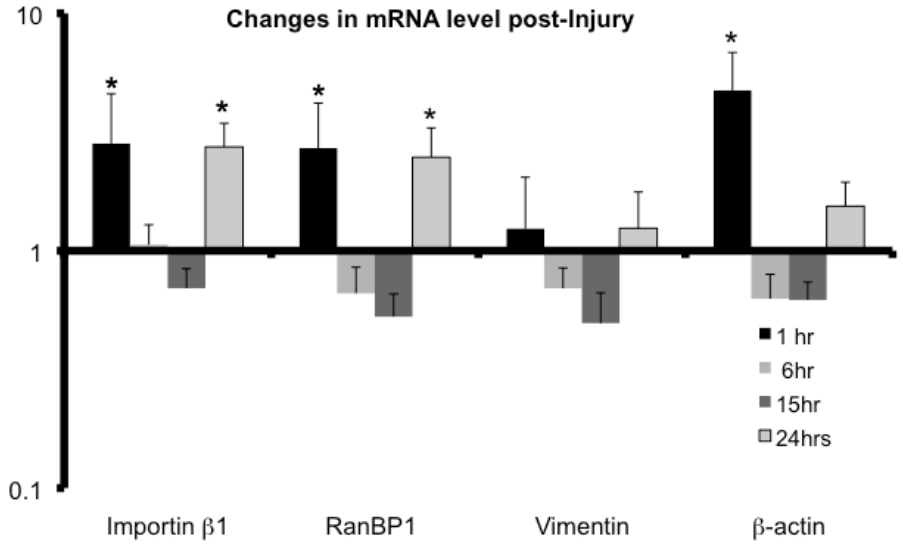

Figure 4-2: Real-time RT-PCR was used to quantitate levels of specific mRNAs in the axonal RNA samples post axotomy.

Results for importin β1, RanBP1, vimentin, and β-actin are illustrated. All values are displayed relative to no injury to axons as a control. Specifically, at 1 hr after axotomy, there is a significant increase in importin Beta, RanBP1, and β-actin mRNA levels. The levels are suppressed at 6 and 15 hrs after axotomy. The levels increase again at 24 hours for importin β1 and RanBP1. No significant changes were observed in vimentin transcript levels. Error bars represent the SD of three - four independent experiments. Significance was calculated based on $P \leq 0.05$ by pair wise fixed reallocation randomization test compared with the control.

Subsection 3: Influence of transcriptional inhibition on axonal mRNA expression

The above results support the hypothesis that an injury-induced signal causes elevation in axonal levels of importin β1, RanBP1, and β-actin at an early stage, within 1 hr after axotomy. We next assessed whether this increase in gene levels required *de novo* transcription, in the cell body. We used the well-characterized antibiotic actinomycin D (AMD) to inhibit transcription, and performed RT-PCR to measure changes in gene expression at 1 hr post-injury. To identify conditions under which AMD inhibited transcription in our culture system, we examined total mRNA content in response to a range of times. A dose of 5 mg/mL of AMD for two hours resulted in ~50% total transcript reduction, which we deemed sufficient to block transcription. AMD treatment suppressed the injury-induced increase in mRNA levels of RanBP1 (0.98 ± 0.34, 2.74) and β-actin (1.29 ± 0.42, 3.79) observed in untreated cells, suggesting that these genes were newly transcribed and rapidly recruited to axons. However, surprisingly, AMD treatment did not inhibit the injury-induced increase in axonal importin β1 mRNA levels (2.64 ± 0.60, 11.5; $p<0.001$). These results suggest that increased axonal importin β1 transcript levels reflect contributions from pre-existing transcript populations in the cell body or axons proximal to harvest level [Fig 3].

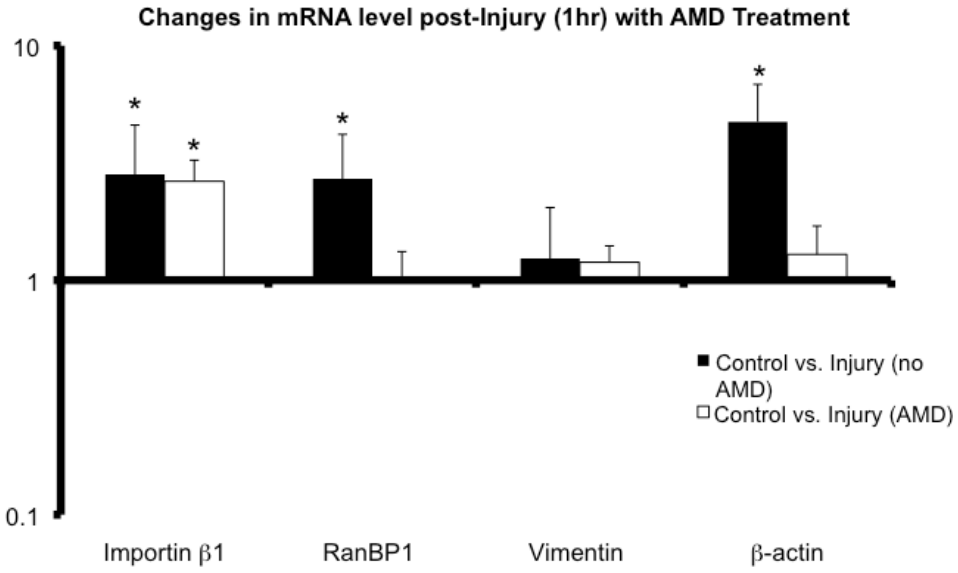

Figure 4-3: RT-PCR was used to measure levels of axonal mRNA in injured hippocampal axons after inhibiting transcription relative to control (uninjured axons).

The results indicate significant elevated mRNA levels in importin β1, suggesting a transport of pre-existing mRNAs from the cell body. The levels of RanBP1, vimentin and β-actin are down-regulated, suggesting a requirement of newly synthesized mRNAs upon injury [white bar]. Comparison of no actinomycin treated injured with respect to control data (previously graphed Figure 2, 1hr) depicts suppression of Ranbp1, vimentin, and β-actin levels after the AMD treatment [black bar]. Error bars represent the SD of three-four experiments. Significance was calculated based on $P \leq 0.05$ by pair wise fixed reallocation randomization test compared with the control.

Subsection 4: Influence of axotomy on axonal protein levels

To test whether and over what time frame early increases in transcript levels ultimately resulted in changes in protein expression, and thus the possible formation of RIS, we explored changes in axonal levels of RIS proteins in response to injury. We

evaluated the expression of importin β1, RanBP1, and vimentin at 0hr, 1hr, 3 hr, and 6 hr after axotomy. As was also the case for mRNA levels, each RIS protein responded uniquely to injury. Consistent with local axonal translation (though not excluding some contribution from the cell body), importin β1 levels increased continuously during the 6 hour observation period, with a significant increase at 6 hr after axotomy (90% increase, $p<0.05$) [Fig 4c,a]. Conversely, Ranbp1 protein levels (60% reduction $p<0.05$) decreased at 3 hours compared to the baseline level (control), but rebounded by 6 hrs [Fig 4d,a]. Vimentin protein levels were significantly reduced at 6 hr after axotomy (50% reduction, $p<0.05$) [Fig 4e,a]. Thus, despite some variability in the temporal coupling between transcriptional and translational changes, these results support an axonal contribution to RIS complexes.

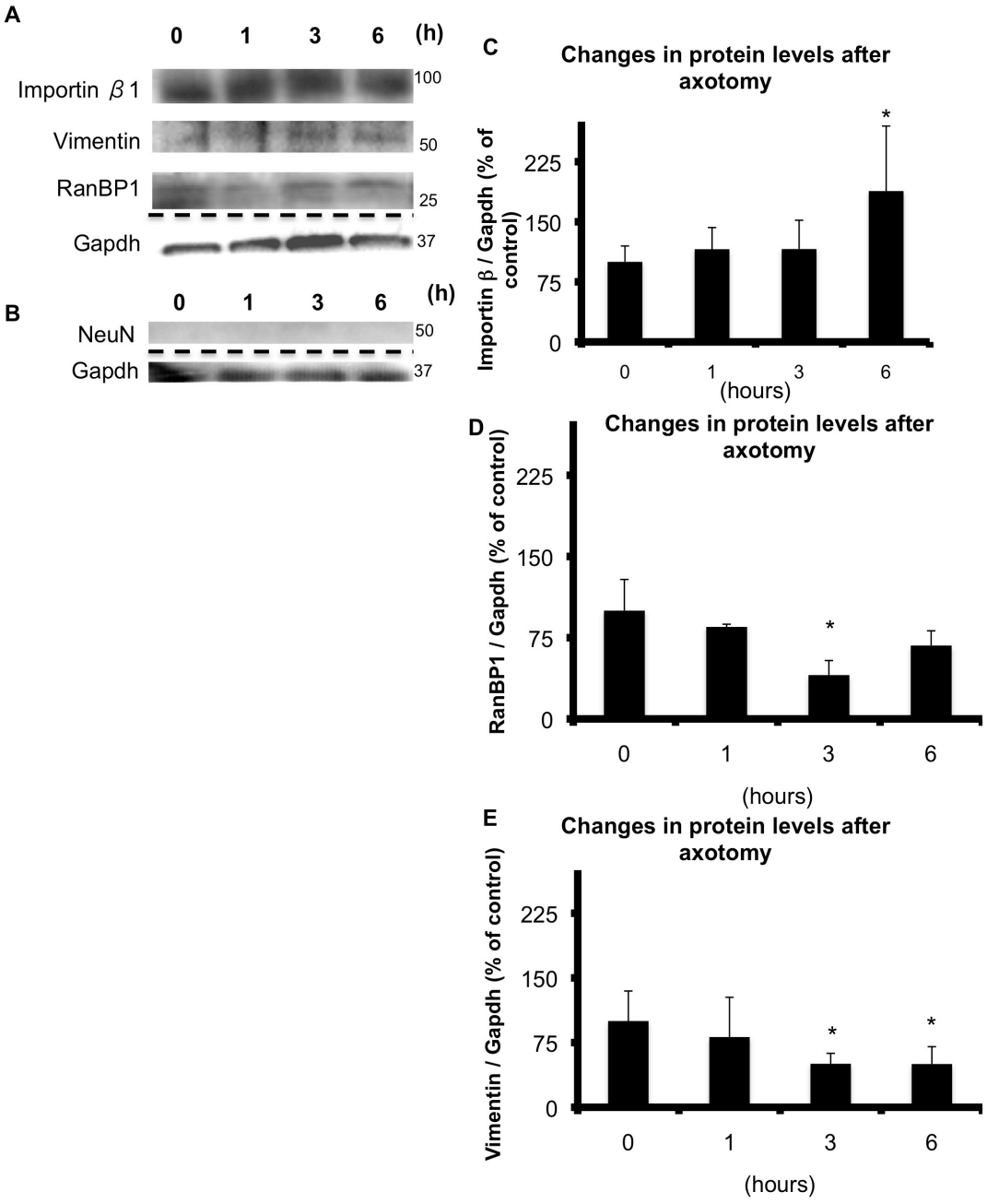

Figure 4-4: Western blot analysis of lysates from axotomized hippocampal explants axons from 0 min to 6 h after axotomy.

(A) Illustrates blots of each protein normalized to GAPDH. (B) Illustrates exclusion of Neun protein from axonal population with respect to GAPDH blot. (C) The graph shows increase in importin β1 axonal protein levels 6 hours after axotomy (D) The graph shows significant decrease in RanBP1

levels 3 hr after axotomy, increases back at 6 hrs post- injury. (E) Vimentin level decrease at 3 and 6 h post axotomy. Data are represented as the percent change in protein levels compared to control (uninjured axons) ± SE of three - seven independent experiments compared with the control (Student's t-test, $p \leq 0.05$).

Subsection 5: Influence of importin β mediated nuclear import on axonal mRNA expression

Having established an increase in both importin β transcript at 1 hour and protein at 6 hours, we next tested whether importin β1-mediated nuclear import was required to transcribe new importin β, RanBP1, and β-actin mRNA observed in the second phase of increased gene expression at 24 hrs. To minimize non-specific perturbation of the diverse functional roles of importin β1, we specifically disrupted nuclear import mediated via importin β using importazole (IPZ). IPZ's role in disrupting importin β mediated nuclear import in non-neuronal cells was extensively characterized by Soderholm et al [139]. However, IPZ inhibition of nuclear import in an explant system, and specifically in neurons, has not yet been characterized. We therefore tracking the localization of the transcription factor NFAT fused to GFP (NFAT-GFP) in response to IPZ treatment. Studies in non-neuronal cells reveal that NFAT-GFP shuttles between the nucleus and cytoplasm in calcium regulated manner, and is imported by importin α/β and exported by CRM1 [140,141,142,143]. As expected, at steady state, NFAT-GFP was predominately cytoplasmic in cells within and at the edge of the explant. Also, as expected, an increase in cytoplasmic calcium induced by ionomycin led to accumulation of NFAT-GFP in the nucleus [Fig 5a].

Explants were then treated with 18μm importazole for 24h hours followed by 1.5 hr treatment of ionomycin in the continued presence of importazole. In stark contrast to control cells, there was no import of NFAT-GFP in importazole treated cells (Fig 5b,c); specifically, IPZ treatment resulted in nuclear exclusion of NFAT-GFP in 75% cells after 12 hrs ($p< 0.015$), and 86% cells after 24 hrs ($p<0.003$) (Fig 5c) demonstrating effectiveness of IPZ. Because explants contain both neuronal and non-neuronal cells, we also used immunofluorescence with SMI-31 (axonal marker) to verify that IPZ successfully inhibited nuclear import in neuronal cells [Fig 5d]. Importantly, transfection, importazole and ionomycin treatment caused minimal cytotoxicity. Following IPZ and ionomycin treatment of cells expressing NFAT-GFP, we performed a live/dead assay, which indicated over 86-91% survival of cells treated with DMSO (control), as well as transfected cells treated with IPZ followed by ionomycin treatment [Fig 5e,f].

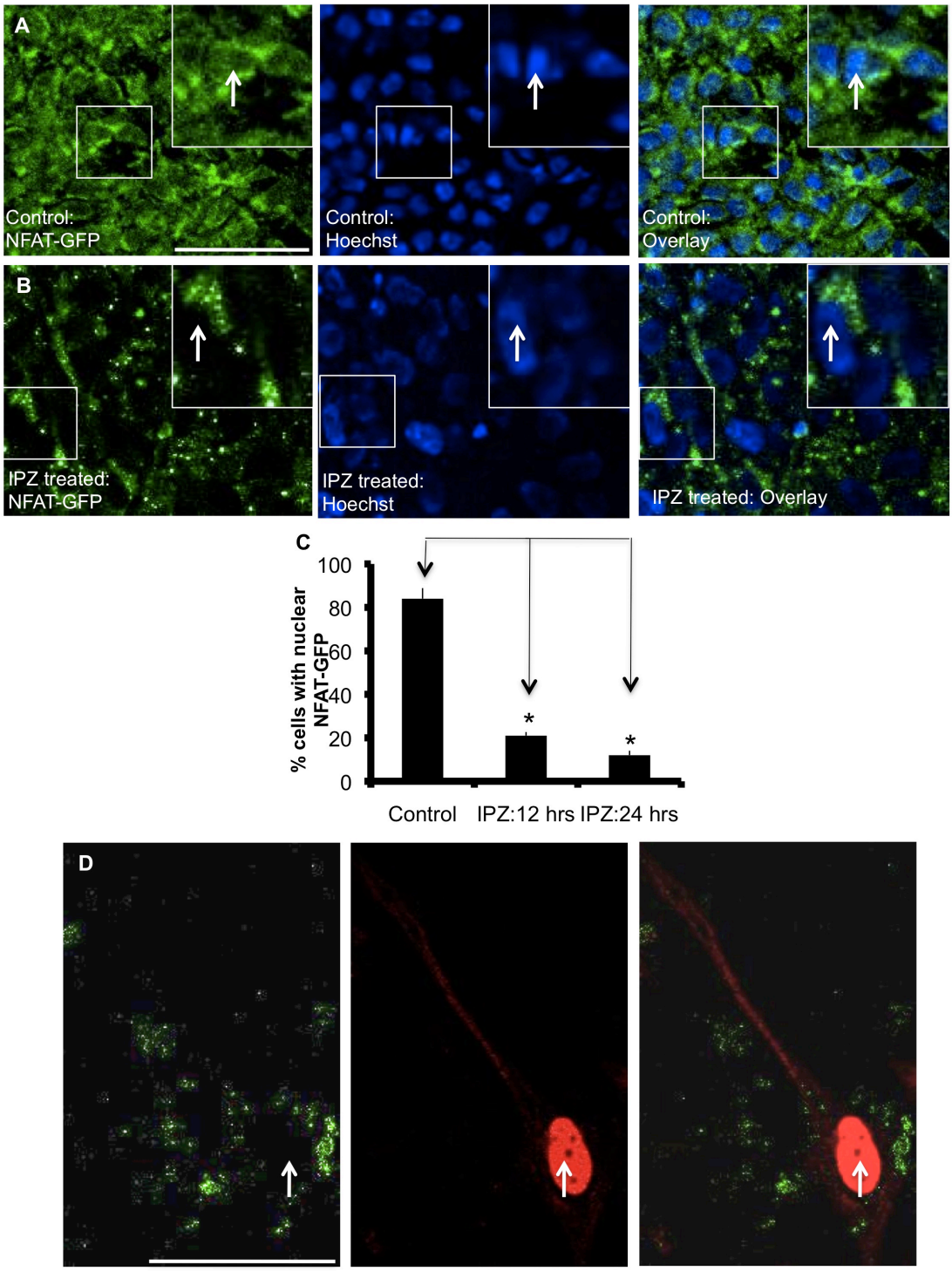
A
Control:
NFAT-GFP
Control:
Hoechst
Control:
Overlay
B
IPZ treated:
NFAT-GFP
IPZ treated:
Hoechst
IPZ treated: Overlay
C
% cells with nuclear NFAT-GFP
100
80
60
40
20
0
*
*
Control
IPZ:12 hrs
IPZ:24 hrs
D

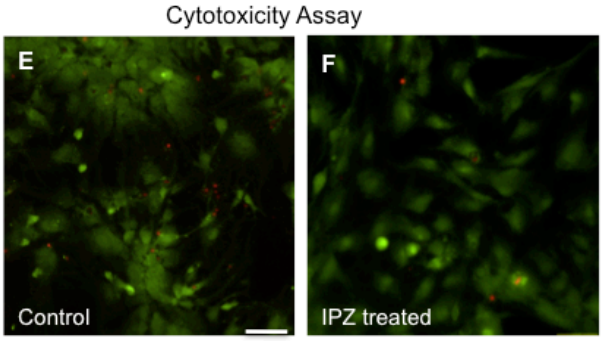

Figure 4-5: Importazole bocks Importin beta-mediated nuclear import in hippocampal explant. (A) Cells stably expressing NFAT-GFP were not-treated with importazole prior to a 1.5 hr treatment with ionomycin to induce nuclear import of NFAT-GFP. Presence of nuclear localized GFP signal indicate expression within nucleus, NFAT-GFP illustrates signal within nucleus (Hoechst, arrows) and surrounding regions (overlay, arrows) (Inset – expanded for more clear visualization). (B) Cells stably expressing NFAT-GFP were treated with 18uM of importazole for 24 hours prior to a 2 hr treatment with ionomycin to induce nuclear import of NFAT-GFP. Absence of nuclear localized GFP signal indicate exclusion of nuclear GFP signal, NFAT-GFP excluded from nucleus (Hoechst, arrows) and presence of GFP signal in cytoplasmic regions (overlay, arrows) (Inset – expanded for more clear visualization). (C) Results were quantified as the percentage of cells with nuclear NFAT-GFP N=2, 150 or more cells counted under each conditions. The treatment blocks nuclear import in 75% of cells within 12 hrs, and 86% of cells within 24 hrs (Student's t-test, $p \leq .05$). (D) Cells expressing NFAT-GFP were immunostained for axonal marker (SMI-31- red) after IPZ treatment illustrate population of neuronal cells also affected by the IPZ treatment. Presence of GFP signal is observed in the proximal axons. Arrows indicate absence of GFP signal within in the nucleus. SMI-31 also labels the nucleus. (E) Live/dead assay of either control or treated (F) with IPZ and Ionomycin after transfection show no toxicity both in control and treated cells. Bar is 50µm. Values represent means ± SEM

We then evaluated changes in axonal mRNA levels 24 hrs post-injury followed by IPZ treatment. IPZ treatment suppressed the second wave of increased axonal mRNA for all RIS-related genes and β-actin, as indicated by the lack of significant changes in axonal mRNA levels of all genes after IPZ treatment at 24 hrs post-injury relative to control [Fig 6]. When viewed in combination with the transcriptional and translational up regulation of several key RIS proteins at earlier time points, these results support a model whereby an RIS feedback mechanism is required for secondary amplification of both RIS-associated and unassociated mRNA at later time points.

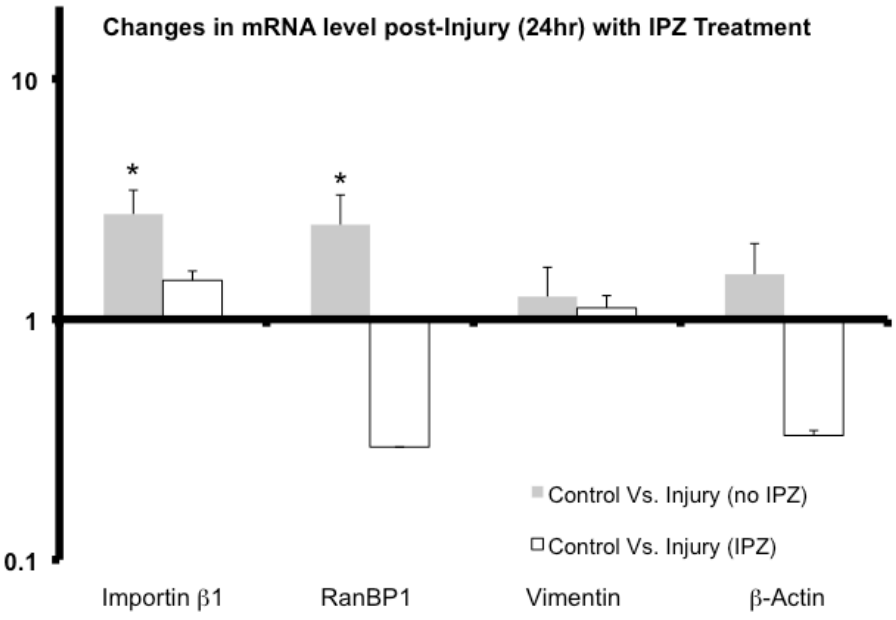

Figure 4-6: RT-PCR was used to measure levels of axonal mRNA in injured hippocampal axons after inhibiting nuclear transport relative to control (uninjured axons).

The results indicate suppression of elevated mRNA levels in importin β1, RanBP1, vimentin and β-actin [white bar]. Comparison no IPZ treated injured with respect to control data (previously graphed Figure 2, 24 hr, light gray bar) clearly depicts suppression of gene levels after the IPZ

treatment. Error bars represent the SD of three-four experiments. Significance was calculated based on $P \leq 0.05$ by pair wise fixed reallocation randomization test compared with the control.

Section 4: Discussion

In this study, we examined axonal levels of RIS-associated genes, which will ultimately be translated to activate RIS pathways. Our findings suggest that axotomy results in biphasic elevation of axonal mRNA, at 1 and 24 hours after injury. Regulation of this biphasic response appears gene-specific at the early time point, with importin β mediated nuclear import required for the second wave of axonal gene expression.

Subsection 1: Biphasic elevation in mRNA levels after axotomy

Inhibition of protein synthesis in axons significantly impairs growth cone activity and axonal extension [28,46], emphasizing the importance of local protein synthesis for regeneration. Among the many axonally synthesized proteins, translation of importin β1, RanBP1, and/or vimentin following axonal injury suggests a role for local protein synthesis in RIS. In particular, local translation of RanBP1 following injury results in RanGTP dissociation from importins, allowing binding of newly synthesized importin β to importin α and dynein-bound RIS complexes that are transported to neuronal cell bodies [36,47,53,57].

To execute these retrograde signaling pathways, required transcripts must be in place beforehand, or must be rapidly recruited to the site of injury [21]. The rapid increase in mRNA transcripts within the axon implies rapid localization to the injury site [Fig 2]. This response is consistent with the rapid retrograde propagation of an

electrophysiological response, possibly mediated by calcium, which provides the first indication of a lesion even [47,48,49,50,51,144]. On the other hand, electrical activity alone is not sufficient to initiate regeneration [52,145], and thus our observed secondary elevation in mRNA transcripts 24 hours post-injury is consistent both with RIS and the requirement for an additional signal for effective regeneration. The dip in axonal transcript levels at time points between 1 and 24 hours, as opposed to steadily increasing or stably increased levels, also supports the notion of two different mechanisms for transcript recruitment to the axon.

Subsection 2: Specificity and differential regulation of axonal transcript levels: early injury response

A number of transcripts have been shown to alter their axonal levels following axotomy of central neurons [21]. As expected, mRNA levels for β-actin, whose local synthesis has been extensively characterized, increased after axotomy, serving as a sort of positive control. Consistent with RIS signaling, we also observed rapid increases in both importin β and RanBP1 transcript levels, but interestingly, not vimentin. Transcriptional inhibition also revealed differences in the response of evaluated genes. The early increase in axonal levels of RanBP1 and β-actin, like GAP-43, depended on newly synthesized mRNAs (Fig 3; [22,146]). Conversely, importin β, like several other genes, such as CGRP, moved into axons [146,147], indicating an additional non-transcriptional contribution to axonal synthetic capacity.

Differential regulation of importin β1 compared to RanBP1 (or vimentin) genes may in part be a consequence of the functional diversity of importin β, and thus the potential for its recruitment away from other functional roles. In addition to nuclear

transport in the cell body, such roles for importin β include quality control of ER proteins [138], assembly of mitotic spindles and centrosomes [135,136], and in learning-related plasticity in CNS [148]. On the other hand, though, importin isoform localization is dictated by its 3' UTR, with a short 3' UTR variant of importin more prominent in cell bodies and a longer variant more prominent in axons [54]. Thus, any pre-existing recruitable pool of importin β1 mRNA must be pre-designated for axonal localization. Candidates for such a transport-ready pool are ribonucleoprotein particles (RNPs), which can migrate to axons and dendrites in response to a given stimulus [149,150]. Such activity has been noted in response to a variety of stimuli, for example, axonal transport of β-actin mRNA following the application of neurotrophins to chick cortical neurons [27,41].

Subsection 3: A role for importin β in regulating axonal levels of mRNAs: delayed injury response

Several lines of evidence suggest that importin β plays an important, even essential, role in the response to axonal injury. In the PNS, importin-associated RIS complexes transport signaling proteins, including transcription factors such as JNK, Erk, ATF2, and ATF 3, from the injury site [36,55,151], and the depletion of importin β results in suppressed gene transcription and delayed functional recovery following nerve injury [54]. Importin β also stimulates axotomy-induced axonogenesis in the CNS, in part by transporting the transcription factor STAT3 [56,57].

Our data support an important role for importin β1 post-injury, and reveal novel and intriguing temporal dynamics of an importin-mediated neuronal response. Based on

RIS complex transport rates, transcription rates, and mRNA transport rates [68,152], it is unlikely that importin β mediated nuclear import plays a role in transcriptional changes at 1 hr post-axotomy. However, our data suggest that importin β plays a critical role in the secondary wave of axonal transcript elevation upon injury. Increased importin β1 expression over 6 hours [Fig. 4c] indicates that early increases in importin β1 transcript are translated. In addition, axonal elevation of importin β1 and RanBP1 transcripts was suppressed following specific pharmacological inhibition of nuclear import, with other importin functions, including RIS complex formation, presumably intact [Fig 6]. Together, these data suggest that rapidly synthesized importin β1 feeds back to further upregulate the axonal localization RIS associated genes.

Subsection 4: RIS in the CNS versus PNS

Our work points to interesting similarities and differences between RIS signaling in the PNS and CNS. On one hand, we confirm that axonal levels of the RIS-associated genes importin β1and RanBP1 indeed increase following central axonal injury, and importin β plays a key role in regulating this increase. Our observed increase in axonal levels of importin β1 after 6hrs of axotomy [Fig 4a] is similar to that in the PNS, with maximum increases observed 6-8 hrs after axotomy [36]. A recent study by Ohara and colleagues suggested that, unlike our results, several axonal proteins, including importin β1, slightly increased 10 mins after axotomy of dissociated cortical neurons, before returning to control levels 1 hr post-injury [57]. However, isolated axons were harvested only from regions distal to the injury site, which were presumably degenerating. Axonal regions proximal to the injury site in this study were not separated from cell bodies

[56,57], precluding direct comparison with our results. Additionally, no further quantification was performed beyond 1hr.

On the other hand, in contrast to studies in the PNS, which show a gradual increase in axonal protein levels of vimentin and RanBP1 over period of 6hrs after axotomy in the PNS [53,55], we observed neither. In fact, our study, which examined for the first time in the CNS axonal protein expression of RanBP1 and vimentin, indicated unchanged vimentin transcripts over 24 hours, and, in fact, a reduction in axonal protein levels of vimentin within 6 hrs after axotomy [Fig 4e]. While in the PNS, calpain-cleaved vimentin binds to phosphorylated ERKs (pErk), linking pErk to dynein via importin β1 [55], this regulatory pathway does not appear to be conserved in our CNS model. Our observed RanBP1 axonal levels also differed from observations in the PNS studies. It is not clear why axonal levels of RanBP1 were reduced at 3 hours post-injury; however, the subsequent increase at 6 hrs post-axotomy is consistent with increased transcript levels [Fig 2 vs. 4d] and possible inclusion in RIS complexes.

Section 5: Conclusions

Our observed novel biphasic increase in axonal gene expression suggests tightly and differentially regulated control of local protein synthesis in hippocampal neurons, including a key role for importin β-mediated nuclear import [Illustration 1, Table 1]. While our focus was on the regulation of RIS associated genes, additional details regarding local protein synthesis and RIS signaling in CNS axons, including the exact set of transcription factors responsible for de novo mRNA synthesis as well as details regarding zip-code-like proteins that regulate axonal mRNA transport for RIS genes, remain to be elucidated. Additionally, how such details influence localized protein

synthesis and axonal outgrowth must also be elucidated. Our findings confirm intrinsic regenerative capabilities in the CNS, and have important implications for exploiting RIS and local protein synthetic pathways towards enhanced CNS repair.

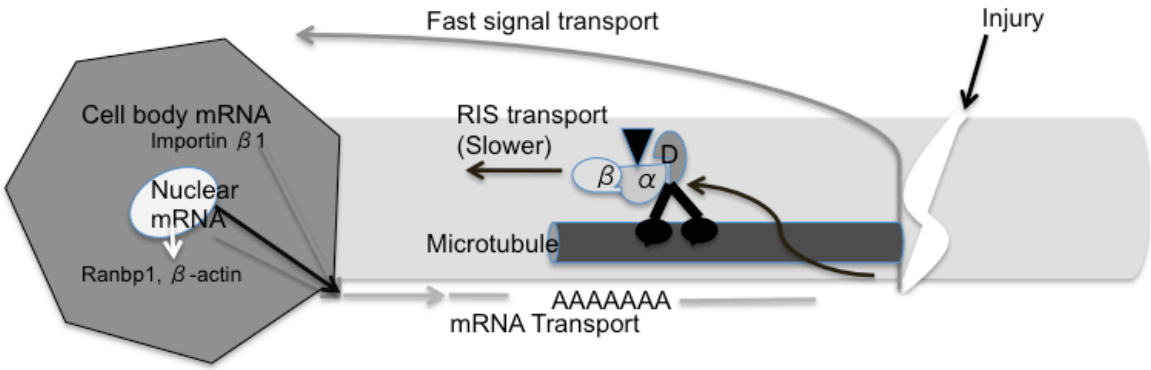

Illustration 4-1: Schematic presentation of RIS-associated axonal transcript levels post-injury. The schematic summarizes the findings of the study. Specifically, injury triggers biphasic elevation in axonal transcript levels. At an earlier time point, these levels are differentially regulated; where, some require new transcription and others do not. Injury triggers increase in axonal importin β protein levels suggesting contribution in formation of RIS-complex. And, at later time point, importin β is required for increase in the second wave of mRNA transcripts.

Table 4-1: Summarized Results

Genes	Axonal mRNA levels after Injury		Axonal mRNA levels after AMD treatment & Injury	Axonal mRNA levels after IPZ treatment & Injury	Axonal protein levels after injury		
	1 h	24h			1h	3h	6h
importin β1	↑	↑	↑	↓	—	—	↑
RanBP1	↑	↑	↓	↓	—	↓	—
β-actin	↑	—	↓	↓	n/a	n/a	n/a
Vimentin	—	—	—	—	—	↓	↓

Section 6: Methods

Ethics statement: All animal protocols were approved by University of Maryland Institutional Animal Care and Use Committee (IACUC).

Explant culture:

C57/Black 6 mouse neonates (P1) were euthanized. Brains were harvested and maintained in cold Hank's Balanced Salt Solution (HBSS) (HBSS 500 mL, D glucose .4g, HEPES .834g, and Penicillin 15 mL). Curved forceps were used to split the left and right hemispheres of the brain, meninges carefully removed, and hippocampus detached from surrounding tissue and maintained in ice cold HBSS (2). For explant culture, the hippocampus was placed on a ~0.2 μL drop of Matrigel on lysine (1mg/ml)-coated glass cover slips. An additional 0.2 μL of matrigel was introduced to the underside of the explant as needed with a micropipette, to further secure the explant to the substrate. After

30 minutes incubation, culture media (Neurobasal media supplemented with 2% B-27) was added. Media was changed carefully every 3 days, so as not to dislodge the explant. All cells were maintained at 37°C and 5% CO_2. Detached explants or fragmented hippocampi were discarded.

Axon Isolation:

Explants were allowed to grow for seven days, after which axons were severed with a needle at a distance ~2/3 of the longest axons away from the explant edge. Injured or non-injured axons were collected using appropriate lysis buffer and a micropipette, through careful observation under a light microscope. To avoid any cell body and dendritic contamination, we avoided regions at the explant edge. For severed axons, tissue was collected both proximal and distal to the injury site, to enable comparison with corresponding control axons. We performed additional analysis on each sample to assess the exclusive axonal nature of the preparation. For gene expression assays, we confirmed the absence of γ–actin mRNA by PCR, which resides only in the soma but is restricted from axons [118,119,120]. For protein assays, we confirmed the absence of Neun, a neuron-specific nuclear, and thus axon-excluded, protein by immunoblotting [153]. Any samples that were contaminated with cell body markers were not used for further analysis.

Axonal gene expression:

Control or uninjured axonal samples were collected at 1, 6, 15, and 24 hours post-injury. For detection of axonal transcripts, ~ 100 ng of RNA from axons was used as a template

for reverse transcription (RT) with M-MLV Reverse Transcriptase (Invitrogen, Carlsbad, CA) and an oligo (dT) primer at 90°C for 1 h. The RT reactions were diluted 10-fold and used for transcript specific PCR. For primer sequence, we used Primer 3 tool based on specific nucleotide sequence found on PubMed. Primer sequences used for PCR are outlined in Table 1. Negative controls were performed on each sample, and consisted of RNA processed without the addition of reverse transcriptase. For quantitative RT-PCR, the control and sample RT reactions above were amplified using the Thermocycler detection system (Bio-Rad, Hercules, CA). These reactions were performed using the Soo Fast Green Eva Mix Master Mix (Bio-rad, Hercules, CA) for all transcripts. All control and samples were assayed in triplicate for four independent experiments. Thermal cycling was initiated with an initial denaturation at 50°C for 2 min and 95°C for 10 min followed by 40 cycles at 95°C for 15 s and 60°C for 1 min. Relative levels of individual transcripts were calculated by normalizing to the CSF1 control using a comparative threshold value (Ct) method. Briefly, the Ct for each transcript was determined using the automatic Ct algorithm of the My IQ software to calculate the optimal baseline range and threshold values. Individual ΔCt values were then determined by subtracting the CSF1 Ct value from the individual transcript Ct values. From this, the calculation of ΔΔCt was determined by subtracting the ΔCt Sample (injury to the axons) from ΔCt control (no injury to axon) The fold difference was then expressed as 2-ΔΔCt, with ΔΔCt+SD and ΔΔCt - SD where SD is the standard deviation attained from Ct values as described in Livak et al**.** [154]. Transcript levels are expressed relative to the ΔΔCt values of the control (uninjured) axons. As some transcripts were expressed at very low levels in axons, primers were validated in whole explant lysate (Fig 1).

Genes	Primers Forward	Primers Reverse
β-Actin	ccaccatgtacccaggcatt	agggtgtaaaacgcagctca
γ-Actin	cttacactgcgcttcttgcc	aatgcctgggtacatggtgg
Importin β1	gtctctactctgcgcgactc	gctaccactccgtccgtatg
RanBP1	ttaagatgcgtgcaaagctg	gcttcagctccatcattggt
Vimentin	tgaaggaagagatggctcgt	ttgagtgggtgtcaaccaga
CSF1 (reference)	agctggatgatcctgtttgc	tcatggaaagttcggacaca

Data were compared statistically using relative expression software tool (REST©, Qiagen, Valencia, CA), as described in the study of Pfaffl et al [155]. Type I error α was set to 0.05.

Actinomycin d-treatment:

Actinomysin-d (AMD) dose was set at 5 μg/ml [156], and treatment duration was varied from 1 to 3 hrs to test transcriptional inhibition in explants. As AMD treatment resulted in inhibition of transcription within two hours, explants were treated with this dose for two hours before being injured (or not, for controls). Samples were collected one hour post-injury and RT-PCR was performed as above, with AMD treated uninjured axons used as controls.

Inhibiting Nuclear Transport:

Importazole (IPZ; Sigma-Aldrich, St. Louis, MO) has been well characterized in non-neuronal cells [139]. We have followed a similar approach to characterize inhibition of importin-mediated nuclear import in our system. Explants were transfected 12 hrs prior to IPZ treatment with NFAT-GFP expression plasmid (pKW520, a kind gift from Dr. Karsten Weis), using Effectene transfection reagent (Qiagen, Valencia, CA) per manufacturer's instructions. All transfections took place in Neurobasal supplemented with 2% B-27 (Life Technologies).

IPZ was used at concentrations of 18 μM for up to 24 hours, supplying fresh media with IPZ every 12 hours. For controls, fresh media without IPZ was used. At 22 hours (1.5 hours prior to 24 hours treatment), ionomycin was added at 15 μM to induce intracellular calcium influx and trigger nuclear import. To assess import, cells were fixed with 4% formaldehyde prior to fluorescence microscopy. DNA was visualized with 1 μg/ml Hoechst dye. For quantification, 100-200 cells for each condition were analyzed and nuclear accumulation of NFAT-GFP was assessed using Image J.

Cell viability:

To test cell viability, after transfection, IPZ and Ionomycin treatments, cultures were washed three times and assessed using Live/Dead reagent (Invitrogen, Grand Island, NY), per manufacturer's protocol. Explants were incubated for 20 minutes, washed, and imaged via an inverted Nikon TE-2000E microscope. Cell viability of explants containing 0.1 to 0.4% of DMSO was performed as a control.

Immunofluorescence and imaging:

Hippocampal explants were fixed with 4% paraformaldehyde in PBS for 10 minutes and rinsed with PBS three times. Following permeabilization with 0.2% Triton X-100 in PBS, the cells were blocked with 10% Fetal goat serum and 3 % BSA for 30 minutes. 1:1000 dilution of SMI-31 (Abcam Inc., Cambridge, MA) and/or 1:500 dilution of MAP2 (Abcam Inc., Cambridge, MA) in BSA was applied for 1 hour at room temperature, followed by three washes in PBS. Fluorescently labeled secondary antibody was applied subsequently for 1 hr at 37°C, followed again by three washes in PBS. Explants were imaged using a Leica SP5X confocal microscope.

Immunoblotting:

After 1, 3, 6 hours of injury, control (uninjured) axons, and positive control (whole explant) samples were lysed using NP40 lysis buffer mixed with protease inhibitor (Fisher-Scientific, Houston, TX) and phosphatase inhibitor (Roche Diagnostics, Indianapolis, IN, USA). The homogenate was further lysed in liquid nitrogen, and supernatant was stored at -80ºC. Protein concentration was measured using a bicinchoninic acid (BCA) protein assay kit (Pierce; Thermo Fisher Scientific, Rockford, IL, USA). An equal amount of the protein (60 μg) was loaded into each lane, run on 4-15% Mini-Protean Precast gel (Bio-rad, Hercules, CA), and transferred to PVDF membranes (Millipore, Billerica, MA). The membranes were blocked overnight using casein-blocking buffer (Vector Lab**,** Burlingame, CA**)**, and incubated for 2 h at RT either with RanBP1 antibody (diluted 1 : 100; Santa Cruz, Dallas, TX) or vimentin antibody (diluted 1 : 100; Abcam, Cambridge, MA). Alternately, membranes were incubated for

35 minutes at RT with Importin β1 antibody (diluted 1:300, Abcam, Cambridge, MA), GAPDH (diluted 1:60000, Fitzgerald, Acton, MA) or, Neun (diluted 1:500, Millipore, Billerica, MA). Appropriate secondary antibodies, and DuoLux Chemiluminescent was used for detection following protocol given in Vectastain-AMC Amp kit (Vector Lab, Burlingame, CA). The membranes were detected using ChemiDoc™ XRS+ (Bio-rad, Hercules, CA), and analyzed using Image Lab software (Bio-rad, Hercules, CA). All data were normalized to GAPDH.

Fluorescence Microscopy:

Imaging was performed on an inverted TE-2000E microscope (Nikon, Melville, NY) outfitted with a Lumen-PRO2000 (Prior Scientific, Rockland, MA) illumination system and Chroma filters (Bellows Falls, VT. EPI: 488 nm, Emission 530 nm). Additionally, a custom built chamber (Precision Plastics, Beltsville, MD) maintained temperature, humidity, and CO2 levels during imaging. Additionally, Leica SP5X confocal microscope (Buffalo Grove, IL) was used for explant imaging and importazole treated sample imaging. The confocal system is equipped with multiple laser lines, including a 405 diode, an Argon laser (458, 476, 488, 496,514nm) and a white light laser (470-670nm in 1 nm increments); they were either imaged using a 10x or 40x objective with Hoechst (Excitation 350 nm, Emission 451 nm), SMI-31 (Excitation 579nm, Emission 599 nm), and Map2 (490 nm, Emission 530 nm) markers.

Statistics and Sample Sizes:

All the PCR experiments were assayed in triplicate for three-four independent experiments. Specifically, axonal injury experiments N=3 for 1 and 24 hrs, and N=4 for 6 and 15 hrs time points. Both the AMD and IPZ treated samples size were N =3, except for Ranb1, in which only a single sample amplified this transcript, possibly due to IPZ effects on both control and injured populations, unrelated to injury response. Data were compared statistically using relative expression software tool (REST©, Qiagen, Valencia, CA), as described in the study of Pfaffl et al. For Importazole characterization, 100-200 cells were quantified from two different explants for each condition, control, IPZ treatment for 12 hrs and 24 hrs. One-way student's t-test was used for statistical analysis. For immunoblots, the following sample sizes were used: Importin β1: N=5, RanBP1: N=3, and vimentin: N =4. Values presented illustrate as percent of control. One-way student's t-test was used for statistical analysis. For all experiments, type I error α was set to 0.05.

Chapter 5: Conclusion

Section 1: Introduction

Unlike PNS neurons, neurons of the CNS do not possess the ability to regenerate after axonal injury. This less effective regeneration capability leads to many chronic CNS functional deficits following spinal cord and brain injury or degeneration. Development of regeneration strategies will be applicable to many CNS disorders, such as spinal cord injury (SCI), genetic disorders such as mental retardation, aphasia, and degenerative diseases such as Alzheimer's disease. One regeneration approach is to understand and exploit the intrinsic growth capacity of neurons. One such intrinsic mechanism post axotomy is localized protein synthesis (LPS). It is a well-established phenomenon that LPS is required for axonal regeneration. Among its several associated processes, LPS requires gene transcription, which has been proposed as a major controlling mechanism for axon growth and after injury [31]. Between PNS and CNS, major gaps exist on this subject, specifically in the context of changes in the localization of mRNA transcripts required for LPS, and injury induced retrograde injury signaling. Importantly, both defects in mRNA transport and RIS mechanisms have been linked to impaired regenerative ability of neurons [46,47]. Thus, our study set out to explore two of these regeneration pertinent mechanisms in local protein synthesis:

- The detailed quantification of mRNA transport during hippocampal neuron development (Chapter 2).

- Regulation of recruitment of retrograde injury signaling complex-related genes in central axons following injury (Chapter 4), using a mouse whole hippocampal explants culture system (Chapter 3).

Section 2: Findings and Implications

The main findings are chapter specific and were summarized with the respective chapters: A comparative quantitative assessment of axonal and dendritic mRNA transport in maturing hippocampal neurons (Chapter 2), a mouse whole hippocampal explant culture system to study isolated axons (Chapter 3), and biphasic increase of retrograde injury signaling complex-related genes in central axons following injury (Chapter 4).

Subsection 1: A comparative quantitative assessment of axonal and dendritic mRNA transport in maturing hippocampal neurons

We have identified unique mRNA transport profiles both in the axons and dendrites at varying stages of neurite maturity. Specifically, neurons at day 4 with a free terminal were designated as immature (growing), differentiated neurons. Neurons at days 7 and 12 were both designated as differentiated neurons with stable synapses, with those at day 12 presumably more mature. Surprisingly, we were able to find two different pools of mRNA populations that were labeled dimly (faster velocities), and brightly (slower velocities). The bright and dim velocities in axons peaked at day 7. The increase in net axonal velocity coincides with the end stages of neurite outgrowth and the initial stages of synapse formation and stabilization. This indicates significance of local translation contributing to synapse stabilization pre-synaptically. This timeline also

parallels the relationship between local translation and the effectiveness of neurotrophic signaling during axonal outgrowth and pre-synaptic signaling. Specifically, BDNF and NT-3 neurotrophins play an important role in effective axonal guidance [4,86]. Net dendritic velocities of bright mRNA particles were linear with highest velocities at day 12. The increase in mRNA transport at later time points in dendrites is consistent with its role for local protein synthesis in the context of sustained synaptic connectivity for long-term potentiation (LTP) [4,17,61,86,87,89]. Proteins relevant for synaptic plasticity are observed in dendritic mRNA pools; these include αCAMKII [91] and cytoplasmic polyadenylation element binding protein (CPEB).

Several studies have indicated that adult CNS neurons lose their regenerative capabilities, whereas embryonic neurons possess the ability to regenerate [31,157]. Since then the focus has been to investigate axonal growth during development and axon regeneration and to examine the factors that could promote axon regeneration in the adult CNS. Here, we have identified mRNA transport profiles in hippocampal neurons as they develop in vitro, with hope to recapitulate the developmental pathway during axonal regeneration. The next step in this direction would be to identify how the transport profiles change during axonal regeneration. The difference between the development and regeneration profiles could be beneficial in identifying key factors that influence CNS regeneration. Additionally, since genetic transcription is imperative in controlling the intrinsic axon growth/regeneration, it would be beneficial to focus on regulation of specific mRNAs before and after injury. Using this logic, the next step in our project was to understand the regulatory mechanism of RIS associated genes in the axons. Because

the study required axonal genetic and protein analysis independent of contamination by the cell body, we developed a novel explant culture system to enable axonal-specific characterization.

Subsection 2: Mouse whole hippocampal explant culture system to study isolated axons

Here, we developed a simple and feasible whole-hippocampal explant culture system to study central neuronal survival and axonal gene and protein expression in the context of regeneration. The explant culture system enabled axon-specific measurements without the need of additional equipment. In this report, we detailed our validation of this model, and its implementation to characterize axonal outgrowth following initial explant harvest and a secondary axonal injury. This model will be useful in probing mechanistic questions in central axons. The simplicity will be beneficial in enabling genetic and pharmacological manipulation to answer neural injury and regeneration questions. We have ourselves utilized the system to understand the underlying mechanisms involved in RIS, a key process underlying for axonal regeneration.

Subsection 3: Biphasic increase of retrograde injury signaling complex-related genes in central axons following injury

Our results suggests biphasic axonal response, in which levels of several axonal transcripts, including those associated with RIS, increase rapidly in axons after injury, contributing to early synthesis of corresponding proteins. Importin β-dependent activity at the nucleus then appears to modulate a second wave of RIS-associated transcripts, which are likely to further support axonal outgrowth. Additionally, these transcripts are

regulated differently where a first wave is probably regulated via an initial early response, and later response is regulated as a feedback mechanism of importin β-mediated RIS pathway itself.

RIS has implications for axonal regeneration in the PNS and CNS. [56]. According to our results, both mRNA and protein localization in axons are highly regulated. We believe that altering/controlling these regulatory pathways could be beneficial in promoting regeneration.

Section 3: Future Experiments and Clinical Significance

Immediate next steps: The identification of the specific signals that are transported from distant injury sites and the mechanism of such transport should provide critical insight into the development of novel therapies to promote neuronal regeneration and functional recovery. The immediate next step in this direction would be to further unveil this mechanism. One of the initial experiments could be to understand what causes the initial changes (~1hr) in mRNA localization post-injury, for example, cascades of calcium-mediated transcriptional or translational regulation in the cell body. Then, we could develop strategies to trigger mRNA changes and localized protein synthesis by manipulating genes or proteins involved in these pathways to improve axonal regeneration. We can also investigate what triggers the differential mRNA response at 1hr post-injury, or what specific cargo is directly responsible for mRNA transcript changes (~24hrs). For example, if STAT3 plays an important role, we could then manipulate STAT3 or other RIS associated signaling molecules genetically or pharmacologically, to observe if mRNA transcripts are altered.

Longer-term studies: Defects in retrograde signaling may underlie the pathophysiological basis of several neurodegenerative diseases. As PNS neurons are able to regenerate compared to CNS neurons, knowing the similarities and differences between the two systems will be beneficial in overcoming the inability of CNS neurons to regenerate. Further, our initial studies were all *in vitro,* allowing us to manipulate the experimental system. However, whether RIS occurs and has a role in recovery after central nervous system injury, such as traumatic brain injury and spinal cord injury is unknown *in vivo*. The next challenge will be to explore mechanisms of RIS *in vivo*, and manipulate RIS pathways in order to promote regeneration.

Our overall goal of the project is to understand the underlying key processes involved in axonal regeneration in order to treat brain injuries. It will be beneficial to consider combining approaches to block extrinsic inhibition while enhancing the intrinsic growth program of the neurons.

The purpose of the thesis is to provide one step forward in promoting axonal regeneration. We hope that the findings will be beneficial in unveiling many regenerative processes both in the CNS and PNS, and eventually lead to therapies promoting axonal regeneration.

Publication and co-author contribution:

I have published:

Publication 1

A comparative quantitative assessment of axonal and dendritic mRNA transport in maturing hippocampal neurons (Chapter 2)

Gunja K. Pathak[1], James M. Love[1], Joshua Chetta[1], and Sameer B. Shah[1,2]*

Pathak GK, Love JM, Chetta J, Shah SB (2013) A comparative quantitative assessment of axonal and dendritic mRNA transport in maturing hippocampal neurons. PLoS One 8: e65917. [Citation].

Co-author contributions:

James Love: experimental, and software help

Joshua Chetta: Development of analytical tool

Dr. Sameer Shah: Writing, project discussion, Mentor, corresponding author.

Publication 2

Variability in membrane continuity between Schwann cells and neurons

James M. Love1, Gunja K. Pathak1, Joshua Chetta1, Sameer B. Shah1,2*

Love J, Pathak G, Chetta J, Shah S (2012) Variability in Membrane Continuity Between Schwann Cells and Neurons. Cellular and Molecular Bioengineering 5: 450-462. [Citation]

Co-author contribution:

Gunja Pathak: writing and project discussion.

I have submitted:

Mouse whole hippocampal explant culture system to study isolated axons

Gunja K. Pathak1, Helim Aranda-Espinoza1, Sameer B. Shah*1,2

Co-author contributions: Dr. Helim Aranda-Espinoza: co-mentor, discussion, and Dr. Sameer Shah: Mentor, writing, and discussion

I will be submitting:

Biphasic increase of retrograde injury signaling complex-related genes in central axons following injury

Gunja K. Pathak1, Hannah Ornstein1, Helim Aranda-Espinoza1, Amy Karlsson1, Sameer B. Shah*1,2

Co-author contribution:

Hannah Ornstein: Westernblot experiments

Dr. Helim Aranda-Espinoza: co-mentor, project-discussion

Dr. Amy Karlsson: western blot troubleshooting

Dr. Sameer Shah: mentor, writing and project discussion.

Appendices

Section 1: Chapter 2 Supplementary Tables

Table S1: Summary of maximum velocities for various classes of labeled cargoes. * Significant difference (day 4 vs. day 12 *p<.05). ✦ Significant difference (p<.05). ✷Significant difference (day 7 vs. day 12 p<.05).

Average Maximum Velocity	**Day 4**	**Day 7**	**Day 12**
Mitochondria Dendrite anterograde	0.002±.0008	0.007±.003	0.004±.0007
Mitochondria Dendrite retrograde	-0.009±.003[*]	-0.004±.001	-0.003±.001[*]
mRNA Axon anterograde (Dim)	0.08± .02	0.09±.01	0.11±.01
mRNA Axon retrograde (Dim)	-0.04±.01	-0.04±.007	-0.05±.01
mRNA Dendrite anterograde (Dim)	0.13±.03	0.12±.02	0.2±.03
mRNA Dendrite retrograde (Dim)	-0.05±.02	-0.04±.009	-0.07±.05
mRNA Axon anterograde (Bright)	0.01±.003	0.02±.004	0.007±.003
mRNA Axon retrograde (Bright)	-0.004±.0009	-0.006±.001	-0.008±.002
mRNA Dendrite anterograde (Bright)	0.008±.004	0.02±.005	0.008±.003
mRNA Dendrite retrograde (Bright)	-0.02±.009[*]	-0.01±.003	-0.005±.001[*]
Mitochondria Axon anterograde	0.008±.001	0.01±.002	0.008±.002
Mitochondria Axon retrograde	-0.009±.002	-0.008±.002	-0.007±.001

Table S2: Summary of average velocities for various classes of labeled cargoes. * Significant difference (day 4 vs. day 12 p<.05). ✦Significant difference (day vs. day 7 p< .05). ✷Significant difference (day 7 vs. day 12 p<.05).

Average Velocity	**Day 4**	**Day 7**	**Day 12**
mRNA Axon anterograde (Dim)	.06±.02	0.08±.02	0.08±.02
mRNA Axon retrograde (Dim)	-0.03±.01	-0.03±.01	0.03±.01
mRNA Dendrite anterograde (Dim)	0.1±.02	0.08±.009	0.12±.009
mRNA Dendrite retrograde (Dim)	-0.03±.01	-0.03±.007	-0.06±.03
mRNA Axon anterograde (Bright)	0.005±.001	0.009±.001	0.004±.001
mRNA Axon retrograde (Bright)	-0.003±.0004	-0.004±.0005	-0.004±.0009
mRNA Dendrite anterograde (Bright)	0.004±.003	0.01±.008	0.007±.002
mRNA Dendrite retrograde (Bright)	-0.02±.006[*][✦]	-0.004±.002[✦]	-0.003±.0008[*]

Mitochondria Axon anterograde	0.003±.0005	0.004±.0009	0.004±.0005
Mitochondria Axon retrograde	-0.006±.002	-0.004±.0009	-0.003±.0005
Mitochondria Dendrite anterograde	0.001±.0003[✦]	0.005±.002[✦]	0.002±.0003
Mitochondria Dendrite retrograde	-0.03±.01[*]	-0.03±.01	-0.03±.01[*]

Table S3: Summary of duration spent moving in each direction for various classes of labeled cargoes. * Significant difference (day 4 vs. day 12 p<.05). ✦ Significant difference (day 4 vs. day 7p<.05). ✷Significant difference (day 7 vs. day 12 p<.05).

Particle Duration	**Day 4**	**Day 7**	**Day 12**
mRNA Axon anterograde (Dim)	144 ±34[✦]	143±17[✦]	179±19
mRNA Axon retrograde (Dim)	84±20	100±16	83±15
mRNA Dendrite anterograde (Dim)	110±21	200±22	168±18
mRNA Dendrite retrograde (Dim)	67±23	61±14	27±18
mRNA Axon anterograde (Bright)	297±34	234±26[✷]	330±24[✷]

mRNA Axon retrograde (Bright)	363±40	300±34	311±36
mRNA Dendrite anterograde (Bright)	225±50	281±32	320±31
mRNA Dendrite retrograde (Bright)	294±86	278±71	331±56
Mitochondria Axon anterograde	472±36[*]	473±37[✷]	255±26[*][✷]
Mitochondria Axon retrograde	308±33[*]	260±33[✷]	517±31[*][✷]
Mitochondria Dendrite anterograde	264±50[*]	342±42	449±47[*]
Mitochondria Dendrite retrograde	399±49	398±42	298±48

Table S4: Summary of net velocities for various classes of labeled cargoes. * Significant difference (day 4 vs. day 12 $p<.05$). ✦ Significant difference (day 4 vs. day 7$p<.05$). ✷Significant difference (day 7 vs. day 12 $p<.05$).

Net Average Velocity	Day 4	Day 7	Day 12
mRNA Axon (Dim)	0.03±.02	0.04±.01	0.04±.01
mRNA Dendrite (Dim)	0.0705±.03	0.05±.02	0.1±.02
mRNA Axon (Bright)	0.0002±.0003	0.002±.001	0.0001±.0004
mRNA Dendrite (Bright)	-0.003±.001[*]	-0.0001±.002	0.001±.0006[*]
Mitochondria Axon	-0.0002±.0002	-0.0004±.0007	0.0006±.0003
Mitochondria Dendrite	-.002±.0005[*] [✦]	.0008±.0009[✦]	.0008±.0004[*]

Bibliography

1. Qianx122 (2012) Biological Psychology. Psychology.
2. Yiu G, He Z (2006) Glial inhibition of CNS axon regeneration. Nat Rev Neurosci 7: 617-627.
3. Williams WH, Potter S, Ryland H (2010) Mild traumatic brain injury and Postconcussion Syndrome: a neuropsychological perspective. J Neurol Neurosurg Psychiatry 81: 1116-1122.
4. Zhang X, Poo MM (2002) Localized synaptic potentiation by BDNF requires local protein synthesis in the developing axon. Neuron 36: 675-688.
5. Russo CA, Steiner C (2006) Hospital Admissions for Traumatic Brain Injuries, 2004: Statistical Brief #27.
6. Coronado VG, Xu L, Basavaraju SV, McGuire LC, Wald MM, et al. (2011) Surveillance for traumatic brain injury-related deaths--United States, 1997-2007. MMWR Surveill Summ 60: 1-32.
7. Wood MD, Kemp SW, Weber C, Borschel GH, Gordon T (2011) Outcome measures of peripheral nerve regeneration. Ann Anat 193: 321-333.
8. Shi R, Asano T, Vining NC, Blight AR (2000) Control of membrane sealing in injured mammalian spinal cord axons. J Neurophysiol 84: 1763-1769.
9. Gurgo RD, Bedi KS, Nurcombe V (2002) Current concepts in central nervous system regeneration. J Clin Neurosci 9: 613-617.
10. Horner PJ, Gage FH (2000) Regenerating the damaged central nervous system. Nature 407: 963-970.
11. Huebner EA, Strittmatter SM (2009) Axon regeneration in the peripheral and central nervous systems. Results Probl Cell Differ 48: 339-351.
12. Kim JE, Li S, GrandPre T, Qiu D, Strittmatter SM (2003) Axon regeneration in young adult mice lacking Nogo-A/B. Neuron 38: 187-199.
13. Simonen M, Pedersen V, Weinmann O, Schnell L, Buss A, et al. (2003) Systemic deletion of the myelin-associated outgrowth inhibitor Nogo-A improves regenerative and plastic responses after spinal cord injury. Neuron 38: 201-211.
14. Zheng B, Ho C, Li S, Keirstead H, Steward O, et al. (2003) Lack of enhanced spinal regeneration in Nogo-deficient mice. Neuron 38: 213-224.
15. Bomze HM, Bulsara KR, Iskandar BJ, Caroni P, Skene JH (2001) Spinal axon regeneration evoked by replacing two growth cone proteins in adult neurons. Nat Neurosci 4: 38-43.
16. Sotelo-Silveira JR, Calliari A, Kun A, Koenig E, Sotelo JR (2006) RNA trafficking in axons. Traffic 7: 508-515.
17. Martin KC, Casadio A, Zhu H, Yaping E, Rose JC, et al. (1997) Synapse-specific, long-term facilitation of aplysia sensory to motor synapses: a function for local protein synthesis in memory storage. Cell 91: 927-938.
18. Zelena J (1970) Ribosome-like particles in myelinated axons of the rat. Brain Res 24: 359-363.

19. Zelena J (1972) Ribosomes in myelinated axons of dorsal root ganglia. Z Zellforsch Mikrosk Anat 124: 217-229.
20. Koenig E, Martin R, Titmus M, Sotelo-Silveira JR (2000) Cryptic peripheral ribosomal domains distributed intermittently along mammalian myelinated axons. J Neurosci 20: 8390-8400.
21. Taylor AM, Berchtold NC, Perreau VM, Tu CH, Li Jeon N, et al. (2009) Axonal mRNA in uninjured and regenerating cortical mammalian axons. J Neurosci 29: 4697-4707.
22. Willis DE, van Niekerk EA, Sasaki Y, Mesngon M, Merianda TT, et al. (2007) Extracellular stimuli specifically regulate localized levels of individual neuronal mRNAs. J Cell Biol 178: 965-980.
23. Steward O, Levy WB (1982) Preferential localization of polyribosomes under the base of dendritic spines in granule cells of the dentate gyrus. J Neurosci 2: 284-291.
24. Twiss JL, van Minnen J (2006) New insights into neuronal regeneration: the role of axonal protein synthesis in pathfinding and axonal extension. J Neurotrauma 23: 295-308.
25. Swanger SA, Bassell GJ (2011) Making and breaking synapses through local mRNA regulation. Curr Opin Genet Dev 21: 414-421.
26. Phillips LL, Pollack AE, Steward O (1990) Protein synthesis in the neuropil of the rat dentate gyrus during synapse development. J Neurosci Res 26: 474-482.
27. Yoo S, van Niekerk EA, Merianda TT, Twiss JL (2010) Dynamics of axonal mRNA transport and implications for peripheral nerve regeneration. Exp Neurol 223: 19-27.
28. Verma P, Chierzi S, Codd AM, Campbell DS, Meyer RL, et al. (2005) Axonal protein synthesis and degradation are necessary for efficient growth cone regeneration. J Neurosci 25: 331-342.
29. Willis DE, Twiss JL (2006) The evolving roles of axonally synthesized proteins in regeneration. Curr Opin Neurobiol 16: 111-118.
30. Huang YS, Richter JD (2004) Regulation of local mRNA translation. Curr Opin Cell Biol 16: 308-313.
31. Park KK, Liu K, Hu Y, Smith PD, Wang C, et al. (2008) Promoting axon regeneration in the adult CNS by modulation of the PTEN/mTOR pathway. Science 322: 963-966.
32. Edbladh M, Tonge D, Golding J, Ekstrom AR, Edstrom A (1994) Early regeneration in vitro of adult mouse sciatic axons is dependent on local protein synthesis but may not involve neurotrophins. Neurosci Lett 168: 37-40.
33. Gaete J, Kameid G, Alvarez J (1998) Regenerating axons of the rat require a local source of proteins. Neurosci Lett 251: 197-200.
34. Li C, Sasaki Y, Takei K, Yamamoto H, Shouji M, et al. (2004) Correlation between semaphorin3A-induced facilitation of axonal transport and local activation of a translation initiation factor eukaryotic translation initiation factor 4E. J Neurosci 24: 6161-6170.
35. Zheng JQ, Kelly TK, Chang B, Ryazantsev S, Rajasekaran AK, et al. (2001) A functional role for intra-axonal protein synthesis during axonal regeneration from adult sensory neurons. J Neurosci 21: 9291-9303.

36. Hanz S, Perlson E, Willis D, Zheng JQ, Massarwa R, et al. (2003) Axoplasmic importins enable retrograde injury signaling in lesioned nerve. Neuron 40: 1095-1104.
37. Bassell GJ, Warren ST (2008) Fragile X syndrome: loss of local mRNA regulation alters synaptic development and function. Neuron 60: 201-214.
38. Richter JD (2007) CPEB: a life in translation. Trends Biochem Sci 32: 279-285.
39. Christie SB, Akins MR, Schwob JE, Fallon JR (2009) The FXG: a presynaptic fragile X granule expressed in a subset of developing brain circuits. J Neurosci 29: 1514-1524.
40. Farina KL, Huttelmaier S, Musunuru K, Darnell R, Singer RH (2003) Two ZBP1 KH domains facilitate beta-actin mRNA localization, granule formation, and cytoskeletal attachment. J Cell Biol 160: 77-87.
41. Zhang HL, Eom T, Oleynikov Y, Shenoy SM, Liebelt DA, et al. (2001) Neurotrophin-induced transport of a beta-actin mRNP complex increases beta-actin levels and stimulates growth cone motility. Neuron 31: 261-275.
42. Lin AC, Holt CE (2008) Function and regulation of local axonal translation. Curr Opin Neurobiol 18: 60-68.
43. Ross AF, Oleynikov Y, Kislauskis EH, Taneja KL, Singer RH (1997) Characterization of a beta-actin mRNA zipcode-binding protein. Mol Cell Biol 17: 2158-2165.
44. Huttelmaier S, Zenklusen D, Lederer M, Dictenberg J, Lorenz M, et al. (2005) Spatial regulation of beta-actin translation by Src-dependent phosphorylation of ZBP1. Nature 438: 512-515.
45. Tiruchinapalli DM, Oleynikov Y, Kelic S, Shenoy SM, Hartley A, et al. (2003) Activity-dependent trafficking and dynamic localization of zipcode binding protein 1 and beta-actin mRNA in dendrites and spines of hippocampal neurons. J Neurosci 23: 3251-3261.
46. Gumy LF, Tan CL, Fawcett JW (2010) The role of local protein synthesis and degradation in axon regeneration. Exp Neurol 223: 28-37.
47. Hanz S, Fainzilber M (2006) Retrograde signaling in injured nerve--the axon reaction revisited. J Neurochem 99: 13-19.
48. Berdan RC, Easaw JC, Wang R (1993) Alterations in membrane potential after axotomy at different distances from the soma of an identified neuron and the effect of depolarization on neurite outgrowth and calcium channel expression. J Neurophysiol 69: 151-164.
49. Mandolesi G, Madeddu F, Bozzi Y, Maffei L, Ratto GM (2004) Acute physiological response of mammalian central neurons to axotomy: ionic regulation and electrical activity. FASEB J 18: 1934-1936.
50. Abe N, Cavalli V (2008) Nerve injury signaling. Curr Opin Neurobiol 18: 276-283.
51. Rishal I, Fainzilber M (2010) Retrograde signaling in axonal regeneration. Exp Neurol 223: 5-10.
52. Ben-Yaakov K, Fainzilber M (2009) Retrograde injury signaling in lesioned axons. Results Probl Cell Differ 48: 327-338.
53. Yudin D, Hanz S, Yoo S, Iavnilovitch E, Willis D, et al. (2008) Localized regulation of axonal RanGTPase controls retrograde injury signaling in peripheral nerve. Neuron 59: 241-252.

54. Perry RB, Doron-Mandel E, Iavnilovitch E, Rishal I, Dagan SY, et al. (2012) Subcellular knockout of importin beta1 perturbs axonal retrograde signaling. Neuron 75: 294-305.
55. Perlson E, Hanz S, Ben-Yaakov K, Segal-Ruder Y, Seger R, et al. (2005) Vimentin-dependent spatial translocation of an activated MAP kinase in injured nerve. Neuron 45: 715-726.
56. Ohara R, Fujita Y, Hata K, Nakagawa M, Yamashita T (2011) Axotomy induces axonogenesis in hippocampal neurons through STAT3. Cell Death Dis 2: e175.
57. Ohara R, Hata K, Yasuhara N, Mehmood R, Yoneda Y, et al. (2011) Axotomy induces axonogenesis in hippocampal neurons by a mechanism dependent on importin beta. Biochem Biophys Res Commun 405: 697-702.
58. Fink DJ, Gainer H (1980) Axonal transport of proteins. A new view using in vivo covalent labeling. J Cell Biol 85: 175-186.
59. Willis D, Li KW, Zheng JQ, Chang JH, Smit A, et al. (2005) Differential transport and local translation of cytoskeletal, injury-response, and neurodegeneration protein mRNAs in axons. J Neurosci 25: 778-791.
60. Zelena J (1972) Ribosomes in the axoplasm of myelinated nerve fibres. Folia Morphol (Praha) 20: 91-93.
61. Martin KC, Zukin RS (2006) RNA trafficking and local protein synthesis in dendrites: an overview. J Neurosci 26: 7131-7134.
62. Fletcher TL, Cameron P, De Camilli P, Banker G (1991) The distribution of synapsin I and synaptophysin in hippocampal neurons developing in culture. J Neurosci 11: 1617-1626.
63. Matus A (2001) Moving molecules make synapses. Nat Neurosci 4: 967-968.
64. Banker GA, Cowan WM (1977) Rat hippocampal neurons in dispersed cell culture. Brain Res 126: 397-342.
65. Craig AM, Banker G (1994) Neuronal polarity. Annu Rev Neurosci 17: 267-310.
66. Ligon LA, Steward O (2000) Movement of mitochondria in the axons and dendrites of cultured hippocampal neurons. J Comp Neurol 427: 340-350.
67. Aronov S, Aranda G, Behar L, Ginzburg I (2002) Visualization of translated tau protein in the axons of neuronal P19 cells and characterization of tau RNP granules. J Cell Sci 115: 3817-3827.
68. Knowles RB, Sabry JH, Martone ME, Deerinck TJ, Ellisman MH, et al. (1996) Translocation of RNA granules in living neurons. J Neurosci 16: 7812-7820.
69. Sanchez-Carbente Mdel R, Desgroseillers L (2008) Understanding the importance of mRNA transport in memory. Prog Brain Res 169: 41-58.
70. Skup M (2008) Dendrites as separate compartment - local protein synthesis. Acta Neurobiol Exp (Wars) 68: 305-321.
71. Yoon BC, Zivraj KH, Holt CE (2009) Local translation and mRNA trafficking in axon pathfinding. Results Probl Cell Differ 48: 269-288.
72. Knowles RB, Kosik KS (1997) Neurotrophin-3 signals redistribute RNA in neurons. Proc Natl Acad Sci U S A 94: 14804-14808.
73. Roegiers F, Jan YN (2000) Staufen: a common component of mRNA transport in oocytes and neurons? Trends Cell Biol 10: 220-224.
74. Davis L, Banker GA, Steward O (1987) Selective dendritic transport of RNA in hippocampal neurons in culture. Nature 330: 477-479.

75. Cambray S, Pedraza N, Rafel M, Gari E, Aldea M, et al. (2009) Protein kinase KIS localizes to RNA granules and enhances local translation. Mol Cell Biol 29: 726-735.
76. Davidovic L, Jaglin XH, Lepagnol-Bestel AM, Tremblay S, Simonneau M, et al. (2007) The fragile X mental retardation protein is a molecular adaptor between the neurospecific KIF3C kinesin and dendritic RNA granules. Hum Mol Genet 16: 3047-3058.
77. Elvira G, Wasiak S, Blandford V, Tong XK, Serrano A, et al. (2006) Characterization of an RNA granule from developing brain. Mol Cell Proteomics 5: 635-651.
78. Kanai Y, Dohmae N, Hirokawa N (2004) Kinesin transports RNA: isolation and characterization of an RNA-transporting granule. Neuron 43: 513-525.
79. Ling SC, Fahrner PS, Greenough WT, Gelfand VI (2004) Transport of Drosophila fragile X mental retardation protein-containing ribonucleoprotein granules by kinesin-1 and cytoplasmic dynein. Proc Natl Acad Sci U S A 101: 17428-17433.
80. Shan J, Munro TP, Barbarese E, Carson JH, Smith R (2003) A molecular mechanism for mRNA trafficking in neuronal dendrites. J Neurosci 23: 8859-8866.
81. Sotelo-Silveira J, Crispino M, Puppo A, Sotelo JR, Koenig E (2008) Myelinated axons contain beta-actin mRNA and ZBP-1 in periaxoplasmic ribosomal plaques and depend on cyclic AMP and F-actin integrity for in vitro translation. J Neurochem 104: 545-557.
82. Dynes JL, Steward O (2007) Dynamics of bidirectional transport of Arc mRNA in neuronal dendrites. J Comp Neurol 500: 433-447.
83. Bramham CR (2008) Local protein synthesis, actin dynamics, and LTP consolidation. Curr Opin Neurobiol 18: 524-531.
84. Brittis PA, Lu Q, Flanagan JG (2002) Axonal protein synthesis provides a mechanism for localized regulation at an intermediate target. Cell 110: 223-235.
85. Martin KC (2004) Local protein synthesis during axon guidance and synaptic plasticity. Curr Opin Neurobiol 14: 305-310.
86. Kang H, Schuman EM (1996) A requirement for local protein synthesis in neurotrophin-induced hippocampal synaptic plasticity. Science 273: 1402-1406.
87. Bramham CR, Wells DG (2007) Dendritic mRNA: transport, translation and function. Nat Rev Neurosci 8: 776-789.
88. Sutton MA, Ito HT, Cressy P, Kempf C, Woo JC, et al. (2006) Miniature neurotransmission stabilizes synaptic function via tonic suppression of local dendritic protein synthesis. Cell 125: 785-799.
89. Sutton MA, Schuman EM (2006) Dendritic protein synthesis, synaptic plasticity, and memory. Cell 127: 49-58.
90. Woo NH, Nguyen PV (2003) Protein synthesis is required for synaptic immunity to depotentiation. J Neurosci 23: 1125-1132.
91. Miller S, Yasuda M, Coats JK, Jones Y, Martone ME, et al. (2002) Disruption of dendritic translation of CaMKIIalpha impairs stabilization of synaptic plasticity and memory consolidation. Neuron 36: 507-519.
92. Si K, Giustetto M, Etkin A, Hsu R, Janisiewicz AM, et al. (2003) A neuronal isoform of CPEB regulates local protein synthesis and stabilizes synapse-specific long-term facilitation in aplysia. Cell 115: 893-904.

93. Miller KE, Sheetz MP (2006) Direct evidence for coherent low velocity axonal transport of mitochondria. J Cell Biol 173: 373-381.
94. Morris RL, Hollenbeck PJ (1993) The regulation of bidirectional mitochondrial transport is coordinated with axonal outgrowth. J Cell Sci 104 (Pt 3): 917-927.
95. Overly CC, Rieff HI, Hollenbeck PJ (1996) Organelle motility and metabolism in axons vs dendrites of cultured hippocampal neurons. J Cell Sci 109 (Pt 5): 971-980.
96. Ligon LA, Steward O (2000) Role of microtubules and actin filaments in the movement of mitochondria in the axons and dendrites of cultured hippocampal neurons. J Comp Neurol 427: 351-361.
97. Cai Q, Sheng ZH (2009) Mitochondrial transport and docking in axons. Exp Neurol 218: 257-267.
98. Hollenbeck PJ, Saxton WM (2005) The axonal transport of mitochondria. J Cell Sci 118: 5411-5419.
99. Wang W, van Niekerk E, Willis DE, Twiss JL (2007) RNA transport and localized protein synthesis in neurological disorders and neural repair. Dev Neurobiol 67: 1166-1182.
100. Chetta J, Shah SB (2011) A novel algorithm to generate kymographs from dynamic axons for the quantitative analysis of axonal transport. J Neurosci Methods 199: 230-240.
101. Ferguson TA, Son YJ (2011) Extrinsic and intrinsic determinants of nerve regeneration. J Tissue Eng 2: 2041731411418392.
102. Liu H, Kim Y, Chattopadhyay S, Shubayev I, Dolkas J, et al. (2010) Matrix metalloproteinase inhibition enhances the rate of nerve regeneration in vivo by promoting dedifferentiation and mitosis of supporting schwann cells. J Neuropathol Exp Neurol 69: 386-395.
103. Liu K, Lu Y, Lee JK, Samara R, Willenberg R, et al. (2010) PTEN deletion enhances the regenerative ability of adult corticospinal neurons. Nat Neurosci 13: 1075-1081.
104. Hayashi H, Campenot RB, Vance DE, Vance JE (2004) Glial lipoproteins stimulate axon growth of central nervous system neurons in compartmented cultures. J Biol Chem 279: 14009-14015.
105. Hellman AN, Vahidi B, Kim HJ, Mismar W, Steward O, et al. (2010) Examination of axonal injury and regeneration in micropatterned neuronal culture using pulsed laser microbeam dissection. Lab Chip 10: 2083-2092.
106. Willis D, Li KW, Zheng JQ, Chang JH, Smit AB, et al. (2005) Differential transport and local translation of cytoskeletal, injury-response, and neurodegeneration protein mRNAs in axons. J Neurosci 25: 778-791.
107. Ivins KJ, Bui ET, Cotman CW (1998) Beta-amyloid induces local neurite degeneration in cultured hippocampal neurons: evidence for neuritic apoptosis. Neurobiol Dis 5: 365-378.
108. Le Nel A, Minc N, Smadja C, Slovakova M, Bilkova Z, et al. (2008) Controlled proteolysis of normal and pathological prion protein in a microfluidic chip. Lab Chip 8: 294-301.

109. Yu L, Huang H, Dong X, Wu D, Qin J, et al. (2008) Simple, fast and high-throughput single-cell analysis on PDMS microfluidic chips. Electrophoresis 29: 5055-5060.
110. Abate AR, Lee D, Do T, Holtze C, Weitz DA (2008) Glass coating for PDMS microfluidic channels by sol-gel methods. Lab Chip 8: 516-518.
111. Quinto-Su PA, Lai HH, Yoon HH, Sims CE, Allbritton NL, et al. (2008) Examination of laser microbeam cell lysis in a PDMS microfluidic channel using time-resolved imaging. Lab Chip 8: 408-414.
112. Parsley CP, Cheng KW, Song L, Hochman S (1998) Thin slice CNS explants maintained on collagen-coated culture dishes. J Neurosci Methods 80: 65-74.
113. Spenger C, Braschler UF, Streit J, Luscher HR (1991) An Organotypic Spinal Cord - Dorsal Root Ganglion - Skeletal Muscle Coculture of Embryonic Rat. I. The Morphological Correlates of the Spinal Reflex Arc. Eur J Neurosci 3: 1037-1053.
114. Masuko S, Kuromi H, Shimada Y (1979) Isolation and culture of motoneurons from embryonic chicken spinal cords. Proc Natl Acad Sci U S A 76: 3537-3541.
115. Tuttle R, Matthew WD (1995) Neurotrophins affect the pattern of DRG neurite growth in a bioassay that presents a choice of CNS and PNS substrates. Development 121: 1301-1309.
116. Tsai HH, Macklin WB, Miller RH (2006) Netrin-1 is required for the normal development of spinal cord oligodendrocytes. J Neurosci 26: 1913-1922.
117. Ayaz D, Leyssen M, Koch M, Yan J, Srahna M, et al. (2008) Axonal injury and regeneration in the adult brain of Drosophila. J Neurosci 28: 6010-6021.
118. Grooms SY, Noh KM, Regis R, Bassell GJ, Bryan MK, et al. (2006) Activity bidirectionally regulates AMPA receptor mRNA abundance in dendrites of hippocampal neurons. J Neurosci 26: 8339-8351.
119. Bassell GJ, Zhang H, Byrd AL, Femino AM, Singer RH, et al. (1998) Sorting of beta-actin mRNA and protein to neurites and growth cones in culture. J Neurosci 18: 251-265.
120. Bassell G, Singer RH (1997) mRNA and cytoskeletal filaments. Curr Opin Cell Biol 9: 109-115.
121. Park J, Koito H, Li J, Han A (2012) Multi-compartment neuron-glia co-culture platform for localized CNS axon-glia interaction study. Lab Chip 12: 3296-3304.
122. Atsma DE, Bastiaanse EM, Ince C, van der Laarse A (1994) A novel two-compartment culture dish allows microscopic evaluation of two different treatments in one cell culture simultaneously. Influence of external pH on Na+/Ca2+ exchanger activity in cultured rat cardiomyocytes. Pflugers Arch 428: 296-299.
123. Saijilafu, Zhou FQ (2012) Genetic study of axon regeneration with cultured adult dorsal root ganglion neurons. J Vis Exp.
124. Shen KF, Crain SM (1994) Nerve growth factor rapidly prolongs the action potential of mature sensory ganglion neurons in culture, and this effect requires activation of Gs-coupled excitatory kappa-opioid receptors on these cells. J Neurosci 14: 5570-5579.
125. Smalheiser NR, Peterson ER, Crain SM (1981) Specific neuritic pathways and arborizations formed by fetal mouse dorsal root ganglion cells within organized

spinal cord explants in culture: a peroxidase-labeling study. Brain Res 254: 383-395.
126. Streit J, Spenger C, Luscher HR (1991) An Organotypic Spinal Cord - Dorsal Root Ganglion - Skeletal Muscle Coculture of Embryonic Rat. II. Functional Evidence for the Formation of Spinal Reflex Arcs In Vitro. Eur J Neurosci 3: 1054-1068.
127. Mariotti C, Askanas V, Engel WK (1993) New organotypic model to culture the entire fetal rat spinal cord. J Neurosci Methods 48: 157-167.
128. Zhang L, Palmer R, McClellan AD (2004) Conditioning lesions enhance axonal regeneration of descending brain neurons in spinal-cord-transected larval lamprey. J Comp Neurol 478: 395-404.
129. Shoemaker SE, Sachs HH, Vaccariello SA, Zigmond RE (2005) A conditioning lesion enhances sympathetic neurite outgrowth. Exp Neurol 194: 432-443.
130. Bonnici B, Kapfhammer JP (2008) Spontaneous regeneration of intrinsic spinal cord axons in a novel spinal cord slice culture model. Eur J Neurosci 27: 2483-2492.
131. Lee YS, Baratta J, Yu J, Lin VW, Robertson RT (2002) AFGF promotes axonal growth in rat spinal cord organotypic slice co-cultures. J Neurotrauma 19: 357-367.
132. Grimpe B, Dong S, Doller C, Temple K, Malouf AT, et al. (2002) The critical role of basement membrane-independent laminin gamma 1 chain during axon regeneration in the CNS. J Neurosci 22: 3144-3160.
133. Lind D, Franken S, Kappler J, Jankowski J, Schilling K (2005) Characterization of the neuronal marker NeuN as a multiply phosphorylated antigen with discrete subcellular localization. J Neurosci Res 79: 295-302.
134. Cavalli V, Kujala P, Klumperman J, Goldstein LS (2005) Sunday Driver links axonal transport to damage signaling. J Cell Biol 168: 775-787.
135. Chang WL, Tarn WY (2009) A role for transportin in deposition of TTP to cytoplasmic RNA granules and mRNA decay. Nucleic Acids Res 37: 6600-6612.
136. Harel A, Forbes DJ (2004) Importin beta: conducting a much larger cellular symphony. Mol Cell 16: 319-330.
137. Lonhienne TG, Forwood JK, Marfori M, Robin G, Kobe B, et al. (2009) Importin-beta is a GDP-to-GTP exchange factor of Ran: implications for the mechanism of nuclear import. J Biol Chem 284: 22549-22558.
138. Zhong Y, Wang Y, Yang H, Ballar P, Lee JG, et al. (2011) Importin beta interacts with the endoplasmic reticulum-associated degradation machinery and promotes ubiquitination and degradation of mutant alpha1-antitrypsin. J Biol Chem 286: 33921-33930.
139. Soderholm JF, Bird SL, Kalab P, Sampathkumar Y, Hasegawa K, et al. (2011) Importazole, a small molecule inhibitor of the transport receptor importin-beta. ACS Chem Biol 6: 700-708.
140. Flanagan WM, Corthesy B, Bram RJ, Crabtree GR (1991) Nuclear association of a T-cell transcription factor blocked by FK-506 and cyclosporin A. Nature 352: 803-807.
141. Shibasaki F, Price ER, Milan D, McKeon F (1996) Role of kinases and the phosphatase calcineurin in the nuclear shuttling of transcription factor NF-AT4. Nature 382: 370-373.

142. Kehlenbach RH, Dickmanns A, Gerace L (1998) Nucleocytoplasmic shuttling factors including Ran and CRM1 mediate nuclear export of NFAT In vitro. J Cell Biol 141: 863-874.
143. Zhu J, McKeon F (1999) NF-AT activation requires suppression of Crm1-dependent export by calcineurin. Nature 398: 256-260.
144. Ziv NE, Spira ME (1993) Spatiotemporal distribution of Ca2+ following axotomy and throughout the recovery process of cultured Aplysia neurons. Eur J Neurosci 5: 657-668.
145. Harvey PJ, Grochmal J, Tetzlaff W, Gordon T, Bennett DJ (2005) An investigation into the potential for activity-dependent regeneration of the rubrospinal tract after spinal cord injury. Eur J Neurosci 22: 3025-3035.
146. Donnelly CJ, Fainzilber M, Twiss JL (2010) Subcellular communication through RNA transport and localized protein synthesis. Traffic 11: 1498-1505.
147. Toth CC, Willis D, Twiss JL, Walsh S, Martinez JA, et al. (2009) Locally synthesized calcitonin gene-related Peptide has a critical role in peripheral nerve regeneration. J Neuropathol Exp Neurol 68: 326-337.
148. Thompson KR, Otis KO, Chen DY, Zhao Y, O'Dell TJ, et al. (2004) Synapse to nucleus signaling during long-term synaptic plasticity; a role for the classical active nuclear import pathway. Neuron 44: 997-1009.
149. Sephton CF, Cenik C, Kucukural A, Dammer EB, Cenik B, et al. (2011) Identification of neuronal RNA targets of TDP-43-containing ribonucleoprotein complexes. J Biol Chem 286: 1204-1215.
150. Egan MJ, McClintock MA, Reck-Peterson SL (2012) Microtubule-based transport in filamentous fungi. Curr Opin Microbiol 15: 637-645.
151. Ambron RT, Walters ET (1996) Priming events and retrograde injury signals. A new perspective on the cellular and molecular biology of nerve regeneration. Mol Neurobiol 13: 61-79.
152. Pathak GK, Love JM, Chetta J, Shah SB (2013) A comparative quantitative assessment of axonal and dendritic mRNA transport in maturing hippocampal neurons. PLoS One 8: e65917.
153. Mullen RJ, Buck CR, Smith AM (1992) NeuN, a neuronal specific nuclear protein in vertebrates. Development 116: 201-211.
154. Livak KJ, Schmittgen TD (2001) Analysis of relative gene expression data using real-time quantitative PCR and the 2(-Delta Delta C(T)) Method. Methods 25: 402-408.
155. Pfaffl MW, Horgan GW, Dempfle L (2002) Relative expression software tool (REST) for group-wise comparison and statistical analysis of relative expression results in real-time PCR. Nucleic Acids Res 30: e36.
156. Bensaude O (2011) Inhibiting eukaryotic transcription: Which compound to choose? How to evaluate its activity? Transcription 2: 103-108.
157. Park KK, Liu K, Hu Y, Kanter JL, He Z (2010) PTEN/mTOR and axon regeneration. Exp Neurol 223: 45-50.